Review of the liquid line of descent in iron-rich basalts

by

Marnus Gert Ferreira

Submitted in partial fulfilment of the requirements for the degree

MSc Geology

In the Faculty of Natural & Agricultural Sciences

University of Pretoria

27 November 2014

DECLARATION OF ORIGINALITY / DECLARATION ON PLAGIARISM

The ***Department of Geology (University of Pretoria)*** places great emphasis upon integrity and ethical conduct in the preparation of all written work submitted for academic evaluation. While academic staff teaches you about referencing techniques and how to avoid plagiarism, you too have a responsibility in this regard. If you are at any stage uncertain as to what is required, you should speak to your lecturer before any written work is submitted.

You are guilty of plagiarism if you copy something from another author's work (e.g. a book, an article or a website) without acknowledging the source and pass it off as your own. In effect you are stealing something that belongs to someone else. This is not only the case when you copy work word-for-word (verbatim), but also when you submit someone else's work in a slightly altered form (paraphrase) or use a line of argument without acknowledging it. You are not allowed to use work previously produced by another student. You are also not allowed to let anybody copy your work with the intention of passing if off as his/her work.

Students who commit plagiarism will not be given any credit for plagiarised work. The matter may also be referred to the Disciplinary Committee (Students) for a ruling. Plagiarism is regarded as a serious contravention of the University's rules and can lead to expulsion from the University.

The declaration which follows must accompany all written work submitted while you are a student of the ***Department of Geology (University of Pretoria)***. No written work will be accepted unless the declaration has been completed and attached.

I, the undersigned, declare that:

1. I understand what plagiarism is and am aware of the University's policy in this regard.
2. I declare that this assignment (e.g. essay, report, project, assignment, dissertation, thesis, etc) is my own original work. Where other people's work has been used (either from a printed source, Internet or any other source), this has been properly acknowledged and referenced in accordance with Departmental requirements.
3. I have not used work previously produced by another student or any other person to hand in as my own.
4. I have not allowed, and will not allow, anyone to copy my work with the intention of passing it off as his or her own work.

Full names of student: _____

Student number: _____

Date submitted: _____

Topic of work: _____

Signature: _____

Supervisor: _____

ABSTRACT

This research project aims to highlight and identify the main assumptions made, and the methods implemented during the construction of the liquid line of descent (LLD) for iron-rich basalts. The project investigates the potential influence of these assumptions on the resultant LLD. The most important factors involved in the construction of a LLD, namely oxygen fugacity (fO_2) and H_2O are examined and presented here in some detail. Alternative methods for analysing the evolution of these iron-rich rocks are discussed and critically assessed. In order to investigate the assumptions and methods for the construction of the LLD, two case studies were performed on iron-rich intrusions, namely: the Birds River Complex in the Eastern Cape, South Africa; and the Skaergaard layered intrusion, Greenland. For Skaergaard, four of the main LLDs proposed for its liquid evolution were chosen and critically assessed. The Birds River Complex is a small and relatively unknown intrusion, therefore it has received significantly less attention, but presents a good example of a local iron-rich intrusion. These two intrusions were used as testing grounds for the application of the thermodynamic modelling software AlphaMELTS to investigate the potential influence of fO_2 and H_2O on crystallising melts. It was found that H_2O had the most significant influence on the maximum iron-enrichment possible for a melt, and that maximum iron-enrichment is attained under anhydrous conditions for all the starting compositions investigated. The effect of fO_2 was significant, however, its influence varied between starting compositions.

TABLE OF CONTENTS

Page

LIST OF FIGURES

Page

LIST OF TABLES

Page

1. Introduction

Layered igneous intrusions have baffled and intrigued scientists for over a hundred years. In no other geological formations is there a more outstanding display of magmatic differentiation than in layered intrusions. There has been great debate over their formation and evolution, especially the famous ones such as the Bushveld Complex; Dufek; Stillwater; the Great Dyke; and Skaergaard. The major interest in these layered intrusions is the large amount of often economic oxide, sulfide and platinum group ores. Layered igneous provinces, such as these, are the source of a whole host of economically mineable elements and minerals, such as: platinum group elements; chromite; Ni-Cu-Fe sulfides; rare earth elements; gold; silver; magnetite etc. (Naldrett, 2004; Barnes and Lightfoot, 2005; Cawthorn *et al.*, 2005). These elements and minerals occur in large concentrated layers within the intrusions, often stretching over great distances (hundreds of kilometres in the Bushveld Complex). The concentration mechanisms and controls remain a greatly debated topic, not only for the ores, but for these provinces as a whole. The key to understanding the evolution of these provinces is to investigate the gradual change in composition of the residual melt. This compositional change can be modelled by constructing a liquid line of descent.

The liquid line of descent (LLD) is a graphical representation of the compositional change of the liquid, during differentiation of the magmatic body. It is especially useful in evaluating and assessing the evolutionary history of the liquid. It is imperative to understand the evolution of the liquid if the formation of layered intrusions is to be better constrained. A sample of the presumed final product of differentiation can be taken, and a reverse model constructed to obtain the chemical composition of the parent magma. The same is true for the opposite scenario. The assumed parental magma can be sampled and analysed for major and trace elements, plugged into a forward model and the final product of differentiation can be predicted. Therefore, a step by step analysis of the liquid's evolution is possible.

Several other methods exist, other than forward and reverse modelling, that can be used to construct a LLD. The importance of the LLD, however, is not the focus of this thesis. That being said, its importance does necessitate a review of the LLD in its entirety. Certain issues regarding the LLD need to be addressed. Take Skaergaard as an example. How is it that ten or so different LLDs can exist for the same intrusion (Fig. 1)? Surely something is amiss. Upon closer inspection it is found that the inherent assumptions made during the construction of the LLD can lead to severe alteration. Skaergaard is considered to be a differentiation product that displays iron enrichment of the liquid during its evolution. Several other intrusions also display this iron enrichment trend. Is this iron enrichment trend real, or is it merely a result of the assumptions?

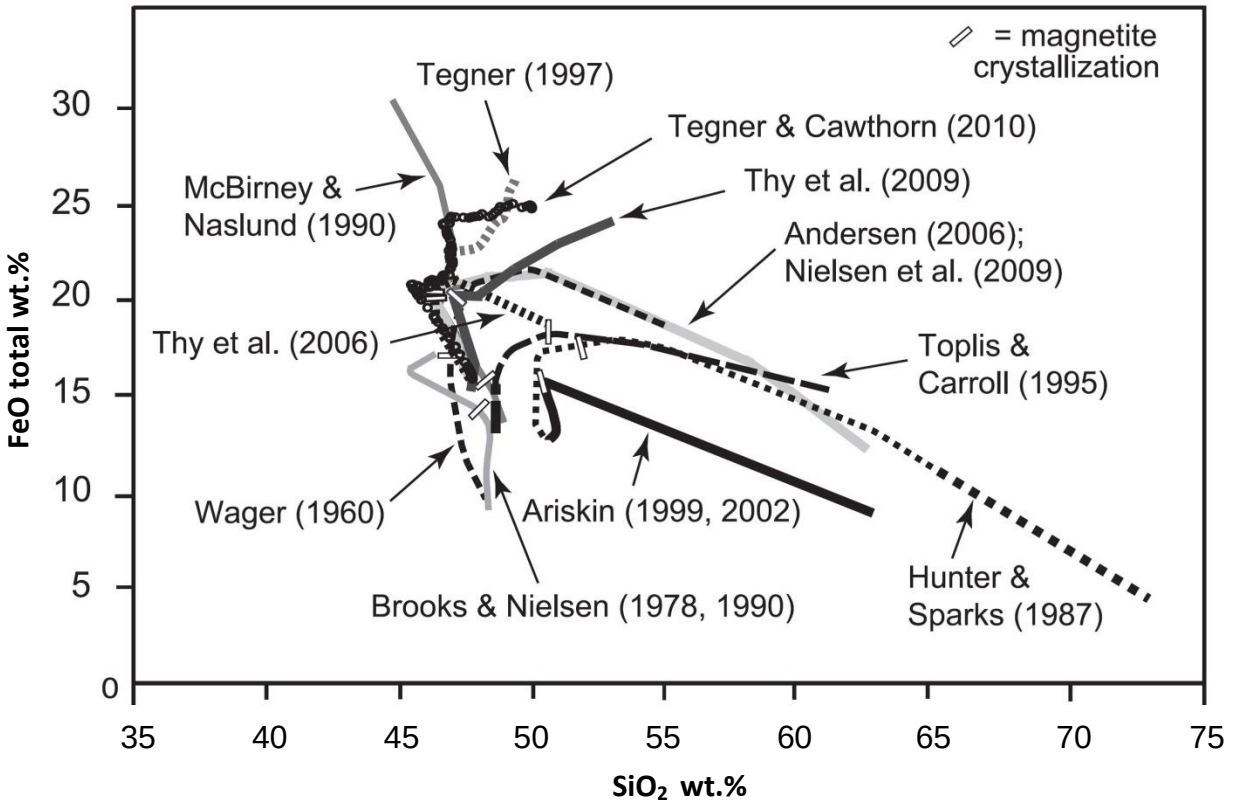

Figure 1. Various proposed LLDs for the Skaergaard intrusion. The suggested onset of magnetite crystallisation (LZc) is indicated for all the LLDs. From Jakobsen *et al.* (2011).

It is assumed that the differentiation of shallow seated sub-alkaline basalt will lead to a liquid becoming enriched in iron (tholeiitic trend) during low degrees of differentiation, and subsequently being depleted in iron and enriched in silica during higher degrees of differentiation (Toplis and Carrol, 1995). The controlling factors

that could lead to extreme iron enrichment are not well understood, nor is it clear just how iron-enriched a liquid can become (Toplis and Carrol, 1995). Looking at the Skaergaard and Kiglaplait intrusions, Wager and Brown (1967) and Morse (1981) calculated the late-stage melts to contain ≥22 wt.% FeO, and McBirney and Naslund (1990) experimentally produced melts of up to 30 wt.% FeO. Others, however, produced melts with <15 wt.% FeO, which is not excessive for a normal tholeiitic basalt.

It should be noted that there are problems surrounding the idea of a residual liquid that becomes increasingly rich in iron as differentiation progresses. One of the main issues is that of the incremental density increase associated with an increase in iron-content of that liquid. Such effects would inhibit the settling of crystals that are less dense than the surrounding liquid, and yet plagioclase crystals accumulated on the floor of the Layered Series, Skaergaard (McBirney and Noyes, 1979).

The focus of this thesis is to review and assess the assumptions made during the construction of the LLD for tholeiitic basalts. The assessment will be done using two igneous intrusions as case studies, one in South Africa, and one abroad. These two are the Birds River complex, Eastern Cape, South Africa, and the Skaergaard layered intrusion, Greenland. A thorough literature review for these two intrusions will be done, focussing specifically on their respective liquid lines of descent. Birds River represents a tholeiitic liquid that has undergone a supposed extreme iron-enrichment trend, and contains a highly iron-rich restite. Skaergaard, as mentioned above, has numerous possible liquid evolutionary paths, a few toward extreme iron-enrichment, and the others to silica enrichment. These are the two very contrasting liquid evolutionary trends proposed by Bowen (1928) and Fenner (1929), but which is the correct one? Debate on this topic has, in the 80 odd years since its introduction, not ceased, nor has it unequivocally been laid to rest.

Consider Figure 2. These five LLDs, constructed for Skaergaard, demonstrate the two enrichment trends, i.e. the Bowen trend (Wager, 1960; Hunter and Sparks, 1987; Toplis and Carrol, 1995) and the Fenner trend (McBirney and Naslund, 1990; Tegner, 1997). Four of these five LLDs will be the focal point for the Skaergaard review, as they represent four main studies performed in the last 70 odd years. Each

one of these LLDs will be assessed and reviewed in order to determine: the assumptions made; their potential impact on the LLD; the method of construction; and the positives and negatives for each method. The starting liquids used for these four LLDs will be remodelled using new modelling software AlphaMELTS and the findings will be compared to work done in literature.

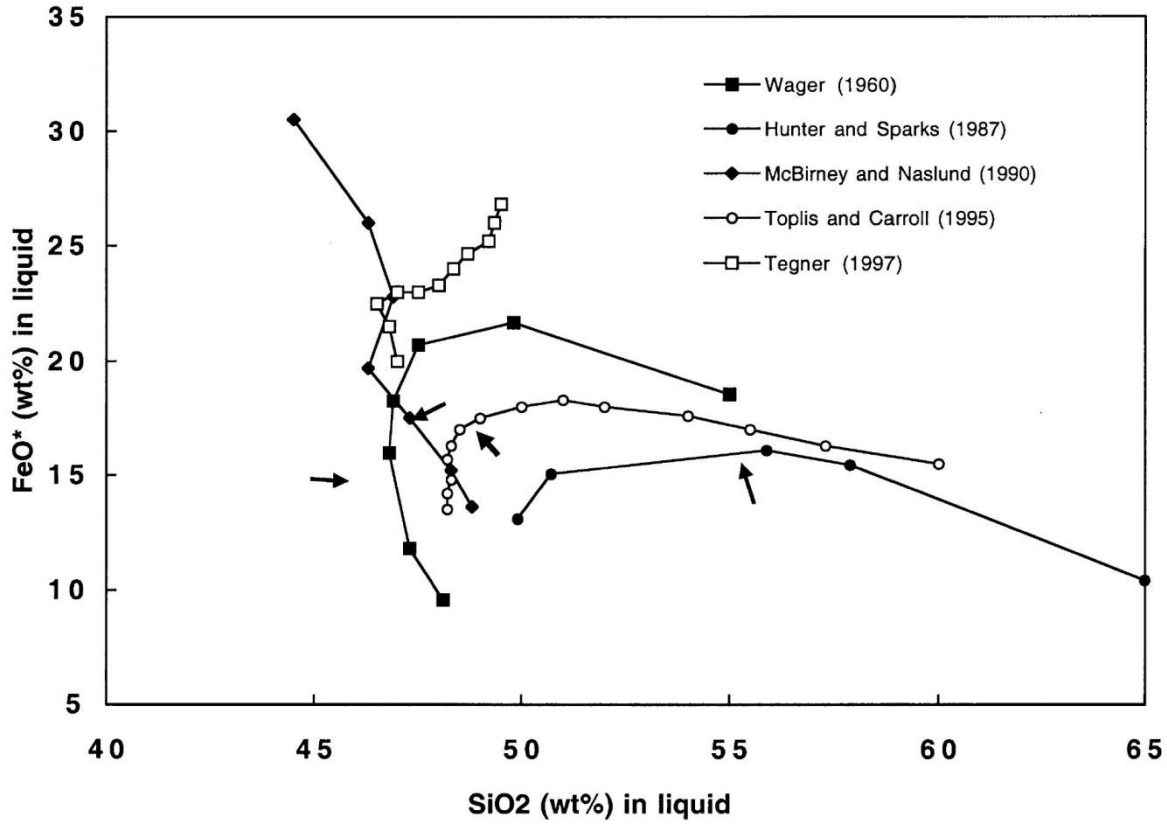

Figure 2. The five main proposed liquid lines of descent for the Skaergaard Intrusion, Greenland. Note the relatively similar initial trends below 50 wt.% SiO_2. Arrows indicate timing of magnetite crystallisation. From Jang *et al.* (2001).

2. Literature Review

2.1 Background

2.1.1 Bowen vs. Fenner

One of the oldest rivalries in geological history involves the LLD, and was between N.L. Bowen and C.N. Fenner. The argument was concerned with which evolutionary path the LLD would take during the differentiation of a magmatic body. These two introduced the world to the appropriately named Bowen and Fenner trends. Bowen (1928) suggested that the liquid would evolve toward a silica-rich end, and Fenner (1929) believed it would follow a Fe-rich trend.

Bowen's trend originally becomes slightly enriched in iron relative to silica, or not at all, but after the precipitation of Fe-Ti oxides from the melt it becomes enriched in silica with a steady decrease in iron. Bowen hypothesised that if a magmatic body was left to differentiate and crystallise from the bottom up, due to fractional crystallisation and crystal settling, the bottom would be magnesium-rich, then becoming iron-rich and ultimately topped by a silica-rich one. The lack of such a silica-rich layer in the Skaergaard intrusion is explained by Bowen purists to have been erupted and eroded, due to the large difference in density between the silica-rich melt and the lower, heavier ferromagnesian, which would be too heavy to erupt (Bottinga and Weill, 1970; McBirney and Noyes, 1979). The lack of any iron-rich lava is also evidence against the existence of the Fenner-trend in nature, despite the lack of silica-rich lavas present near any iron-enriched intrusions.

Fenner's trend becomes enriched in iron, but continues to become enriched in iron even after the precipitation of Fe-Ti oxides, with stable or slightly decreasing silica content. Fenner's (1929) original works related to the crystallisation of basalt. He too hypothesised that a magmatic body left to differentiate only through fractionation and crystal settling would produce at first a magnesium rich layer at the bottom, due to augite precipitation, followed by a gradual increase in iron moving towards the top. Fenner (1929) predicts that all differentiating magma bodies' liquid will become enriched in iron; it is just a question of to what extent. External processes acting in on a magmatic body during crystallisation will affect the degree to

which iron enrichment can take place (Fenner, 1929). The external processes include the likes of: oxygen fugacity (fo_2), hydrous or anhydrous conditions etc. (Thy *et* al., 2006; Giehl *et al.*, 2012). fo_2 is considered to have the strongest effect (Thy *et al.*, 2006), but the partitioning of Fe_2O_3 into oxides and silicate minerals in turn controls fo_2 in the melt, assuming conditions closed to oxygen (Osborn 1959, 1962; Roeder and Osborn 1966). Fenner (1929) states that if only fractionation and crystal settling were active during differentiation and all of these external processes negated, the iron enrichment trend would always be visible in nature. All these external processes will be assessed later on, but it is clear that because of the vast number of processes acting in on the differentiating liquid, many assumptions must be made in order to construct a LLD. These assumptions will inherently alter the outcome of the LLD.

The topic of this thesis is focussed on extreme iron enrichment, in the range of ≥22 wt.% Fe-Ti oxides, as can be seen in Skaergaard, Bird's River etc. The question of how and why such extreme iron enrichment occurs is the subject of on-going debate. Take Skaergaard as an example; if the magma followed a calc-alkaline trend, or even the standard tholeiitic trend, how is it possible to have such a high quantity of Fe-Ti oxides in the crystallised body? To produce cumulate layers significantly enriched in iron, some degree of iron enrichment must occur in the liquid. Looking at it from a mass balance perspective, it is just not possible to have that much iron in the system, unless the parental magma contained up to 20 wt.% iron. That is highly unlikely and there is no evidence of such a melt ever existing. The iron content must have steadily increased in the liquid due to differentiation, until it was partitioned into titanomagnetite and ilmenite.

2.1.2 Starting Composition

Choosing the starting composition correctly, i.e. the parental magma, is key when doing forward modelling of the LLD. Wager and Brown (1967) chose to sample from the chilled margin of Skaergaard and used this as the parental magma. In this case there was very little contamination of from the host rock, but it should be noted that care needs to be taken when making use of this method, as interaction processes can take place along contacts and may render them heterogeneous

(Snyder *et* al., 1993; Abu El-Ela, 1996). Heterogeneity can result from accumulation of wall rock, provided enough heat is present, or through the accumulation of phenocrysts settling out of the fractionating magma (Snyder *et al.*, 1993). Furthermore, the use of chilled margins as potential parental magma has been strongly cautioned for two reasons: layered intrusions and the sills that are associated with them do not generally form from a single pulse of magma of a homogenous composition; and the magma slowly fills the sills, becoming more primitive over time, thus the chilled margins might reflect the fractionated version of the original parental melt (Latypov *et al.*, 2007).

As previously mentioned there are more than two ways to calculate a LLD, for example: Tegner (1997) made use of the iron content in plagioclase combined with bulk summation of the gabbro compositions in Skaergaard to approximate melt compositions in the Upper Zone. McBirney (1975) and McBirney and Naslund (1990) experimentally determined the LLD by melting Skaergaard gabbros. McBirney and Naslund (1990) also used trapped liquids in cumulates to determine the LLD. Hunter and Sparks (1987) took the Tinden Sill as the final differentiation product and used mass balance. These different methods are all valid, and it should be noted that all of these techniques produced vastly diverse LLDs, albeit two main trends: the Bowen and the Fenner, though some were extreme. It should be noted that almost all of these trends begin with very similar starting compositions, and it is only after the onset of magnetite and ilmenite precipitation, which is during the olivine-pigeonite peritectic reaction, that the LLDs start to vary dramatically (Veksler, 2009). It is therefore quite obvious that the Fe-Ti oxide precipitation is the most important factor when constructing LLDs for iron-enriched igneous bodies (Veksler, 2009). Two techniques that will be focussed on in particular are bulk summation and linear regression using the least squares method.

2.1.3 Bulk Summation

Bulk summation is a very useful technique specially designed for layered igneous bodies. It is based on the principle that the igneous body as a whole is essentially the differentiated product of the parent magma. Thus, it follows that if an average bulk composition of the differentiated body can be calculated, it should equal

the starting composition of the parent magma. It involves taking a number of samples from each defined cumulate layer, weighting each layer according to stratigraphic thickness and volume, and calculating a bulk average for the entire body. It assumes however that each layer is, although different in composition from one layer to the next, certainly more or less homogenous in itself. Jang *et al.* (2001) points out that in Skaergaard, the LLDs produced from summation procedures are affected because of heterogeneity in individual layers. The composition of each layer is the result of a mixture between early formed minerals, precipitated minerals from circulating interstitial liquids and final trapped liquids (Jang *et al.*, 2001).

This method also assumes that no amount of liquid was lost during the cooling history; in fact it assumes no volume was lost whatsoever. If there was any eruption of liquid at any point, particularly the final differentiation product, this method would produce a false starting composition. It also makes assumptions on the size, shape and dimensions of the intrusion. It stands to reason that if the volume of any layer is incorrectly assumed, within a certain margin of error, that the whole final composition might be wrong. The shape and size of igneous bodies are often only assumed, as the lack of outcrop is usually a major obstacle. One of the central focus points of this thesis is to ascertain the extent to which the assumed volume can skew the resultant starting composition, the error range if you will, and to determine what effect the assumed shape of the intrusion can have. Real data will be used along with a number of different thickness, shape and volume alterations to determine this.

One question that should be mentioned at this time is why there is such a large difference between the inferred liquid line of descent and iron contents in the evolved magmas for Kiglapait, Skaergaard and the Bushveld, which were all modelled using the bulk summation method (Tegner and Cawthorn, 2010). In terms of iron enrichment, it is suggested that Kiglapait's liquid evolved up to 23 wt.% total FeO (Morse, 1981) and the Bushveld only 15 wt.% total FeO (Tegner *et al*., 2006). The reason why this is bizarre is because their final stages of differentiation are dominated by the assemblage magnetite, ilmenite, plagioclase (An_{30-50}), clinopyroxene, apatite and olivine and/or orthopyroxene, or inverted pigeonite (Tegner and Cawthorn, 2010). If their differentiation evolution is so similar in terms of

final assemblage, why is it that the iron content in the evolved liquid is so different? It is possible that the chamber conditions were very different for each intrusion, as iron content in the liquid is so heavily influenced by external processes. However, the inferred iron content for Kiglapait and Skaergaard seem very similar.

Tegner and Cawthorn (2010) suggest that the reasons behind why the inferred LLDs are so different need to be re-examined. The Bushveld is such an intricate and complex problem that solving the reason for its relatively low iron content is most probably beyond the scope of this thesis, but will be reviewed none the less. The summation procedure will be assessed, with step by step instructions on its use, its pitfalls and error margins on assumptions. Hopefully a bulk summation method that is less sensitive to assumptions can be produced. This method will be assessed and modelled using the programming language R, and the code will be provided for further use. The programming language R was chosen for its calculation power, its relative ease of use, the fact that it was designed specifically for geochemical modelling, and because it is downloadable on the internet for free. The other technique that will be critically assessed and described is the least squares method.

2.1.4 Least Squares Method

Least squares modelling is a form of linear regression and is used for fitting a line through points on a scattergram (Ragland, 1989). Least squares was designed specifically to find the best-fit line through data points by minimizing the variation on each point. As Ragland (1989) states, the "term least squares is derived from the fact that when the summation of all squared residuals is at a minimum, the line so defined must be the best-fit line". The residuals being the difference between the actual value and its new value determined from the best-fit line (Ragland, 1989). Simply put, the residual is the amount of deviation from its original value to the value assigned by the best-fit. The point of least squares is to find the line that provides the minimum amount of deviation for all data points concerned.

Least squares modelling is not limited to linear lines, but can also be applied to non-linear problems. The strengths of this method is that mineralogical and bulk data can be used, forward and reverse modelling can be done, and the actual

differentiate can be sampled for reverse modelling. For reverse modelling, the method involves choosing the final differentiation product of the magma, usually by sampling at the top of a differentiated body, as it stands to reason that the final portion of the liquid will be found at the top. Again, this assumes that what is sampled is in fact the final liquid portion and that no eruption took place. For forward modelling, the starting composition has to be assumed which can be difficult if no feeder dykes are exposed or the chilled margin contaminated. The downside is that different mineral phases cannot be accounted for, as it can only handle one mineral phase for each mineral present.

2.2 Oxygen Fugacity

Oxygen fugacity is by and large poorly understood, and not well explained in literature. Its use seems somewhat cavalier in a number of cases and merely used because of well-established oxygen fugacity trends. Thus an attempt will be made to shed some light on this topic. Oxygen fugacity is quoted as being a "powerful mechanism for understanding crystallization of igneous and metamorphic rocks under variable pressure, temperature, and melt composition" (Lac, 2009). It is defined by Lac (2009) as fO_2 = γ*PO_2 where γ is the fugacity coefficient and PO_2 is the partial pressure of oxygen. Lindsey *et al.* (1968) defines it as $\mu O_2 = \mu^\circ O_2$ + RT ln fO_2 where "μO_2 is the chemical potential of oxygen, and $\mu^\circ O_2$ is a constant representing the chemical potential of oxygen in some standard state". Lindsey *et al.* (1968) goes on to state that a "chemical potential (and therefore a fugacity) of oxygen can exist in the *absence* of a gas phase". The redox tendency of the system is reflected by both μO_2 and fO_2 which are intensive variables. Lindsley *et al.* (1968) chooses to use fO_2 because of its close relation to partial pressure, but notes that if log fO_2 or μO_2 was chosen instead the diagrams would be qualitatively correct.

Lindsley (1976) declares that because most oxide minerals contain one or more transition metals that can exist in multiple oxidation states, it is critical to control redox conditions during experiments. Furthermore, these conditions can be expressed in several ways, such as Eh, but oxygen fugacity is by and far the most used in high-temperature experiments (Lindsley, 1976). Lindsley (1976) states that for all realistic, practical and theoretical geological application, oxygen fugacity is

numerically equal to the partial pressure of oxygen (PO_2). In some cases protests have emanated from the fact that when numerical values as low as 10^{-25} atm or lower are used the partial pressure of oxygen is physically unrealistic (Lindsley, 1976). It is vital to specify fO_2 at a certain temperature otherwise the meaning is lost (Lindsley, 1976). For example, a fO_2 value of 10^{-15} atm is intensely oxidizing at 500°C for the majority of minerals, but is strongly reducing at 1000°C (Lindsley, 1976). Pure atmospheric air comprises an oxygen fugacity of 0.21 atm ($fO_2 \approx PO_2 = 0.21$ atm), which is virtually never attained in geological settings (Lindsley, 1976).

2.2.1 Defining Oxygen Fugacity

That being said, Lindsley (1976) simply described it as the partial pressure of oxygen, therefore oxygen fugacity of the atmosphere at 1 atm would be 0.21 atm. This is simply related to the oxygen content of the atmosphere which is 21% of the total composition. But in a geological environment it can be much more byzantine. Geologists can define the redox state of a certain reaction in terms of oxygen activity (aO_2). Take the oxidation of fayalite as an example:

$$3Fe_2SiO_4 + O_2 = 2Fe_3O_4 + 3SiO_2 \quad (1)$$

$$K = \frac{(\mathbf{a}SiO_2)^3(\mathbf{a}Fe_3O_4)^2}{(\mathbf{a}Fe_2SiO_4)^3\mathbf{a}O_2} = \frac{1}{(X_{Fe}^2)^3\mathbf{a}O_2} \quad (2)$$

How is aO_2 defined?

Gibbs' free energy (G) of a gas as a function of pressure can be calculated at a constant temperature and integrated to get the formula:

$$\mathbf{G}(P) - \mathbf{G}(P_0) = \int_{P0}^{P} V\,dP \quad (3)$$

Which is applied to an ideal gas to get:

$$\boldsymbol{G}(P) - \boldsymbol{G}(P_0) = \int_{P_0}^{P} V\,dP = nRT \int_{P_0}^{P} \frac{1}{P} dP \quad (4)$$

and

$$\boldsymbol{G}(P) = \boldsymbol{G}(P_0) + nRT \ln \left(\frac{P}{P_0}\right) \quad (5)$$

This then lead to activity

$$\mu = \mu_i^0 + RT \ln(\boldsymbol{a}_i) \quad (6)$$

where $\boldsymbol{a}_i = \frac{P_i}{P_i^0}$ (7)

and P_i^0 is the reference state (pure gas at 1 bar)

But the gas that geologists deal with is not ideal so it cannot be evaluated by the integral $\int_{P_0}^{P} V\,dP$, therefore the term fugacity was invented to solve this problem. It is defined as:

$$\boldsymbol{G}(P) = \boldsymbol{G}(P_0) + nRT \ln \left(\frac{f}{f_0}\right) \quad (8)$$

Fugacity is similar to corrected pressure:

$$f_i = \gamma_i P_i \quad (9)$$

It has units of pressure and equals the partial pressure in the limit of ideal gas behaviour. The activity of a component *i* in a mixture is simply:

$$\boldsymbol{A}_i = \left(\frac{f_i}{f_i^0}\right) \quad (10)$$

where f_i^0 is the fugacity of *I* at a reference state (taken to be pure *I* at 1 bar). Activity only has meaning relative to a standard state while fugacity has an absolute meaning. If a standard state of 1 bar is used, fugacity and activity is equal.

Oxygen barometers and geothermometers can be used from igneous and metamorphic rocks that contain coexisting solid solution minerals, such as hematite (Fe_2O_3) and ilmenite ($FeTiO_3$); as well as magnetite (Fe_3O_4) and ulvospinel (Fe_2TiO_3). From solid solutions such as these, the aO_2 and T can be determined. Consider the reaction:

$$4Fe_3O_4 + O_2 = 6Fe_2O_3 \quad (11)$$

$$K = \frac{((\gamma Fe_3O_4\, X_{Fe2O3}^{Hm})^2)^6}{} \quad (12)$$

$(aO_2)(\gamma Fe_3O_4\ X_{Fe3O4}^{Mt})^4$

2.2.2 Oxygen Fugacity in Experiments

When conducting experiments on oxide minerals it is necessary to control oxygen fugacity. This can be done in two ways, namely using mixtures of reactive gases or solid-solid oxygen buffers (Lindsley, 1976). Reactive gas mixture takes an oxidizing gas and mixes it with a reducing gas (CO_2 or H_2O mixed with CO or H_2), simultaneously passing it through a furnace in the vicinity of the oxide mineral (Lindsley, 1976). These gases react to produce a new range of gases, one of them being oxygen (Lindsley, 1976). The mixing ratio of the gases and the furnace temperature controls the amount of oxygen produced, thus the oxygen fugacity (Lindsley, 1976). The more regularly used method is that of oxygen buffering. This method involves using solid phases that contain transition elements, i.e. elements that can exist in nature as two different oxidation states, such as the Fayalite + Magnetite + Quartz (FMQ) assemblage where iron exists as both Fe^{3+} and Fe^{2+}. Which phase to use also depends on the phase rule, consequently the number of solids must equal the number of chemical components (Lindsley, 1976). In other words, the number of solid phases must equal the smallest number of chemical entities necessary to describe all the phases in the system (Lindsley, 1976). Looking at the FMQ buffer, the minimum number of chemical components to describe the whole assemblage is three, Fe-O-SiO_2. If Gibbs' Phase Rule is applied to these buffers it is found that the variance is two, and because the two degrees of freedom are temperature and pressure all other intensive variables are fixed (Lindsley, 1976). These other intensive variables include the likes of oxygen fugacity. A review of oxygen buffer methods is given by Huebner (1971).

The majority of fO_2 is examined by the above mentioned mineral equilibria (Lac, 2009). These mineral equilibria provide the basis to calculate thermodynamic equilibrium reactions from, and they can be written so as to associate O_2 gas concentration with the chemical potential (Gibbs free energy at one molar) (Lac, 2009). Here are four commonly used mineral reactions that are associated with iron oxidation and reduction (Lac, 2009):

$2Fe° + SiO_2 + O_2 \Rightarrow Fe_2SiO_4$ QIF (13)

Iron Quartz Fayalite

$3Fe_2SiO_4 + O_2 \Rightarrow 2Fe_3O_4 + 3SiO_2$ FMQ (14)

Fayalite Magnetite Quartz

$4Fe_3O_4 + O_2 \Rightarrow 6Fe_2O_3$ MH (15)

Magnetite Hematite

$2Ni_{(s)} + O_2 \Rightarrow 2NiO$ NNO (16)

Nickel Nickel Oxide

The reactions symbolise a continuously oxidizing system from reaction (13) to (15) and are explained as follows. Reaction (13) is the reaction of pure Fe with quartz and oxygen and produces the iron-rich end-member of olivine, namely fayalite. Natural iron converts to the divalent ion Fe^{2+} and is incorporated into fayalite. This reaction is commonly referred to as the IQF (Iron + Quartz + Fayalite) buffer. Once more oxygen is introduced into the system, thus fayalite will decompose into magnetite and quartz (reaction 14), where iron is oxidated further and is present as both Fe^{2+} and Fe^{3+}. Both these oxidative states of iron are of course present in magnetite and this reaction is commonly known as the FMQ (Fayalite + Magnetite + Quartz) buffer.

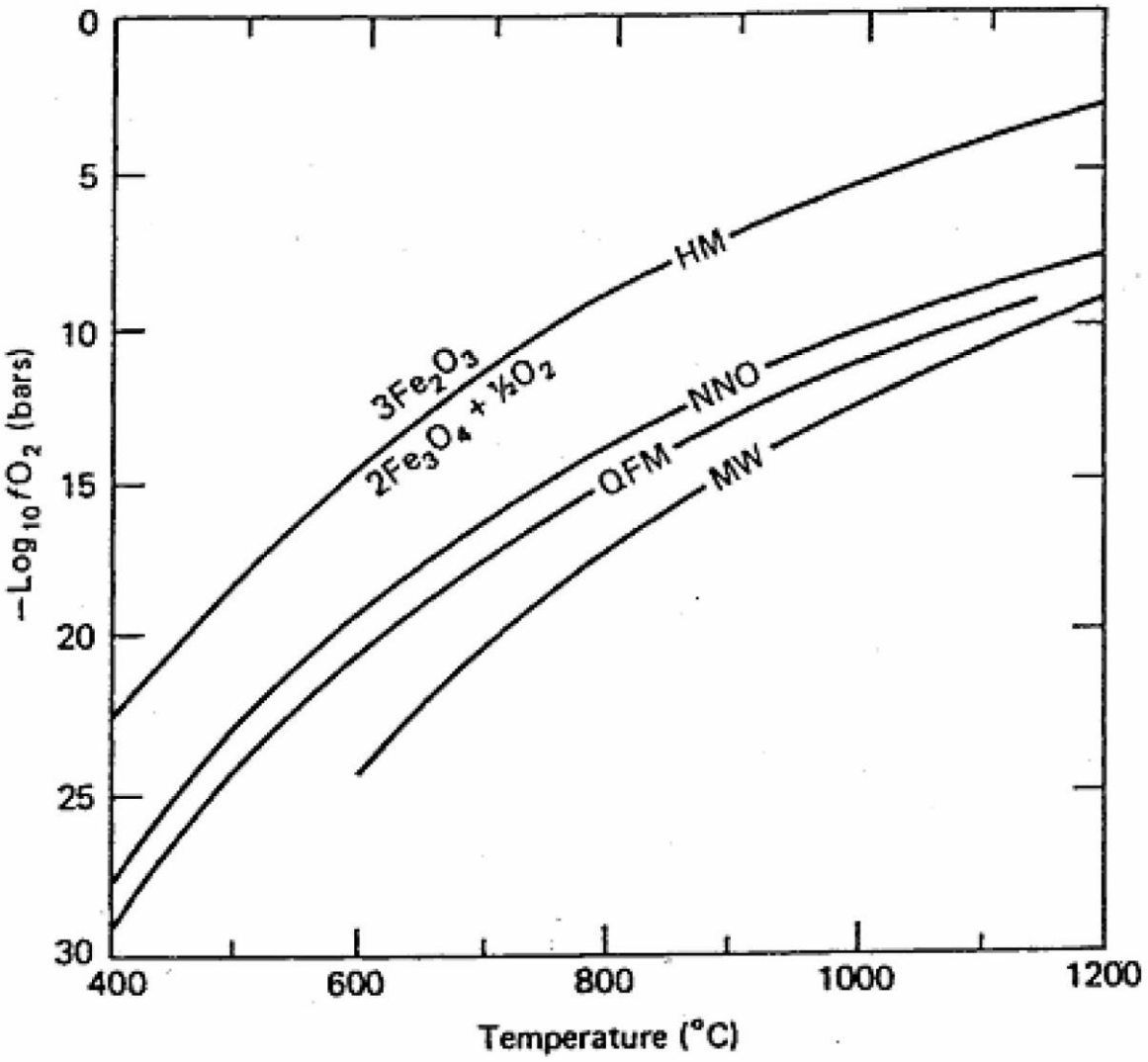

Figure 3. LogfO_2 plotted against temperature indicating the stabilities of the various oxidative states of iron in the system Fe-Si-O. From Philpotts (1990).

Further increase of oxygen leads to all Fe^{2+} being converted to Fe^{3+}, as shown by reaction (15), and hematite will crystallise at the expense of magnetite. Reaction (15) is abbreviated as the MH (Magnetite + Hematite) buffer. These three reactions are known as oxygen buffers. It is assumed that only pure mineral phases exist within these reactions. They are termed this because oxygen controls the mineral equilibria at constant temperature and pressure. Reaction (16) is also a common oxygen buffer, known as the NNO (Nickel + Nickel oxide) buffer, and is a nickel oxide buffer which is not related with iron in any way. It lies between the MH and FMQ buffer, as shown in Figure 3 (Philpotts, 1990).

Assuming the above mentioned phases exist as pure phases at a given temperature and pressure, values for oxygen fugacity can be determined from the equilibrium reactions (13-16) (Lac, 2009). The fO_2 values are calculated on the basis of the following equations:

$$\Delta G^*_{(P,T)} = \Delta G^\circ_{(P,T)} + RT\ln(K_{eq}) = 0 \quad (17)$$

$$RT\ln(K_{eq}) = -\Delta G^\circ_{(P,T)} \quad (18)$$

$$\ln(K_{eq}) = -\Delta G^\circ_{(P,T)}/RT \quad (19)$$

$\Delta G^\circ_{(P,T)}$ is the standard value for Gibb's free energy. R is the gas constant (8.314472 $J \cdot K^{-1} \cdot mol^{-1}$) and K_{eq} is the equilibrium constant (Lac, 2009). Focussing specifically on the QIF buffer K_{eq} can be written as:

$$K_{eq} = (a_{fayalite}) / [(a_{iron})^2 (a_{quartz})] \quad (20)$$

where a_i = the activity component of i. If the phases fayalite, iron and quartz are present as pure solid phases, then their activities will all be equal to one (Lac, 2009).

$$K_{eq} = (a_{O2})^{-1} = (fO_2 / f^\circ O_2)^{-1} \quad (21)$$

$$\ln(fO_2) = \Delta G^\circ_{(P,T)}/RT \quad (22)$$

$$\Rightarrow \log(fO_2) = \Delta G^\circ_{(P,T)}/2.303RT \quad (23)$$

In this instance fO_2 = oxygen fugacity at pressure (P) and temperature (T). $f^\circ O_2$= oxygen fugacity at the standard state of 1 bar and T of interest (i.e. fO_2 = 1). The 2.303 preceding RT in equation (23) is the value used to convert natural logarithms (ln) to logarithm (log) on base 10). Equation (23) displays that the log of fO_2 can be solved for as function of temperature, but once again only if pure phases are present and if $\Delta G^\circ_{(P,T)}$ is known. Activities in equation (20) have to be attuned to calculate the K_{eq} (Frost, 1991).

Considering the QIF, FMQ and MH buffers, when solving for fO_2 using equation (7), it is possible to calculate the iron equilibrium phase boundaries for pure solid phases (as can be seen in Figure 1). Figure 1 depicts these equilibrium phase boundary curves of iron as a function of temperature and fO_2. In this scenario iron oxidation is reflected by the upward trend of the curve toward higher temperature and fO_2 (Lac, 2009). In other words, the higher the temperature and fO_2 the more oxidised iron will become. This of course leads to iron species becoming increasingly concentrated as Fe^{3+} rather than Fe^{2+}, and is reflected in the change of mineralisation in reactions (13-15).

An empirical formula relating Gibbs free energy to fO_2 was experimentally derived and used to relay Fe^{3+}/Fe^{2+} ratios in the melt, fO_2, temperature and composition of the melt by Sack *et al.* (1980), Kilinc *et al.* (1983) and Kress and Carmicheal (1988, 1989, 1991). These experiments were conducted over an extensive range of crystalline free melt compositions at 1 bar (Lac, 2009). These equations (24a and 24b), describe the oxidation of iron in silicate melts and are given below:

$$2FeO_{(melt)} + 0.5O_2 = Fe_2O_{3(melt)} \quad (24a)$$

$$\text{or } FeO_{(melt)} + ¼O_2 = FeO_{1.5(melt)} \quad (24b)$$

Thermodynamic equilibrium for equation (12a and 12b) is determined by equation (25):

$$\Delta G^*_{(1,T)} = 0 = \Delta H^\circ_{(1,T)} - T\Delta S^\circ_{(1,T)} + RT\ln(K_{eq}) \quad (25)$$

where $\Delta G^\circ_{(1,T)} = \Delta H^\circ_{(1,T)} - T\Delta S^\circ_{(1,T)}$

$\Delta H^\circ_{(1,T)}$ equals the change in enthalpy, and $\Delta S^\circ_{(1,T)}$ the change in entropy. In this instance the equilibrium constant (K_{eq}) relates to activities of the products and reactants of the reaction:

$$K_{eq} = (a_{Fe2O3}) / [(a_{FeO})^2(fO_2)^{0.5}] \quad (26)$$

where a_{Fe2O3} and a_{FeO} are present as liquid phases.

Combining equation (25) and (26) the following equation is made:

$$\ln(X_{Fe2O3} / X_{FeO}^2) = ½\ln fO_2 - \Delta H^\circ_{(1,T)} / RT + \Delta S^\circ_{(1,T)} / R \quad (27)$$

where X is the mole fraction of component *i*.

But an upgrade on equation (27) was made, one that better fit observed values of fO_2 (Kress and Carmichael, 1988, 1990, 1991).

$$\ln(X_{Fe2O3} / X_{FeO}) = a \ln fO_2 + b/T + c + \Sigma d_i X_i \quad (28)$$

where a,b,c and d_i are experimentally calibrated constants and *i* refers to melt oxide components (Sack *et al.*, 1980; Kilinc *et al.,* 1983; Kress and Carmichael, 1991). Equation (15) very accurately predicts fO_2 in anhydrous melts to within 0.5 units (Sack *et al.*, 1980; Kilinc *et al.,* 1983; Kress and Carmichael, 1991). This is very agreeable, except for the fact that in nature melts contain volatiles.

2.2.3 Effect of Volatiles on Oxygen Fugacity

Volatiles can sometimes have a colossal effect on the viscosity, cation diffusion, electrical conductivity, eruptive potential, crystallisation temperature etc. in a melt. Lac (2009) mentions that volatile content can even affect the Fe^{3+}/Fe^{2+} ratio. Burnham (1975) and Mysen *et al.* (1980) state that when H_2O enters a silicate melt, presumably through an external source of water, it will react with bridging oxygen (O^{2-}) to form two OH^- groups for each oxygen bond. Non-bridging oxygen (NBO) reacts with water to form T-OH bonds and M(OH) or $M(OH)_2$ complexes, where T represents the tetrahedral site and can be anything from $Si^{4+} > Al^{3+} \geq Fe^{3+}$ (Mysen *et al.* 1980).

The redox ability of iron was appraised by Dickenson and Hess (1981, 1986) by means of altering melt compositions at constant T, P and fO_2. Their results indicated that Al^{3+} and Fe^{3+} work toward charge balance by acting as network forming cations in the tetrahedral site with monovalent and divalent network

modifiers. They found that water will be accepted into the silicate melt until equilibrium is reached. Low water contents (< 3 wt.%) in the melt lead to a rapid increase in the amount of water that reacts with O^{2-} to form hydroxyl groups, i.e. low water content equals higher water activity (Lac, 2009). Anything higher than that and the ratio between OH^- and H_2O decreases (Stolper, 1982). Reaching a water content of 4 wt.% in the melt the ratio is more or less equal, thus more molecular water is dissolved into the melt than hydroxyl groups (Stolper, 1982).

Assuming fixed water content, the proportion of dissolved water as hydroxyl groups will increase with an increase in temperature (Stolper, 1982). Moore *et al.* (1995) believes that the redox state of iron in silicate melts is not affected by the dissolution of water, concluding this after experimenting on the Fe^{3+}/Fe^{2+} ratios in hydrous and anhydrous liquids at known T, P and fO_2 and finding the ratios to be identical. Baker and Rutherford (1996) disagree with this conclusion and found that the Fe^{3+}/Fe^{2+} ratio does increase with increased water content. This argument has gone on for many years and is still undecided. What is clear is that in experiments it is not only one variable controlling the Fe^{3+}/Fe^{2+} ratio, but many. In the grand scheme of things oxygen fugacity is still the supreme factor governing the oxidation state of iron in silicate melts (Botcharnikov *et al.*, 2005). However, the activity of water does control the redox state of the melt and thus exerts a profound influence on oxygen fugacity and the crystallisation of oxide minerals (Botcharnikov *et al.*, 2005).

The combination of fO_2 and H_2O has a strong influence on the path the liquid line of descent takes. When fO_2 and H_2O are present in low concentrations, i.e. a reducing and dry melt, the evolutionary path is toward iron enrichment, decreasing SiO_2 and increased alkalinity index (≤ 3.55; Giehl *et al.*, 2012). The reverse is very foreseeable in that a wet and oxidized melt will produce low iron contents, high SiO_2 and constant alkalinity index (Giehl *et al.*, 2012). The condition of the latter suppresses olivine crystallisation and drives that of magnetite and clinopyroxene with less or no alkalis and nepheline (Giehl *et al.,* 2012). These results were determined experimentally at ~5 wt.% H_2O and fO_2 between ~ΔlogFMQ -3 to +1 and were applied to a peralkaline phonolitic melt. Direct comparisons between the

experimental work conducted by Giehl *et al.* (2012) and the focus of this thesis should not be made as this thesis focuses on tholeiitic magmas. But the overwhelming evidence for iron enrichment in wet melts has to be mentioned and will most probably apply to tholeiitic melts as well.

2.3 Alternative Analytical Methods

2.3.1 Trace Elements

A problem with examining crystallised bodies of magma is that is all the melt has crystallised. This leaves no portion of residual melt or "final product" to analyse directly and determine the evolutionary trend from. There is also no parent magma as it has undergone differentiation. The LLD provides estimates of the major element composition of the parent and residual melt, without having direct access to these stages in the magma bodies' evolution. In order to construct a LLD, however, a number of assumptions have to be made. Inconsistencies between authors' LLDs, for the same magma body, sneak in because of all these assumptions. In many cases authors use the same data but tweak the assumptions, which lead to a LLD evolving toward a silica-rich end instead of an iron-rich end. These assumptions are inherent to the method chosen for calculating the bulk composition of the differentiated body. As the body is no longer similar in composition to the parent magma, a method must be used to calculate its average bulk composition.

To properly assess the evolution and history of an iron-enriched igneous body many tools are available and should be used. The first of those should always be petrography. The use of trace elements has long been a major tool igneous petrology, specifically for determining magma source, contamination, magma mixing, new injections, the number of injections etc. Trace element contents of coexisting mafic minerals can also be used to assist with determining the timing or stratigraphic height of magnetite crystallisation (Jang *et al.,* 2001). Oxide minerals, specifically magnetite, control the content of V in an evolving magma (Jang *et al.*, 2001). The partition coefficient for V (D_V) is > 25 in magnetite, but is low or insignificant for silicate phases (Dostal *et al.*, 1983; Rollinson, 1993). V is present in large quantities in Skaergaard's oxides, with magnetite containing up to 1.74 wt.% V_2O_5 (Vincent and

Phillips, 1954; Naslund, 1980). This advocates that the presence of plentiful magnetite would intensely deplete the evolving magma and coexisting minerals in V (Jang *et al.*, 2001).

In other intrusions, for example the Basistoppen sill, the liquid line of descent indicates that after magnetite appears on the liquidus the V content in pyroxene declines sharply from 443 ppm to 10 ppm (Naslund, 1989). Another example a bit closer to home is the Bushveld Complex, where the V content is more or less constant throughout early pyroxenes, but undergoes a sharp decline with the first appearance of magnetite on the liquidus (Atkins, 1969).

The V content in Skaergaard, measured in pyroxene, does not decline significantly until the end of the MZ (Jang *et al*., 2001). It stays relatively constant throughout the LZ and does therefore not decrease at the first appearance of magnetite, as expected. This implies that either the magma responsible for magnetite precipitation ponded on the floor of the chamber, as previously mentioned, or it percolated down through the crystal mush into the LZ (Jang *et al.*, 2001). If iron enrichment took place as high up as the MZ, then such a liquid would be denser than the surrounding silicates and could percolate down due to gravitational forces. If it percolated down into the LZ, it would precipitate a phase that does not appear on the liquidus at that level (Jang *et al*., 2001). The LZc therefore represents the level where the Fe-Ti oxides reached saturation in the liquid, or this was as far as the denser iron-rich interstitial liquid could percolate down through the crystal mush from the MZ (Jang *et al.*, 2001). Irrespective of the process, the constant amount of V throughout the LZ and MZ would appear to indicate that the crystallisation of magnetite did not have a profound effect on the evolution of the main magma reservoir (Jang *et al.*, 2001). Thus, the concentration of V is clearly a potentially very good tool in testing how high into the stratigraphy Fe-Ti oxides were carried in the evolving liquid, and at which point they crystallised. The amount of crystallisation at that height is a very important factor though.

2.3.2 Oxygen Fugacity in Plagioclase

Because of the high compatibility of Fe^{3+} with feldspar, the use of plagioclase as an oxygen barometer by measuring Fe content is a potentially important one (Sugawara, 2001). Experimental work done by Sato (1989) on the partitioning of iron between plagioclase and liquid in iron-rich basalts at various oxygen fugacities, suggests that the partition coefficient of iron (total iron as FeO) increases with an increase in oxygen fugacity (Sugawara, 2001). Fe^{3+} partitions into plagioclase about 20 times more readily than Fe^{2+}, with respective partition coefficients of 0.2-0.9 and 0.01-0.05 (Phinney, 1992; Lundgaard and Tegner, 2004). The Fe^{3+}/Fe_{total} ratio in plagioclase increases with increasing anorthite (An) content (Hofmeister and Rossman, 1984). This is presumably due to the fact that anorthite ($CaAl_2Si_2O_8$) has more Al^{3+} (2 moles) than albite ($NaAlSi_3O_8$) (1 mole). Fe^{3+} exists in plagioclase as a trace element, substituting for Al^{3+} (Smith, 1974). Therefore anorthite is able to house more Fe^{3+} simply because it contains more Al^{3+} that can be substituted for. Both oxidation states of Fe substitute for Al in the tetrahedral T site with Fe^{2+} also substituting for Ca in the interstitial M site (Smith and Brown, 1987).

Partitioning is also influenced by the polymerisation of the liquid (Tegner and Cawthorn, 2010). The effect is such that partitioning of both oxidation states of Fe into plagioclase is increased with an increase of SiO_2 into the liquid (Lundgaard and Tegner, 2004). Another possibility is that partitioning is influenced by the availability of M and T sites for substitution (Tegner, 1997). There is an increase in Si and Na over Al and Ca with a decrease in An content, which leads to a decrease in available sites (Tegner and Cawthorn, 2010). This applies if compositional and f_{O2} effects are excluded.

Erupted plagioclase contains a higher amount of iron than plagioclase in layered intrusions, which leads to the idea that partition coefficients derived from experiments cannot be applied (Lundgaard and Tegner, 2004). Nonetheless, the iron content in plagioclase can be used as a tool for direct comparison between the iron content of ingeous bodies, as the iron content in plagioclase reflects the original magma composition (Tegner and Cawthorn, 2010). This is supported by the fact that major element diffusion in plagioclase is extremely slow, relative to magmatic

processes, because of the coupled substitution of CaAl-NaSi (Grove *et al*., 1984). Tegner and Cawthorn (2010) further found no evidence to support any re-equilibration or diffusion between plagioclase and mafic phases. It should be noted however, that certain aspects of iron partitioning between plagioclase and the liquid is still uncertain, especially temperature and compositional dependencies (Sugawara, 2001).

Recently, Lac (2009) conducted an experiment on the possibility of determining the oxygen fugacity of the melt based on Fe^{3+}/Fe_{Total} in plagioclase. Volcanic rocks preserve the magma chamber conditions during the time of eruption through mineral assemblages and chemical composition (Lac, 2009). Oxygen and water fugacity and pressure and temperature are but some of the common characteristics embedded within these rocks (Lac, 2009). Although there are no known volcanic equivalents to the layered series for Skaergaard, Kiglapait or the Bushveld, this approach remains a conceivably valuable tool.

These characteristics can also be determined through thermodynamic phase relationship calculations (Lac, 2009). Ideally, crystal-free melts are used to determine Fe^{3+}/Fe^{2+} ratios as a way of ascertaining the oxygen fugacity (Lac, 2009). Crystal-free melts are ideal because the possibility of sampling a phase which is not in equilibrium with the melt is eliminated. Mineral assemblages that do in fact coexist with the melt can of course be used, but a risk is taken by sampling these minerals as they may in fact be earlier formed phenocrysts. It is consequently not worth the risk if it can be avoided. Oxygen concentration is mirrored by the Fe^{3+}/Fe^{2+} ratio and can possibly be used to ascertain fO_2 (Sack *et al.*, 1980; Kilinc *et al.*, 1983; Kress and Carmichael, 1988, 1991). The Fe^{3+}/Fe^{2+} ratio in plagioclase can record fO_2 in the melt (Clowe *et al.*, 1988; Phinney, 1992; Redhammer *et al.,* 1993; Tegner, 1997; King *et al.*, 2000; Sugawara, 2001). This ratio is directly proportional to that of the melt (Longhi *et al.,* 1976; Phinney, 1992; Tegner, 1997; Sugawara, 2000, 2001; Lundgaard and Tegner, 2004).

An empirical formula relating Fe^{3+}/Fe^{2+} to fO_2 is derived in Kress and Carmichael (2001). Fe-Ti oxide barometry is commonly used to estimate the fO_2 of oxide minerals during the time of their crystallisation (Lac, 2009). As previously

stated, Fe^{3+} is substituted more readily than Fe^{2+} during proliferated oxidizing conditions (fO_2 increase) and the extent to which this occurs can be surveyed by the iron partition coefficient (wt.% Fe_2O_3/FeO in plagioclase / wt.% Fe_2O_3/FeO in melt) (Phinney, 1992). Lac (2009) seeks to devise a method of determining fO_2 using Fe^{3+}/Fe^{2+} in plagioclase and other mineral phases, so as not to rely on Fe-Ti oxide barometry. Lac (2009) chose to use volcanic rocks, as they represent the melt just prior to eruption, and are therefore devoid of the effect of high temperature diffusion of ions (Clowe *et al.,* 1988). The study made use of "quantitative analysis of plagioclase phenocrysts by using synchrotron-generated high-energy X-rays" and the micro-beam Fe-XANES (X-Ray Absorption Near-Edge Structure; Delaney *et al.*, 1998; Dyar *et al.*, 2001; Wilke *et al.*, 2001) method of analysis of Fe^{3+}/Fe_{Total} ratio in plagioclase" (Lac, 2009). This method is preferentially used to determine the oxidative state of Fe over wet chemistry, Mössbauer spectroscopy, optical spectroscopy or electron paramagnetic resonance (EPR) because it provides in situ analysis at a spot size as small as 10x15 µm in size (Dyar *et al.*, 2001; Tegner *et al.*, 2003). For a complete discussion on the technique and subsequent errors refer to Delaney *et al.* (1998).

The Fe-XANES method of analysing iron in plagioclase as a potential monitor of oxygen fugacity in the melt produces results 1 – 4 times more oxidized than results from Fe-Ti oxide barometry (Lac, 2009). Plagioclase grows and records oxygen conditions in the melt for a much longer time than the oxides and is therefore supposedly a better monitor of oxygen fugacity in magma. It stands to reason that the difference in residency time can therefore result in this difference (Lac, 2009). The difference in timing of crystallisation between plagioclase and Fe-Ti oxides will also produce dissimilar results for fO_2. The Fe-XANES method produces large error margins, so the technique is not recommended until adjustments are made (Lac, 2009).

2.3.3 Plagioclase as a Potential Monitor

Plagioclase as a potential monitor of iron enrichment can be used in much the same way as V in pyroxene. This is a relatively new concept, even though Tegner (1997) and McBirney (1998) already made use of the idea to construct a LLD using

the Fe content in plagioclase. Despite the small amounts of Fe in plagioclase, the value of understanding Fe partitioning between the liquid and plagioclase is vital because of plagioclase's abundance in igneous rocks (Sugawara, 2001). As previously mentioned, there is a large discrepancy between the estimated iron values for the evolved differentiated liquid in Kiglapait, Skaergaard and the Bushveld. When comparing igneous bodies, or any geological formation, it is important to try and find a direct comparison. The study undertaken by Tegner and Cawthorn (2010) aimed to do just that, by comparing the iron content of plagioclase from the Bushveld and Skaergaard. They found that a nicely correlated relationship exists between the Fe content in plagioclase and the anorthite content. The opposite is true for Skaergaard, where a weak negative correlation exists. Tegner and Cawthorn (2010) concluded that this is due to inherent differences in the starting liquid composition of the two igneous bodies, despite the similarities in final crystallisation products. However, many authors defer to its potential for an alternative method of analysing igneous rocks.

Tegner (1997) studied Fe in plagioclase in the Skaergaard intrusion and found an inverse correlation between FeO and An content. This is believed to reflect that An content is dependent on fractionation processes rather than fO_2 (Lac, 2009). Lundgaard and Tegner (2004) perused iron oxide interaction between plagioclase and liquid, as a function of melt and plagioclase compositions, temperature and oxygen fugacity, by calculating the partition coefficients of Fe_2O_3 and FeO as a function of An content. They applied Sugawara's (2000, 2001) thermodynamic algorithm to 420 published experiments on basalts ranging in composition from tholeiitic to alkaline liquids For liquids with less than 52 wt.% SiO_2 the relationship between An content and the partition coefficients for Fe_2O_3 in tholeiite and Fe-Ti tholeiite liquids is clear (Lac, 2009). Within these liquids it is apparent that there is a negative correlation between the partition coefficient of Fe^{3+} into plagioclase and the An-content, therefore the amount of Fe^{3+} will decrease with an increase in An-content (Lundgaard and Tegner, 2004) (Fig. 4).

In calc-alkaline liquids there is an increase in the partition coefficient of Fe_2O_3 in plagioclase with a decrease in An-content, but there is no systematic variation in

the alkaline liquid (Fig. 4) (Lundgaard and Tegner, 2004). No systematic variation between the partition coefficient of FeO in plagioclase and An-content exists in any of the liquid compositions (Fig. 4). The fact that there is limited correlation between the partition coefficient of Fe_2O_3 in plagioclase and An-content and no correlation between the partition coefficient of FeO in plagioclase and An-content is strong evidence that plagioclase composition is not a first-order factor in the control of Fe_2O_3 partitioning into plagioclase (Lundgaard and Tegner, 2004). There is no positive correlation between the amount of Al^{3+} and Fe_2O_3 in plagioclase because partitioning of Fe_2O_3 and FeO is independent of fO_2 and plagioclase composition (Lundgaard and Tegner, 2004). Lundgaard and Tegner (2004) state that it is especially clear that there is no correlation between the partition coefficients of Fe_2O_3 and FeO and fO_2 (Fig. 4) (Lundgaard and Tegner, 2004). A relationship may exist between the partition coefficients of both Fe_2O_3 and FeO in plagioclase and temperature, but this cannot be discerned as such a strong positive correlation between An-content and temperature exists (Lundgaard and Tegner, 2004). The distribution of the partition coefficients relative to fO_2 rather reflects the proportions of Fe_2O_3 and FeO in the magma as opposed to changes in the partition coefficients (Lundgaard and Tegner, 2004).

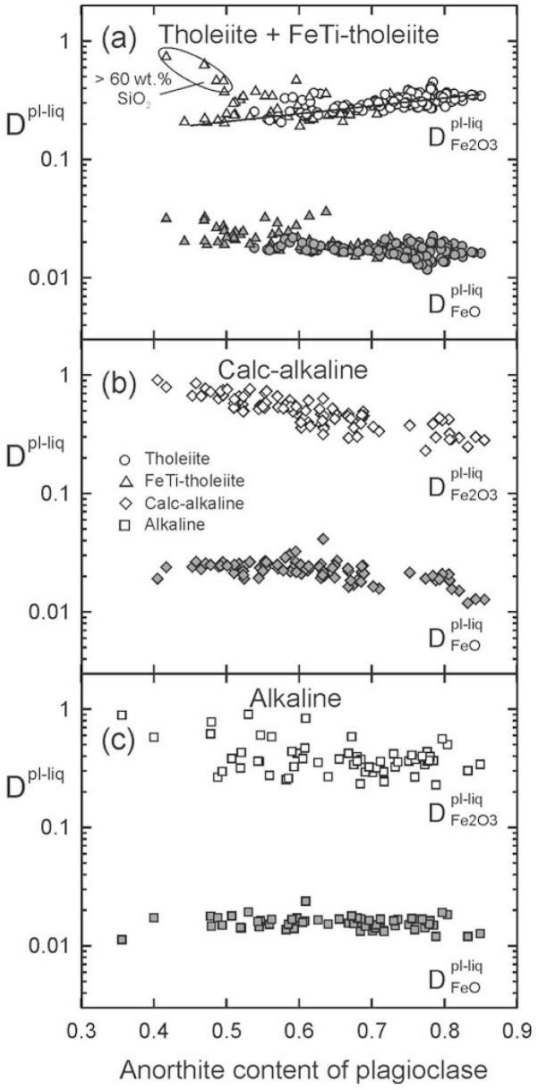

Figure 4. Calculated partition coefficients for Fe_2O_3 and FeO between plagioclase and liquid as a function of anorthite content in plagioclase for (a) tholeiite and FeTi-tholeiite, (b) calc-alkaline and (c) alkaline liquid compositions. Anorthite content is the atomic ratio Ca/(Ca + Na + K). From Lundgaard and Tegner (2004).

There is, however, a positive correlation between the SiO_2 content of magma and the partition coefficients of Fe_2O_3 and FeO (Lundgaard and Tegner, 2004). The activity of iron increases with an increasingly polymerised magma rich in SiO_2 (Lundgaard and Tegner, 2004).

The polymerisation was tested by comparing the partition coefficients for both Fe_2O_3 and FeO with non-bridging oxygens per tetrahedral (NBO/T) for all four liquid compositions (tholeiite, Fe-Ti tholeiite, calc-alkaline and alkaline). The values for NBO/T vary from 0 to 4, 0 represents a fully polymerised melt and 4 a fully

depolymerised melt that consists entirely of isolated tetrahedra (Lundgaard and Tegner, 2004). There is a visible correlation for the partition coefficients of Fe_2O_3 and FeO in plagioclase with NBO/T, where the partition coefficients increase as NBO/T decreases (Lundgaard and Tegner, 2004). This implies a first-order correlation with the melt composition, especially with SiO_2 (Lundgaard and Tegner, 2004). This dependence of elements' partitioning on melt composition extends to trace elements as well (Lundgaard and Tegner, 2004). According to Ewart and Griffin (1994) the partition coefficients of trace elements increased with increasing polymerisation of the liquid (decreasing NBO/T). They determined partition coefficients for trace elements in feldspars, pyroxenes, hornblende, biotite, olivine and Fe-Ti oxides. They assumed these minerals to be in equilibrium with the 32 sampled volcanic rocks ranging in composition from leucitic and picritic basalts to high-silica and per-alkaline rhyolites.

Based on their findings Ewart and Griffin (1994) concluded that melt polymerisation, and therefore composition of the melt, controls element partitioning. This view is shared by others (e.g. Mysen and Virgo, 1980; Kohn and Schofield, 1994 and Toplis and Corgne, 2002). The structure of the melt exerts a strong control on the activity of iron in the liquid, thus also on iron partitioning into plagioclase (Lundgaard and Tegner, 2004).

Because of this and the relations between the partition coefficients of Fe_2O_3 and FeO and the An-content in tholeiitic basalts (< 52 wt.% SiO_2) the iron content and Fe^{3+} / ΣFe of the parental liquid can be calculated (Lundgaard and Tegner, 2004). If FeO_{total} and Fe^{3+} / ΣFe is known for plagioclase the Fe^{3+} / ΣFe and FeO_{total} for the equilibrium magma can be projected using the partition coefficients of Fe_2O_3 and FeO in plagioclase. It is important not to use partition coefficients that display a weak correlation with An-content as large error margins of the projected value will occur, such as the coefficient for FeO (Fig. 4). Lundgaard and Tegner (2004) recommend that the exchange coefficient of K_D should be used instead because it provides a better correlation with An-content. From Beattie *et al.* (1993) the following definition of K_D is given:

$$K_D^{pl\text{-}liq}\ (Fe_2O_3FeO) = \frac{(\text{wt \% } Fe_2O_3 \text{ / wt \% FeO})^{pl}}{(\text{wt.\% } Fe_2O_3/\text{wt \% FeO})^{liq}}$$

$$= \frac{D^{pl\text{-}liq}\ (Fe_2O_3)}{D^{pl\text{-}liq}(FeO)} \qquad (28)$$

where $D^{pl\text{-}liq}$ (Fe_2O_3) is the partition coefficient of Fe_2O_3 in plagioclase from the liquid, and $D^{pl\text{-}liq}$ (FeO) for FeO

$$\ln(K_D^{pl\text{-}liq}(Fe_2O_3/FeO) = 1.262 + 2.185 \cdot An (r^2 = 0.75) \qquad (29)$$

(1 standard error = 0.12)

$$\ln(D^{pl\text{-}liq}(Fe_2O_3) = -2.329 + 1.523 \cdot An (r^2 = 0.71) \qquad (30)$$

1 standard error = 0.09)

Fe^{3+} / ΣFe of the magma can be projected by using equations (28) and (29). The oxygen fugacity of the magma can be calculated by using the formula provided by Kress and Carmichael (1991). FeO_{total} for the magma can be calculated from the plagioclase composition by getting $D^{pl\text{-}liq}(Fe_2O_3)$ from equation (30) and $D^{pl\text{-}liq}$(FeO) by inserting K_D and $D^{pl\text{-}liq}(Fe_2O_3)$ into equation (17). Lundgaard and Tegner (2004) proceeded to calculate the oxygen fugacities for the Palisades Sill, Skaergaard intrusion and the Lake County basalt using these techniques, of which the oxygen fugacity calculated for the Lake County basalt was the first ever estimate.

2.4 Liquid immiscibility

Liquid immiscibility was first conceived as a magmatic process in the early 1900s (e.g. Daly, 1914), but was later abandoned and disregarded (e.g. Greig, 1927; Bowen, 1928). Fifty years on the idea stumbled into revival (e.g. Roedder and Weiblen, 1970, 1971; De, 1974; McBirney and Nakamura, 1974; Philpotts, 1976, 1982; Dixon and Rutherford, 1979; Roedder, 1979), only for it to be ignored in the last few decades. Recently it has once again flickered into literature as a potentially powerful way of explaining petrological problems and features, such as those of Skaergaard's liquid evolution (e.g. Jakobsen *et al.*, 2005; Bogaerts and Schmidt, 2006; Schmidt *et al.*, 2006; Veksler *et al.*, 2006; Veksler *et al.,* 2007).

Philpotts (1976, 1982) showed that some ferrobasaltic liquids became unstable and separated into two compositionally distinct liquids, one that has a very low SiO_2 content (<45 wt.%) and high total iron (FeO + Fe_2O_3) (25-30 wt.%); and the other with much higher SiO_2 (55-60 wt.%) but low total iron (5-10 wt.%). It is therefore potentially possible to have both enrichment paths present, not as separate entities, but as two immiscible liquids in the same magma (Veksler *et al.*, 2007). If liquid immiscibility is the major cause for such extreme enrichment, either iron or silica, it needs to take place at around 50-60% crystallisation and temperatures in the region of 1070-1100°C. That is the point in the crystallisation sequence that magnetite is commonly believed to precipitate and the extreme divergence, from a common initial evolutionary path described by so many for the Skaergaard intrusion, takes place (Fig. 1) (Wager and Brown, 1968; Hunter and Sparks, 1987; McBirney and Naslund, 1990; Toplis and Carrol, 1995; Tegner, 1997). At this point of crystallisation it is believed that the Middle Zone of the Layered Series was crystallising, and it is noted by the disappearance of olivine and appearance of pigeonite on the liquidus (Veksler *et al.*, 2007).

Naslund (1983) performed a series of experiments in order to determine the effect of oxygen fugacity on the immiscibility of silicate melts. The fayalite-tridymite and magnetite-tridymite cotectics in the $Na_2O(K_2O)$-FeO-Fe_2O_3-Al_2O_3-SiO_2 system exhibited a broad region of stable liquid immiscibility in terms of fO_2, from 10^{-12} to 0.2. It also shows that liquid following an evolutionary path for both iron- and silica-

rich paths could coexist irrespective of the direction of magnetite-fayalite reaction (Veksler *et al.*, 2007). The other interesting aspect is that at oxidizing conditions and when the melt was in equilibrium with magnetite, the miscibility gap expanded tremendously and coexisting liquid compositions diverged (Veksler *et al.*, 2007). It perceived that magnetite crystallisation could potentially not have as a great an effect on the evolutionary path of melts compared to chemical interactions taking place in the melt (Veksler, *et al.*, 2007). Apparently, the "strong intrinsic non-ideality of ferrobasaltic liquids" could be a superior factor in magmatic evolution, rather than fO_2 or liquidus mineral assemblage compositions (Veksler *et al.*, 2007).

Veksler *et al.* (2007) points out that experimental studies performed on natural rocks all produced ferrobasaltic glasses with total iron well above 26 wt.%, whereas experiments conducted on synthetic glasses produced liquids with total iron content of 18-22 wt.%. Veksler *et al.* (2007) showed that liquid compositions varying from ferrobasaltic to rhyolitic can potentially be produced under identical conditions and with the sort of cumulates expected in the MZ and UZ of Skaergaard. Powerful non-ideality ingrained in inconsistent incompatibility between iron-rich and silica-rich melts could be the foremost cause of divergent liquid evolution (Veksler *et al.*, 2007).

Veksler *et al.* (2007) proposes that immiscibility started much earlier in the crystallisation sequence of Skaergaard. Immiscibility certainly took place in Skaergaard, as is evident by silicic and iron-rich melt inclusions in cumulus apatite in the UZ gabbros (Jakobsen *et al.*, 2005). The initial rocks of the Layered Series, specifically LZa and LZb, are proposed to have formed from conventional fractional crystallisation and lead to a standard tholeiitic trend, characterised by a large amount of cumulus plagioclase on the cotectic (Veksler *et al.*, 2007). At 60 wt.% crystallisation, which relates to LZc, Veksler *et* al. (2007) proposes that liquid immiscibility took place. Continued iron enrichment would be impossible with conventional fractional crystallisation, as the liquid would inevitably become enriched in silica once magnetite begins to crystallise. The separation of liquids, into a silica-rich and iron-rich liquid respectively, can lead to an unmixing and gravitational separation of the two liquids, assuming immiscibility started early enough in the crystallisation sequence. This unmixing and gravitational separation can be the

catalyst for continued iron enrichment in the denser liquid, regardless of the crystallisation of Fe-Ti oxides (Veksler *et al.*, 2007). Such liquid immiscibility is most likely in large, slow cooling basaltic magmas, where there is enough time for gravitational settling, Ostwald ripening or emulsion coarsening (Veksler *et al.*, 2007).

Veksler (2009) showed that iron enrichment in differentiating tholeiites is heavily dependent on the concentration of alkalis. For extreme iron enrichment to take place (above 22 wt.% total iron) in equilibrium melts that contain the assemblage olivine + plagioclase + augite + pigeonite there has to be a shortage of alkalis (Veksler, 2009). It was previously thought that immiscible liquids could only form in liquids that exhibit such extreme iron enrichment (19-26 wt.% total iron) before reaching the bimodal (~10-20°C). However, experimental work by Philpotts and Doyle (1983) and more recently by Charlier and Grove (2012) showed that this extreme iron enrichment in the melt is not a prerequisite for immiscibility. In fact, in experiments performed by Charlier and Grove (2012), liquid immiscibility took place along the liquid lines of descent during iron depletion and silica enrichment, after Fe-Ti oxides started crystallising. At the time of unmixing, the two liquids in question (SI and M) contained 60.4 wt.% SiO_2 and 9.8 wt.% FeO_{tot}; and 57.4 wt.% SiO_2 and 15.1 wt.% FeO_{tot} respectively (Fig. 5). Charlier and Grove (2012) found that the formation of immiscible liquids at lower iron content was promoted by the presence of high quantities of phosphorous, alkalis and titanium (Fig. 6).

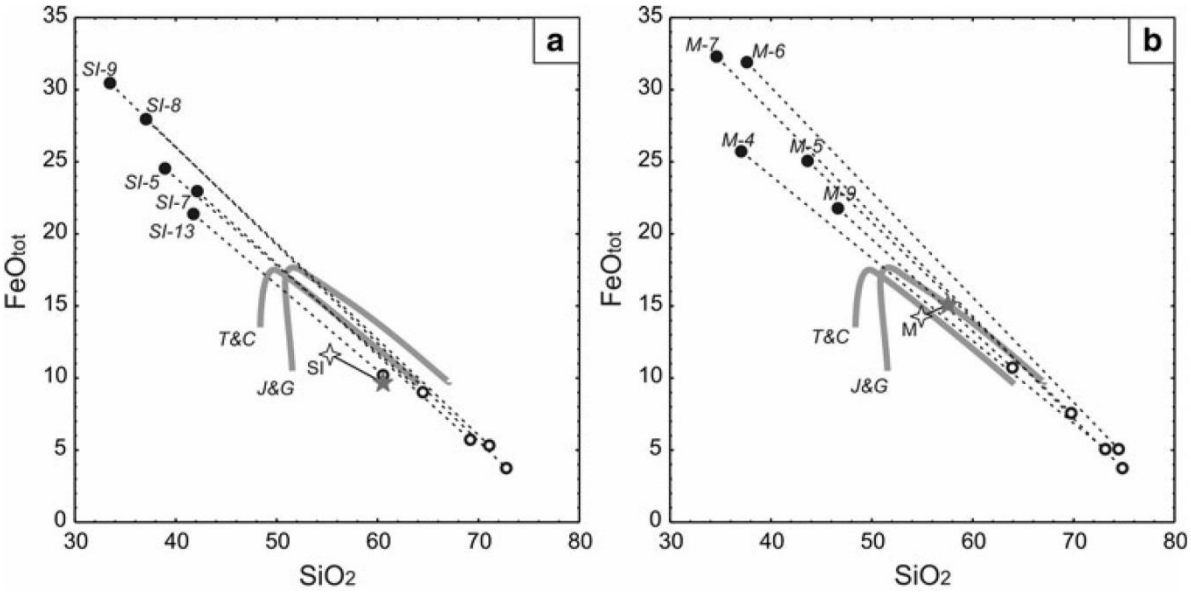

Figure 5. Experimental glasses for starting materials SI and M plotted for FeO_{tot} against SiO_2. Grey lines labelled T&C and J&G represent the liquid lines of descent determined by Toplis and Carrol (1995) and Juster *et al.* (1989), respectively. White stars are starting compositions, grey stars are homogenous melts, and white circles are Si-rich immiscible melts. Tie lines join immiscible pairs. From Charlier and Grove (2012).

Any variation in bulk composition can drastically affect the onset of immiscibility and the size of the two-liquid field, as shown in Figure 7. The two resultant immiscible liquids are also heavily influenced by the liquid composition prior to unmixing (Charlier and Grove, 2012). Homogeneous melt composition at the moment immiscibility occurs, along the liquid line of descent, defines the width of the solvus. Liquids that encounter significant silica enrichment (SI-3), or iron enrichment (M-2), prior to reaching the bimodal, will easily unmix and produce two immiscible liquids that vary greatly in composition (Fig. 8) (Charlier and Grove, 2012). Any composition of liquid will unmix if it plots on the mixing trend, and the amounts can be determined using the lever rule (Charlier and Grove, 2012).

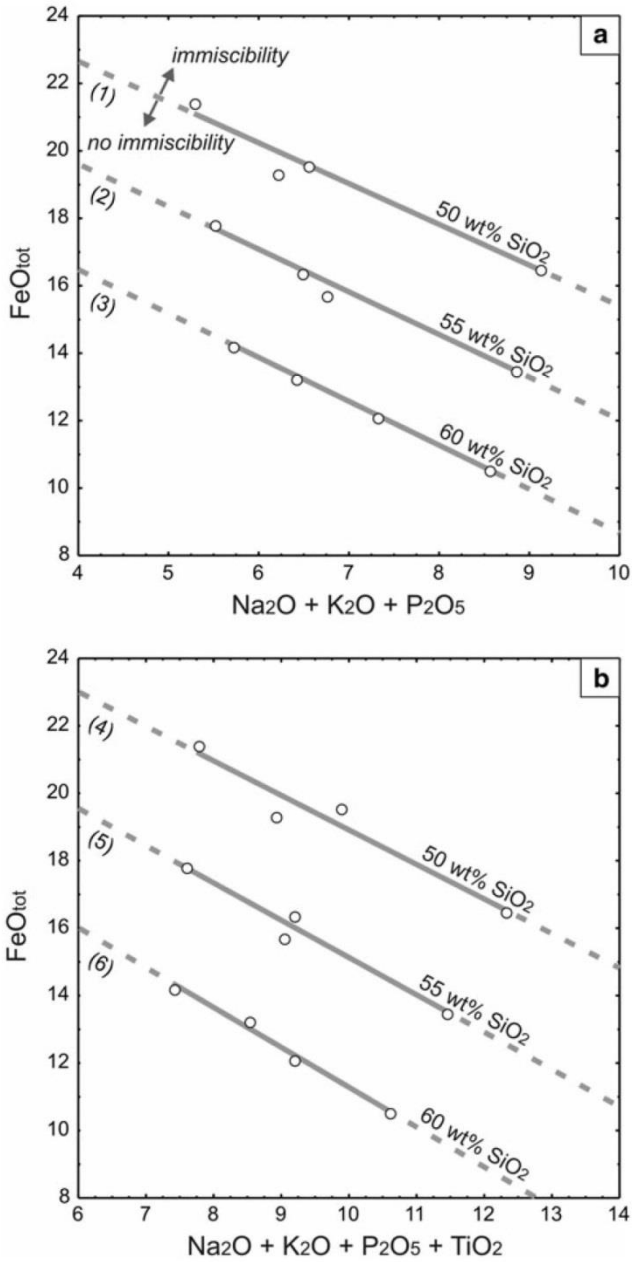

Figure 6. Compositional requirements for silicate liquids to become immiscible along tholeiitic liquid lines of descent. If a liquid of a given SiO_2 content plots above the associated grey line (linear trend of the respective composition) it will become immiscible. (a) FeO_{tot} versus $Na_2O+K_2O+P_2O_5$ (wt.%) and (b) FeO_{tot} versus $Na_2O+K_2O+P_2O_5 \pm TiO_2$ (wt.%) Dashed grey lines represent extrapolated experimental data (reader is referred to Charlier and Grove (2012)). White circles represent immiscible pairs SI-13, M-9, I-3 and S-6 which were proportionally mixed in order to obtain liquid compositions of 50, 55 and 60 wt.% SiO_2. From Charlier and Grove (2012).

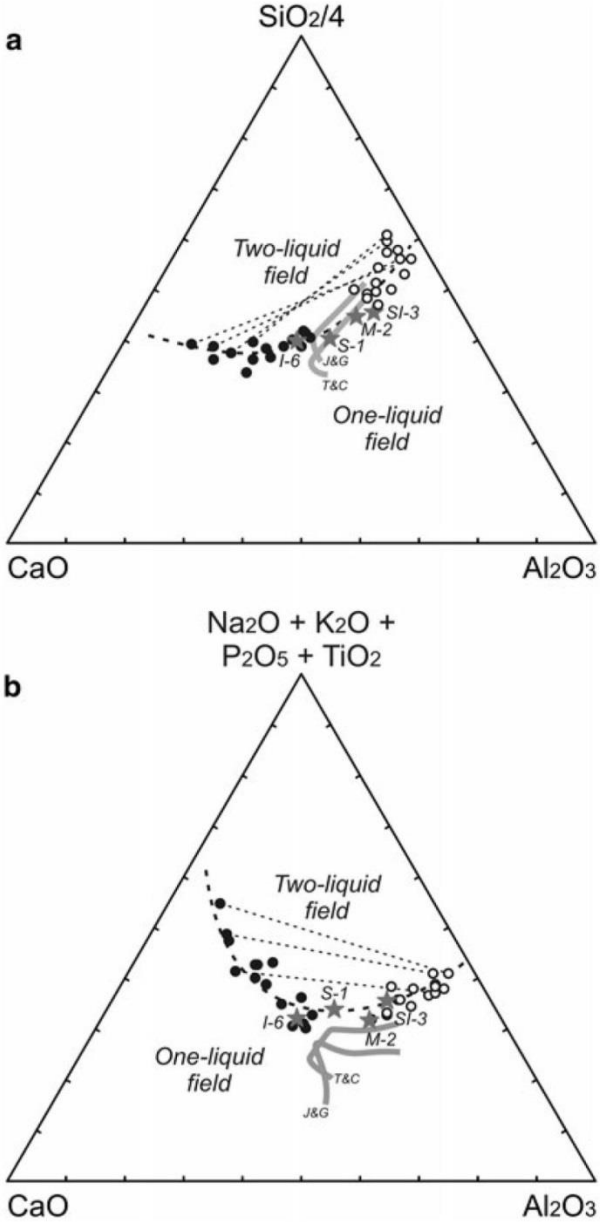

Figure 7. Two ternary diagrams, (a) CaO, Al_2O_3 and $SiO_2/4$; and (b) CaO, Al_2O_3 and $Na_2O+K_2O+P_2O_5+TiO_2$. Experimental glasses plotted onto these in order to show the large influence of variations in bulk composition on the size and width of the immiscible field between the two resultant liquids. Grey lines labelled T&C and J&G represent the liquid lines of descent determined by Toplis and Carrol (1995) and Juster *et al.* (1989), respectively. Grey stars are homogenous melts prior to unmixing (SI-3, M-2, S-1 and I-6). Black circles are Fe-rich immiscible melts, and white circles are Si-rich melts. Tie lines join immiscible pairs. From Charlier and Grove (2012).

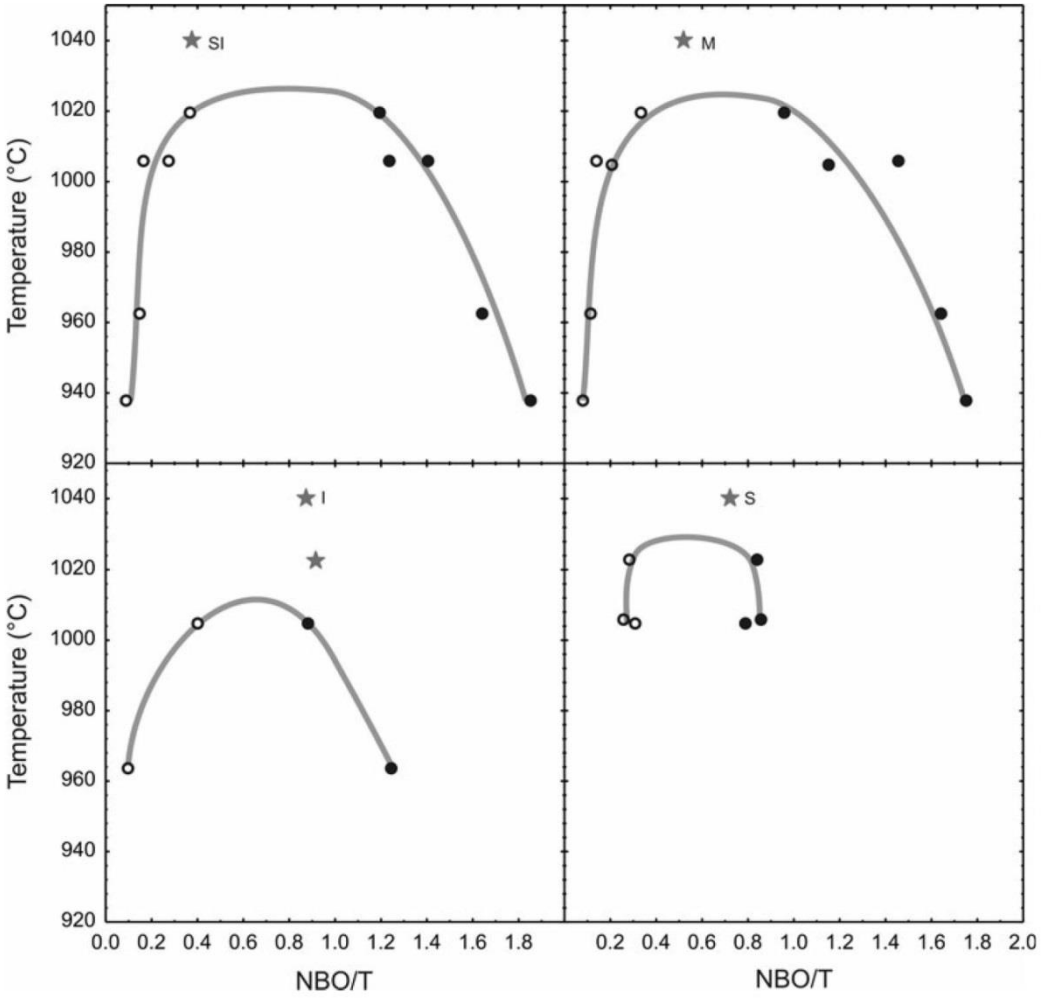

Figure 8. Experimental melts plotted against temperature and degree of polymerization (NBO/T). NBO/T calculated assuming T=Si+A+P+Ti. Grey stars are homogenous melts, black circles are Fe-rich immiscible melts, and white circles are Si-rich, immiscible melts. From Charlier and Grove (2012).

3. Birds River Case Study

3.1 Geological history

The Birds River Gabbro Complex is a small intrusion (~13.5 by 6 km) found in the Eastern Cape Province, approximately 20 km west-south-west of Dordrecht, South Africa (Eales and Booth, 1974). It was emplaced into Stormberg Group sediments during the later stages of Karoo volcanism and seemingly precedes the main stage of flood basalt eruption that occurred in the area (Eales and Booth, 1974). What makes this particular intrusion interesting, is the fact that it contains highly fractionated rocks, some of which have become enriched in iron, described as intersertal tholeiites. These iron-enriched rocks are similar in composition to the likewise enriched New Amalfi dolerites and the melanogranophyres of Skaergaard (Eales and Booth, 1974).

Du Toit (1920) proclaimed that Birds River intruded as an upwelling of magma along an oval-shaped fracture in plan view, thus isolating the central sediments. The roof of the Stormberg sediments was uplifted during gabbroic magma emplacement and later collapsed (Eales and Booth, 1974). The collapse not only triggered the creation of large xenoliths, but served as a mechanism to bring the residual fractions, which were formed from partial fractionation, from deep within the intrusion to a much shallower position (Eales and Booth, 1974; Eales and Robey, 1976). The largest of these xenoliths, the Smuts Pass fragment, is 12 km^2 and more or less rectangular (Eales and Booth, 1974). It is surrounded by intrusive rocks and has adopted the shape of a basin due to its sides being dragged up during settling (Eales and Booth, 1974). Original work done on the intrusion by Du Toit (1920) determined the overall “bell-jar” shape of the intrusion. Later authors agreed with this perception, but disagree that it has vertical contacts on all sides. Instead they propose that the eastern and south-eastern walls of the intrusion gave way and produced a sill-like sheet that dips toward the west (Eales and Booth, 1974). Most of the work done on Birds River was focused on the reaction between Karoo dolerite and the Cave Sandstone xenoliths.

3.2 Stratigraphy

The Birds River complex bounds the Stormberg Group sediments, most notably the underlying fossil-rich Molteno Formation, which is overlain by the Red Bed Formation and that in turn is capped by the Cave Sandstones with associated volcanic breccias. A section along A-B in Figure 9 and 10 is given to illustrate the relative orientation of these sedimentary stratigraphies to the intrusive complex. The Molteno Formation is only represented here by its most upper part and exhibits the normal assemblage of coarse grits, finer cross-bedded sandstones and fossiliferous shales (Eales and Booth, 1974). In contrast the Red Beds Formation is exposed in its entirety, all 440m of it. Its distinguishing red colouration is well exposed at Rooiberg, but in other areas it has undergone metamorphism and changed to a more khaki colour, which makes differentiating it with Molteno Formation problematic (Eales and Booth, 1974). It should be noted that chemical analyses of these Red Beds show that Fe_2O_3 content is less than 2.5 % (Eales and Booth, 1974). The Cave Sandstones are only found as xenoliths, small outliers on higher ground and along the north-eastern rim of the complex, where they barely obtain a thickness of 85 m (Eales and Booth, 1974). There is strong evidence in the form of massive volcanic breccia for erratic explosive volcanics prior to flood basalt eruption (Eales and Booth, 1974). Having said this, there is a small amount of igneous material within these breccias, as determined by chip sampling (Eales and Booth, 1974).

There is no strata underlying the Stormberg that is represented in these volcanic breccias (Eales and Booth, 1974). In that regard the volcanism is very similar to many late-Karoo diatremes that contain sedimentary breccia fillings, as noted by Du Toit (1905). The ostensible thickness of these breccias borders on 120 m (Eales and Booth, 1974). The presence of little or no volcanic material seems to indicate that most of these sedimentary breccias are material ejected from the walls of vents, thus very little volcanic eruptions that produced lava flows were active during Molteno times (Eales and Booth, 1974).

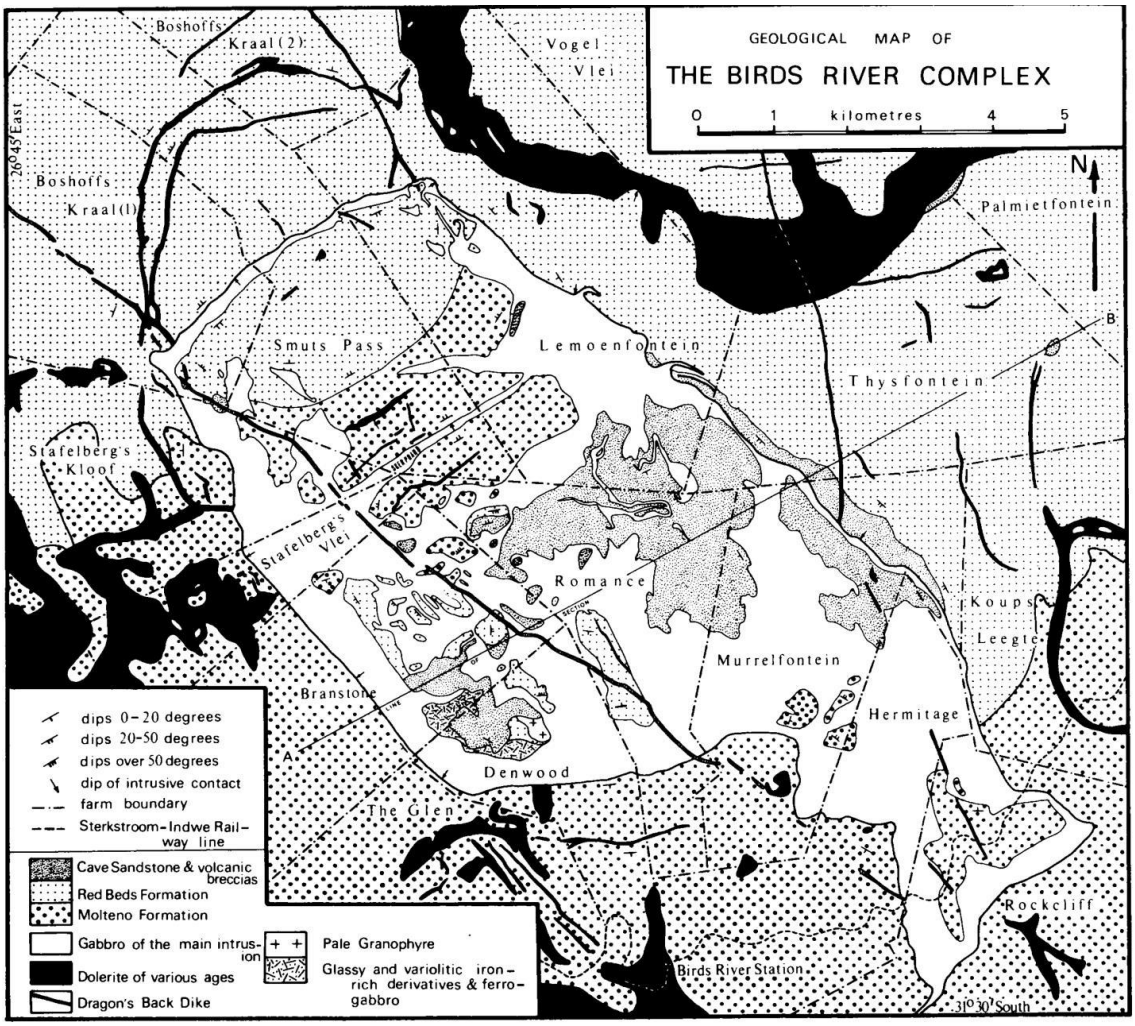

Figure 9. Geological map of the Birds River Gabbro Complex. From Eales and Booth (1974).

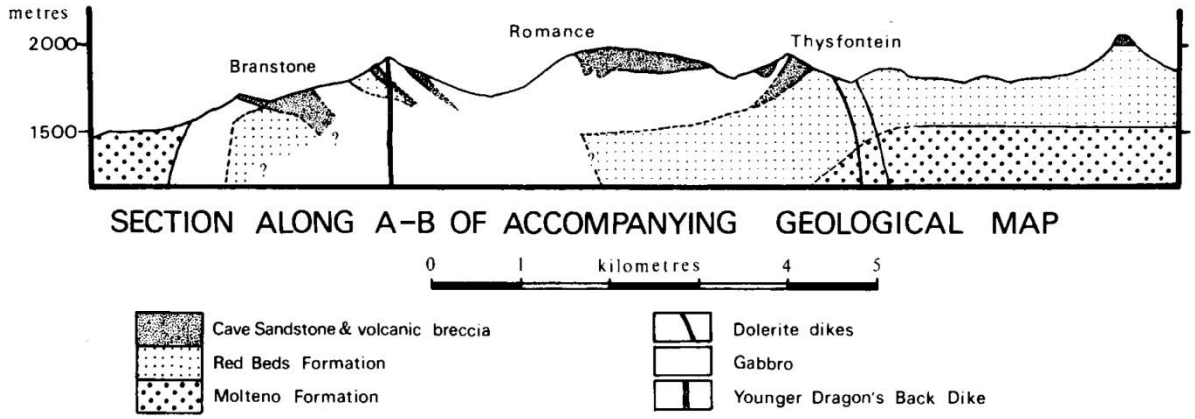

Figure 10. Cross section of the Birds River Gabbro Complex. From Eales and Booth (1974).

Exposed igneous rocks of the Birds River complex show weak rhythmic layering, as identified by Eales and Booth (1974). In the south-east there is visible olivine enrichment near the base of the intrusion, which coincides with the lowest mafic index of all exposed gabbros (Eales and Booth, 1974). Analysis of major elements indicates this portion of gabbros is predominantly calc-alkaline in nature or at least the most calc-alkaline rich gabbro in the whole complex. Compositionally speaking the gabbro from Denwood is a geochemically good match with the characteristics of the Southern Basalt Province (South Africa, Lesotho and Swaziland; Eales and Booth, 1974). A coarse, poikilophitic olivine-rich gabbro or dolerite is the principal rock type for the complex (Eales and Booth, 1974). This rock shows two distinctive features, firstly it is rich in plagioclase (up to 60 % by volume) and secondly amphiboles and biotites are completely absent (Eales and Booth, 1974). This last feature makes it very dissimilar to most Karoo dolerites (Eales and Booth, 1974). It contains up to three pyroxenes, namely dominant augite, subordinate pigeonite and minor orthopyroxene (Eales and Booth, 1974). Electron microprobe analysis of augite shows that distinct marginal enrichment in Fe^{2+} took place, from $Ca_{40}Mg_{47}Fe_{12}$ to $Ca_{36}Mg_{42}Fe_{22}$, however olivine grains display a wide range of Fe contents, thus showing no clear cut compositional zoning (Eales and Booth, 1974).

3.4 Iron-rich Tholeiites

3.4.1 Geological Setting

The main area of interest is of course the ferrogabbros and iron-enriched tholeiites. As can be seen in Figure 11, the portion of the complex containing most of the outcrop of ferrogabbros is found between the farms Denwood and Branstone. The contact between the intrusion itself and the Molteno Formation is a very steeply dipping one, as “bell-jar” intrusions tend to be. From the edge of the complex moving north the exposed rock type is gabbro. North of the gabbros lay the medium-grained ferrogabbros which contain strewn blobs of microcrystalline mesostasis (Eales and Booth, 1974). The ferrogabbros are best exposed in two places (Figure 11), firstly at *POINT A* where there is a steeply dipping contour (the 5600 contour) cutting into the ferrogabbros, providing a suitable place from which to view the exposure in a near

vertical traverse. Secondly, at *POINT B*, and this is the best exposure for this rock type, is the deep kloof running parallel to the north western border of the Denwood farm, i.e. the boundary between Denwood and Branstone. The kloof has a river running through it and some very fresh and clean exposure can be found here.

Two large juts of ferrogabbro are on either side of the kloof, providing good vertical exposure. According to field observation done by Eales and Booth (1974), the gabbros seem to be older than, and on occasion cut into, the ferrogabbros. Fine to glassy black tholeiites, that contain large laths of feldspar and prisms of pyroxene and olivine, alternate with the gabbros (Eales and Booth, 1974). These tholeiites share a chemical similarity with the highly fractionated rocks found at New Amalfi, and are texturally interpreted to have frozen rapidly or formed from a highly viscous melt (Poldervaart, 1944; Eales and Booth, 1974).

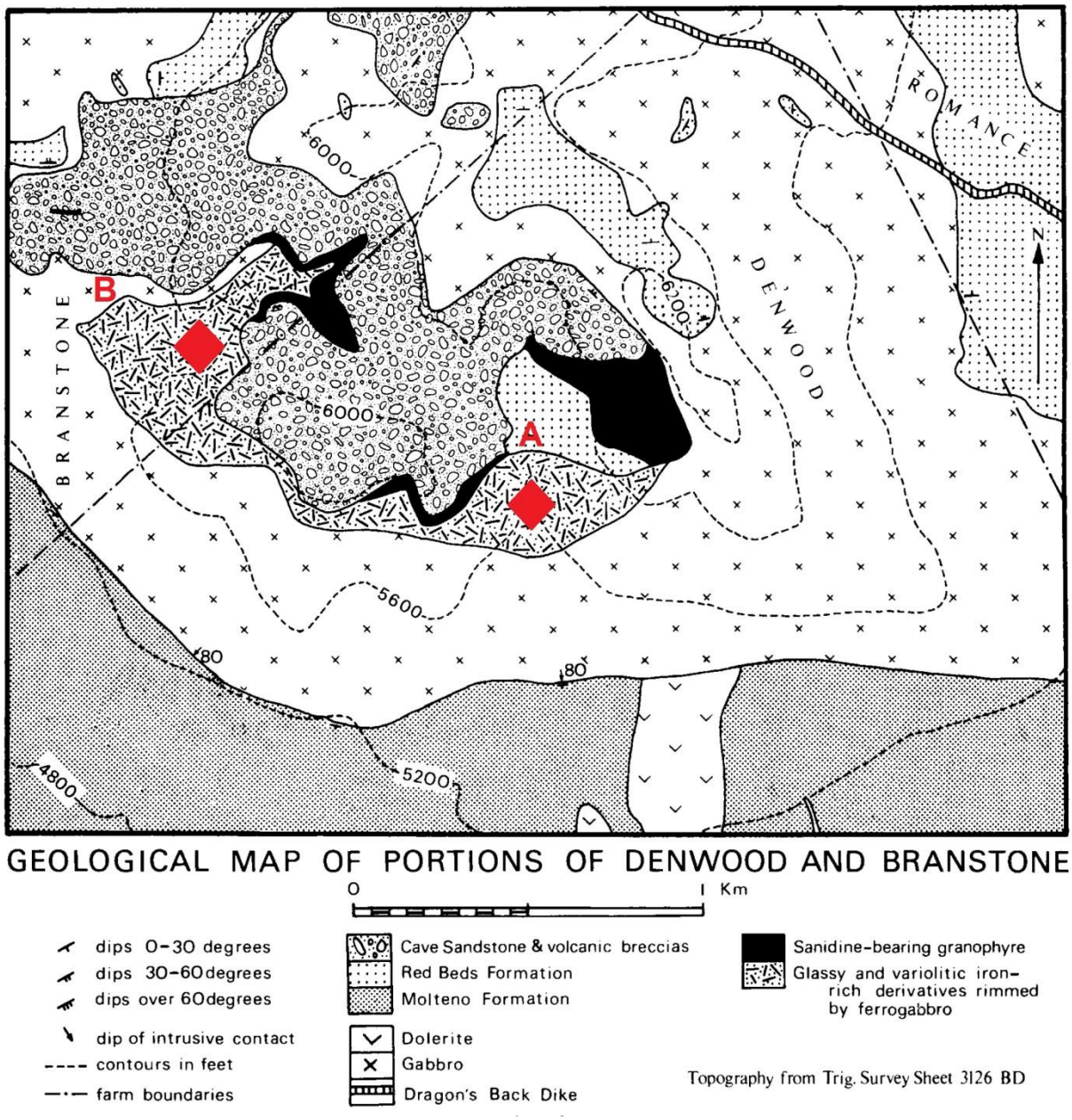

Figure 11. A geological map showing the distribution of ferrogabbro-tholeiites on the portions of Denwood and Branstone. Modified from Eales and Booth (1974).

Moving inward from the south-western margin where the ferrogabbro borders the poikilophitic gabbro, the quartz content in the interstitial mesostasis increases (Eales and Booth, 1974). At the same time zonal structures appear in the pyroxene, where the margins change from brown to green (Eales and Booth, 1974). Augite cores from the ferrogabbros show an average composition of $Ca_{34}Mg_{34}Fe_{32}$, whereas the cores from the poikilophitic gabbros show an average composition of $Ca_{38}Mg_{45}Fe_{17}$ (Table 1). That is an appreciably higher iron content. An even more

ferriferous composition is seen by the co-existing ferropigeonite, $Ca_{16}Mg_{28}Fe_{56}$ (Table 1). The latter composition is very distinctive from the trend in Skaergaard and Bushveld Complexes, but similar to the Ca-poor pyroxenes found in the Red Hill Dike (McDougall, 1962; Wager and Brown, 1967). The mesostasis also becomes increasingly populated by iron ores, sodic plagioclase, alkali feldspar and apatite (Eales and Booth, 1974).

Table 1. Electron microprobe analysis of pyroxenes. From Eales and Booth (1974).

Electron Microprobe Analyses of Pyroxenes.

	1	2	3	4	5	6	7	8	9
SiO_2	52,7	52,3	50,2	48,7	48,8	48,1	47,8	47,7	49,1
TiO_2	0,4	0,5	0,8	0,8	0,9	0,9	1,0	1,0	0,5
Al_2O_3	2,7	3,6	1,5	1,2	1,2	1,3	1,3	1,2	1,1
FeO	7,7	13,0	19,3	25,5	26,3	27,1	28,0	29,5	32,4
MnO	0,2	0,5	0,5	0,6	0,6	0,6	0,6	0,6	0,8
MgO	16,5	14,4	11,6	5,3	4,7	3,5	2,8	2,0	9,3
CaO	19,6	17,1	16,2	18,5	18,6	18,8	18,9	18,9	7,5
Na_2O	0,4	0,5	0,3	0,3	0,3	0,3	0,3	0,3	0,2
TOTAL	100,2	101,9	100,4	100,9	101,4	100,5	100,7	101,2	100,9
Number of Ions on Basis of 6 Oxygens (Z = 2)									
Si	1,936	1,924	1,933	1,941	1,940	1,942	1,936	1,937	1,955
Al	,064	,076	,067	,056	,057	,058	,063	,057	,045
Ti	–	–	–	,003	,003	–	,001	,006	–
Al	,052	,080	,001	–	–	,004	–	–	,005
Ti	,011	,028	,023	,021	,024	,027	,029	,024	,017
Fe	,237	,400	,622	,849	,875	,915	,947	1,001	1,079
Mn	,007	,015	,017	,019	,020	,020	,021	,022	,027
Mg	,904	,789	,667	,316	,279	,208	,171	,122	,549
Ca	,770	,674	,670	,790	,794	,812	,824	,823	,319
Na	,027	,036	,020	,021	,021	,023	,022	,025	,007
X + Y	2,01	2,02	2,02	2,02	2,01	2,01	2,01	2,02	2,00
At. % Mg	47,3	42,4	34,0	16,2	14,3	10,7	8,8	6,3	28,2
Fe	12,4	21,5	31,8	43,4	44,9	47,3	48,7	51,4	55,4
Ca	40,3	36,1	34,2	40,4	40,8	42,0	42,4	42,3	16,4

1–2 Core and margin, respectively, of augite oikocrysts in poikilophitic olivine gabbro (No. 1 of Table III).
3 Augite of ferrogabbro (No. 1 of Table V).
4–8 Ferroaugites and ferrohedenbergites of fractionated tholeiites with microcrystalline mesostasis.
9 Ferropigeonite (subcalcic ferroaugite) co-existing with augite of 3 above.

The ferrotholeiites found in Birds River did not crystallise slowly and the melt did not exhibit low viscosity, therefore they are not autochtonous (Eales and Booth, 1974). Furthermore, the expected sequence for such a magma in the upper portion is: gabbro-quartz; gabbro-ferrogabbro-ferrohedenbergite granophyre (Eales and Booth, 1974). Support for this view is given in Table 2, which compares ferrotholeiite-compositions from Birds River to other the rock-type mentioned above.

Table 2. Comparison between Birds River tholeiites and some other late-stage differentiates (wt.%). From Eales and Booth (1974).

	1	2	3	4	5	6	7	8	9
SiO_2	52,2	52,4	54,3	59,3	58,8	62,6	63,2	63,5	63,7
TiO_2	2,4	3,1	2,0	1,4	1,3	0,9	1,1	1,0	1,4
Al_2O_3	13,2	12,2	14,5	11,6	12,0	11,1	10,9	11,3	11,6
Fe_2O_3	4,6	3,5	1,2	5,2	5,8	5,8	7,9	6,5	1,6
FeO	10,1	12,9	11,1	6,3	9,4	3,4	3,8	4,9	8,7
MnO	0,2	0,3	0,2	0,2	0,2	0,2	0,1	0,2	0,2
MgO	3,2	2,6	2,4	1,0	0,7	0,7	0,7	0,7	0,7
CaO	7,7	8,5	8,4	4,6	5,0	3,3	3,4	3,8	4,2
Na_2O	3,0	2,0	2,2	3,3	3,9	3,3	2,8	2,7	2,9
K_2O	1,3	0,9	1,7	2,8	2,3	3,3	2,9	2,7	3,0
P_2O_5	0,4	0,2	0,2	0,4	0,7	0,2	0,6	0,4	0,2
CO_2	n.d	0,1	n.d	0,3	n.d	0,4	n.d	n.d	n.d
H_2O	0,8	1,1	1,8	3,0	0,4	4,3	2,3	2,6	1,6
TOTAL	99,1	99,8	100,0	99,4	100,4	99,5	99,8	100,1	99,8

1. Ferrogabbro with minor interstitial mesostasis, Denwood.
2. Fayalite-quartz dolerite, New Amalfi (Poldevaart, 1944).
3. Quartz dolerite transitional to fayalite granophyre, Red Hill Dike (McDougall, 1962).
4. Porphyritic, microcrystalline Birds River tholeiites.
5. Porphyritic, microcrystalline Birds River tholeiites.
6. Porphyritic, microcrystalline Birds River tholeiites.
7. Granophyre, summit of Red Hill (McDougal, 1962).
8. Granophyre, Gretna, Tasmania (McDougal, 1962).
9. Fayalite-hedenbergite-granophyre, New Amalfi (Poldevaart, 1944).

The composition of the ferrogabbros, tholeiites and some hybrids found in the Denwood Kloof are given in Table 3. It is noted that these rocks contain relatively high values of Fe_{total}, Na_2O and K_2O and SiO_2, but low values of Al_2O_3, CaO and MgO (Eales and Booth, 1974). These rocks are apparently very similar to an iron-enriched dolerite found beneath metasomatic granophyres at New Amalfi (Poldevaart, 1944).

Table 3. Analyses of ferrogabbro, tholeiites and hybrids from Denwood and Branstone (wt.%). From Eales and Booth (1974).

	1	2	3	4	5	6	7	8	9	10
SiO_2	52,2	54,6	54,8	55,7	55,9	59,3	62,6	53,1	61,5	61,7
TiO_2	2,4	2,0	2,1	2,1	2,1	1,4	0,9	2,0	0,8	1,1
Al_2O_3	13,2	11,3	11,2	10,9	10,7	11,6	11,1	11,2	10,7	11,0
Fe_2O_3	4,6	9,8	4,3	4,0	4,3	5,2	5,8	8,7	2,7	4,2
FeO	10,1	6,0	11,0	11,1	10,8	6,3	3,4	6,5	6,9	6,8
MnO	0,2	0,2	0,2	0,2	0,2	0,2	0,2	0,3	0,2	0,2
MgO	3,2	2,3	1,6	1,8	1,5	1,0	0,7	1,7	2,4	0,3
CaO	7,7	5,0	6,0	6,1	5,9	4,6	3,3	6,0	4,6	4,2
Na_2O	3,0	2,8	3,2	2,8	3,2	3,3	3,3	2,8	2,4	2,9
K_2O	1,3	2,2	2,2	2,1	2,3	2,8	3,3	1,9	2,6	3,0
P_2O_5	0,4	0,8	0,7	0,8	0,8	0,4	0,2	0,8	0,1	0,3
CO_2	n.d	0,1	0,1	0,1	0,1	0,3	0,4	2,6	4,0	2,7
H_2O	0,8	2,4	2,2	2,3	2,0	3,0	4,3	1,4	1,4	1,9
TOTAL	99,1	99,5	99,6	100,0	99,8	99,4	99,5	99,0	100,3	100,3
C.I.P.W. NORMS										
q	8,3	20,1	12,0	15,1	13,9	19,7	25,7	22,9	30,1	28,4
or	7,8	12,8	12,8	12,2	13,3	16,7	19,5	11,1	15,6	17,8
ab	25,2	23,6	27,2	23,1	26,7	27,8	27,8	23,6	20,4	24,6
an	18,6	12,0	9,7	11,4	8,3	8,6	5,6	7,8	–	2,2
cor	–	–	–	–	–	–	–	1,7	3,9	2,1
di wo	7,1	2,8	6,0	5,3	6,3	3,9	2,1	–	–	–
di en	3,0	2,4	1,4	1,4	1,5	1,3	1,7	–	–	–
di fs	4,1	–	5,0	4,2	5,2	2,8	0,1	–	–	–
wo	–	–	–	–	–	–	1,2	–	–	–
hy en	5,0	3,4	2,5	3,1	2,2	1,2	0,1	4,3	4,8	0,8
hy fs	7,0	–	8,6	9,8	7,9	2,5	–	2,0	9,5	7,5
il	4,6	3,8	4,0	4,0	4,0	2,7	1,8	3,8	1,5	2,1
mt	6,7	14,1	6,3	5,8	6,5	7,7	8,4	12,5	3,9	6,0
ap	1,0	2,0	1,7	2,0	1,7	1,0	0,3	2,0	0,3	0,7
$CaCO_3$	–	0,2	0,2	0,2	0,2	0,7	0,9	5,9	7,9	6,1
$MgCO_3$	–	–	–	–	–	–	–	–	1,0	–
H_2O	0,8	2,4	2,2	2,3	2,0	3,0	4,3	1,4	1,4	1,9
TOTAL	99,2	99,6	99,6	99,9	99,7	99,6	99,5	99,0	100,3	100,2
Norm. Plag.	An_{41}	An_{32}	An_{25}	An_{32}	An_{23}	An_{23}	An_{16}	An_{24}	An_{00}	An_{08}

1. Ferrogabbro with minor interstitial mesostasis, Denwood.
2-7. Typical tholeiites. (Specimen 2 is partly weathered and Fe_2O_3 value is abnormal). All are taken from Denwood and Branstone.
8. Magnetite-tridymite-feldspar hybrid rock produced by transfusion of sediment at contact with tholeiite, Denwood.
9. Fine granophyre 10 feet beneath Cave Sandstone roof, Branstone.
10. Porphyroblastic metasediment (red beds) at contact with tholeiite, Denwood.

Osborn (1959) shows that strong iron fractionation, with a decrease in SiO_2, occurs due to a drop in oxygen fugacity, assuming the total magma composition stays more or less the same. When fractionation occurs under conditions of constant or increasing oxygen fugacity, it leads to a calc-alkaline trend in the magma (Eales and Booth, 1974). Analysis of the Birds River fractionation trend seems to imply that

fractionation took place under conditions somewhere in-between the calc-alkaline trend and that of Skaergaard, but closer to the latter (Eales and Booth, 1974). Conditions such as these are associated with a slight drop in oxygen fugacity (Eales and Booth, 1974). These conditions are most likely to be met during crystallisation of a hypabyssal intrusion associated with increased water pressure (Eales and Booth, 1974). The increased water pressure limits the drop in oxygen fugacity, but cannot cause it to increase or remain constant (Hamilton and Anderson, 1967). The evolution of these tholeiites is different to the evolution of intrusive Karoo tholeiites described by Poldervaart (1946). Poldervaart (1946) ascribes their evolution to "the distillation of volatiles from contiguous sediments". Contrary to this view, the textural evidence from Birds River supports a much higher viscosity during freezing (Eales and Booth, 1974). In this case structure plays a major role in the chemistry of these rocks (Eales and Booth, 1974). Field observation combined with textural and chemical data supports the theory that these tholeiites intruded as highly fractionated magma along a narrow fracture through oxidized Upper Karoo sediments, early in the history of the complex (Eales and Booth, 1974). The intruded sediments are rich in CO_2, several per cent, and may have assisted oxidation via dissociation, but are more likely to have done this because of their high Fe^{3+} / Fe^{2+} ratio (Eales and Booth, 1974). This being said, their effect is limited, with the major culprit being the controlling magnetite-hematite buffer (Eales and Booth, 1974).

3.5 Determining Differentiation

Eales (1990) attributes gravitational crystal settling as the main mechanism for the differentiation of the Birds River Complex. The on-going separation of residual liquid from the crystals took place by enduring emptying of the hypabyssal chamber (Eales, 1990). Correlations between incompatible elements Ti, Ba, P, K, Rb, Y, Nb, Nd, Ce and La with Zr as the abscissa are shown in Figure 12. Zr is used because of its "almost ideal exclusion from early-crystallizing phases, and the high analytical precision achieved by XRF methods" (Eales, 1990). Covariance between Zr and Ti ends at ~150ppm, and between Zr and Nd, Cem La, P, and Y at ~300ppm (Eales, 1990). There are certain phases into which these incompatible elements are partitioned into, phases like ilmenite-magnetite for Ti and apatite for REEs, Y and P,

and once they start to nucleate it can lead to a break in covariance (Eales, 1990). Trace elements are a useful tool in reconstructing the evolution of differentiated igneous rocks, but the idea that the rocks containing the lowest number of incompatible elements are suitable for use as initial liquid composition is a bad one, as the dilution of liquid in terms of trace elements can occur due to the fortification in cumulus phases (Eales, 1990).

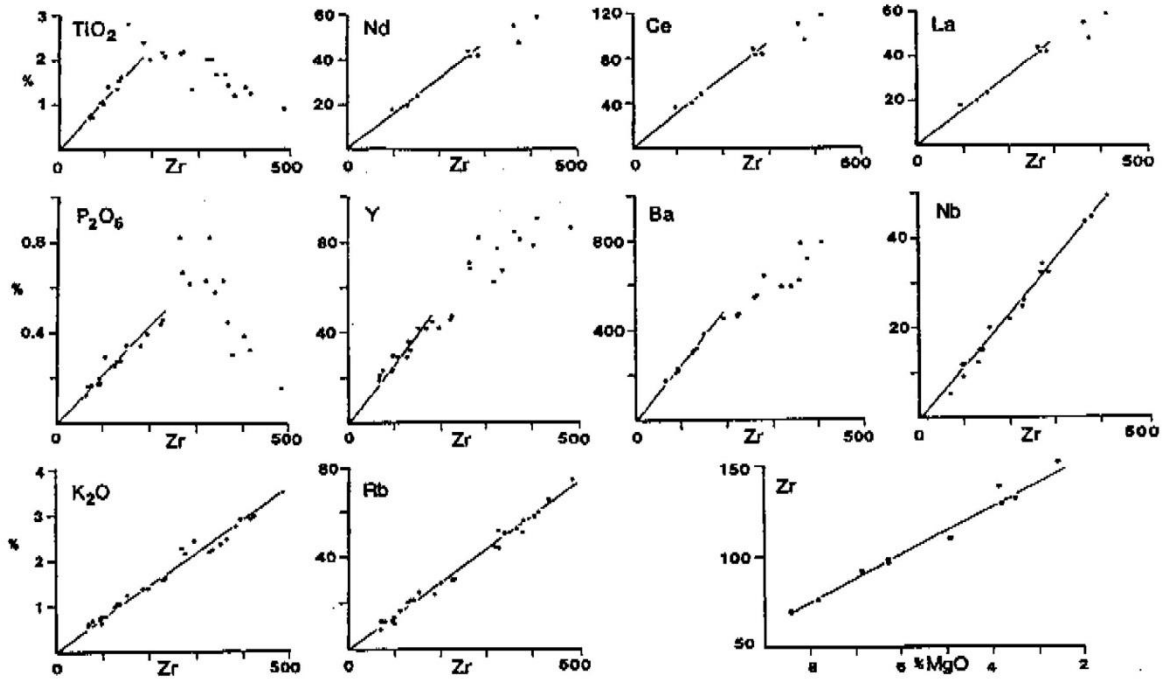

Figure 12. This diagram illustrates the covariance between Zr, Ti, Nd, Ce, La, P, Y, Ba, Nd, K, and Rb, and conversely the inverse linear relationship between Zr and MgO. Regression lines were computed so as to pass through the origin (except Zr vs. MgO). From Eales (1990).

Another point of concern is that the low number of trace elements captured in the aforementioned rocks by analytical techniques can very well be lower than the actual errors in analytical accuracy (Eales, 1990). Therefore Eales (1990) decided to use regression analysis to smooth the data. Data plotting proximally on the regression lines could depict parental liquid that has been diluted by phenocrysts, whereas the distal points are differentiated liquids (Eales, 1990). Therefore the initial liquid composition plots somewhere in-between these ends, but there is no way of independently determining the starting Zr concentration (Eales, 1990). Once a small quantity of phenocrysts crystallise in a melt that contains elements with a high bulk

distribution coefficient, such as Ni, the whole-rock concentration will undergo sudden change (Allegre *et al.*, 1977). Eales (1990) runs with the idea that if an inverse linear relationship between a highly compatible and a highly incompatible element can be determined, then large error values can be accommodated without leading to more than small errors with regards to the estimates of the incompatible element. Eales (1990) reasoned as such:

The Rayleigh fractionation law:

$$C_l^i = C_O^i \, F^{(D-1)} \tag{31}$$

Where C_l^i is the concentration of any trace element *i* in fractionated liquid,

C_O^i is the concentration of trace element *i* in the parent liquid,

F is fraction of liquid remaining, where (l-F) is fraction crystallised,

and

D is the bulk distribution coefficient.

If D is numerically very small it means the element is incompatible. If that is the case, the following applies

$$F = C_O^* / C_l^* \tag{32}$$

then $$C_l^i = C_O^i \ (C_O^* / C_l^*)^{(D-1)} \tag{33}$$

and $$\log C_l^i = \log C_O^i + (D\text{-}1) \log C_O^* - (D\text{-}1) \log C_l^* \tag{34}$$

A plot of log C_l^i against log C_l^* should yield a linear relationship, if D is constant (Eales, 1990). Just such a plot for Birds River is shown in Figure 13, which yields a least squares regression with a correlation coefficient of -0.920 (Eales, 1990). In Figure 13, three independent data sets are used to develop initial liquid compositions

for Ni: (1) the mean of Ni from 22 samples taken from chilled dolerites in the Eastern Cape (Marsh and Eales, 1984); (2) 59 dolerites from the wider Central Igneous Province; and (3) 27 samples from Lesotho Group basalts which are more primitive in composition (Marsh and Eales, 1984). The second batch (4,5 and 6), makes use of the inverse correlation between MgO and Zr (Fig. 12) by substituting the average MgO levels in the relevant equation (Table 4) for the same sample suites (1-3) (Eales, 1990). The third batch (7, 8 and 9) estimates the quantity of Zr in the initial liquid by "fitting the computed mean levels of K, Ti, P, Rb, Y, Ba, Ce, and Nd in the sample suites (1-3) above the regression equations given in" (Table 4). With regression lines passing through the origin, the inversion of y and x in calculating the regression equations produces negligible (largest being 0.8ppm Zr) differences in the estimates of Zr levels (Eales, 1990).

Very good agreement in values are found from (1) to (9) for Zr levels, ranging from 80.3 ppm to 89.0 ppm, with a mean of 84.2 ± 3, which is in accordance with the two Birds River chilled margins samples of 86 ppm, and the 27 basalts in (3) with a mean of 85 ± 6 ppm Zr (Eales, 1990). The summarised data is given in Table 5, with the intitial liquid concentrations for the rest of the incompatible elements determined by assuming a fixed value of 84 ppm for Zr in the respective regression equations (Eales, 1990).

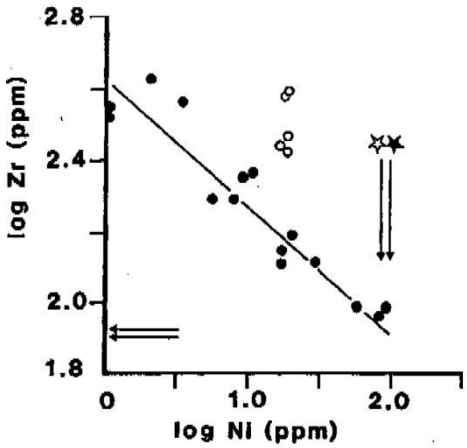

Figure 13. Plot of log Zr (ppm) against log Ni (ppm) in Birds River Rocks. Regression line is calculated for filled-circle datum points only, and yields equation log Zr = -0.3564 logNi + 2.619 (n=15); correlation coefficient -0.920. Calculated average Ni contents of East Cape dolerites (87.0 ppm) shown by open star symbol and 27 Lesotho-type basalts (101 ppm Ni) by filled star. From Eales (1990).

Table 4. Statistical data derived from input data of Figure 12. From Eales (1990).

y	x	n	b	a	Coeff.	Zr limit	100(1–F)
log Zr	log Ni	15	$-3{,}564\times10^{-1}$	2,619	–0,920	420	80
Zr	MgO	10	–13,69	183	–0,988	153	46
K_2O	Zr	27	$7{,}190\times10^{-3}$	–	0,990	506	84
Rb	Zr	27	$1{,}526\times10^{-1}$	–	0,987	506	84
Nb	Zr	17	$1{,}182\times10^{-1}$	–	0,967	506	84
La	Zr	6	$1{,}417\times10^{-1}$	–	0,981	293	72
Ce	Zr	6	$3{,}046\times10^{-1}$	–	0,987	293	72
Nd	Zr	6	$1{,}580\times10^{-1}$	–	0,989	293	72
P_2O_5	Zr	15	$2{,}050\times10^{-3}$	–	0,972	226	64
Y	Zr	12	$2{,}638\times10^{-1}$	–	0,951	226	64
Ba	Zr	9	2,423	–	0,992	200	59
TiO_2	Zr	10	$1{,}158\times10^{-2}$	–	0,965	128	35

Table 5. Estimation of Birds River initial liquid composition. From Eales (1990).

	E. Cape Dolerite	Birds R. Zr	Cent. Prov. Dolerite	Birds R. Zr	Lesotho Basalts	Birds R. Zr	Birds R. Initial Liquid
Ni	87	84,7[a]	87,4	84,6[b]	101	80,3[c]	89
MgO	6,86	89,0[d]	6,92	88,2[e]	7,38	82,0[f]	7,26
TiO_2	1,00	86,4	0,98	84,7	0,93	80,3	0,97
P_2O_5	0,17	82,9	0,16	78,0	0,16	78,0	0,172
K_2O	0,56	78,0	0,58	80,7	0,73	101,5	0,60
Rb	12,5	81,9	12,1	79,3	10,2	66,8	12,8
Y	26	98,6	24,2	91,7	23,3	88,3	22,2
Ba	213	87,9	194	80,1	164	67,7	203
Ce	25	82,1	–	–	–	–	25,6
Nd	14	88,6	–	–	–	–	13,3
Averages:	–	$85{,}8\pm6$[g]	–	$82{,}4\pm5$[h]	–	$80{,}4\pm13$[i]	–

3.6 Derivation of Successive Liquids

In order to model the putative liquid composition as it evolves, it is vital to ascertain the percentage of crystallisation required for each specific element's concentration in the liquid. Using the Rayleigh fractionation equation, estimated values for elements in the initial liquid (C_O) are adopted from Table 5, the successive derivatives (C_l) are taken from subsequent analyses and the bulk distribution coefficient is taken as 0.02 (Eales, 1990). To determine the percentage of crystallisation in the magma chamber the formula 100(l-F) is used, along with the limiting factor that no calculation will allow for covariance that lies outside that which was determined in Figure 12. Table 6 shows the data compiled by Eales (1990) to ascertain the percentage of crystallisation required to yield the residual results described earlier. The F values used are the means of individual values calculated for every element. The coefficient of variation, or rather the level of uncertainty, ranges between 2-6% for all elements. Eales (1990) ascribes this to "sampling or analytical error, presence of phenocrysts phases, and the use of inappropriate distribution coefficients". Furthermore, based on these calculations, Eales (1990) concludes that the fractionation ran continuously and allowed for liquids to be constantly removed as they themselves evolved.

Table 6. The percentage crystallization required to yield residual liquids. From Eales (1990).

Sample No.	MgO	K_2O	Rb	Zr	Nb	P_2O_5	Ba	TiO_2	Ce	Nd	Mean F	% CRYST.	C.V. (%)
3	0,935	0,842	(1,00)	0,911	0,815	0,943	0,922	0,913	–	–	0,897	10,3	5,4
4	0,724	0,775	0,735	0,767	–	(0,560)	0,740	0,688	–	–	0,739	26,1	4,2
5	0,623	(0,554)	0,581	0,635	0,641	0,601	0,632	0,628	0,663	0,653	0,629	37,1	4,0
6	x	0,421	0,424	0,419	0,437	0,418	0,435	(0,475)	–	–	0,426	57,4	1,9
7	x	0,377	0,404	0,363	0,389	0,379	x	x	–	–	0,382	61,8	4,0
8	x	0,258	0,275	0,307	0,295	x	x	x	0,284	0,292	0,285	71,5	6,0
9	x	0,210	0,220	0,213	0,210	x	x	x	x	x	0,213	78,7	2,2
10	x	0,167	0,156	0,160	–	x	x	x	x	x	0,161	83,9	3,5

Negative values for F are attributed to cumulus mineral-enriched varieties. The much higher values for MgO than that of the initial liquid estimate of 7.26% in both column 1 and 2, 8.4% and 7.8% respectively, backs up this sentiment (Eales, 1990).

3.7 Major element variations

Eales (1990) argues that computer methods for determining the composition of liquids produced by the gradual removal of crystals from a melt are much more efficient than graphical methods. To determine the phase compositions, both initial liquid and derivative liquids can be used (Eales, 1990). The mixer programme used in this instance quantitatively measures the compatibility between both input and derived output compositions by minimising the mean discrepancy in oxide values and/or residuals (Eales, 1990). As pointed out by Eales (1990), this does not in any way guarantee that the subsequent solution is exactly correct, but rather that the mathematically most correct answer has been attained with regards to input data. Therefore, the better the compatibility between input data and actual petrography and mineral compositions, the closer the solutions are to being correct (Eales, 1990). The mineral compositions that were used for this computation, as well as the results, are shown in Table 7. The method used for this computation is given as follows: The oxides for the 24 Birds River rocks are plotted against their respective degrees of crystallisation (filled circles in Figure 14). By performing interpolation, the successive derivative's compositions were read off at 10% increments (unfilled circles in Figure 14). These values, and their associated composition for the phases olivine; plagioclase; augite; pigeonite; and titanomagnetite, were used as input compositions (BR10 for 10%, BR20 for 20% etc.) (Table 7). The computer program ran 62 trials for each increment, and the value with the greatest compatibility between input compositions and solutions were used. Table 6 shows a very good alignment between smoothed mean compositions of Birds River and the values potentially achieved during crystal removal. Figure 15 represents a graphical representation of the normative compositions calculated in Table 6, plotted against the per cent crystallisation required to yield such a liquid. The final line in Table 7 summarises the total amount of crystals required to be extracted from the previous liquid in each step. This value can be seen as the degree of match between major element and incompatible trace element data; the closer it is to the 10% increment value, the better the match (Eales, 1990). Due to the fact that vanadium was shown to be a potentially useful monitor of Fe-Ti oxide crystallisation, it is included here (Fig. 16). One issue evident in Figure 14, is where some of the data plots away from the

smoothed trends, more so than analytical error allows, e.g. SiO_2 depletion and Fe_2O_3 and TiO_2 enrichment at 49.5% and 53.5% crystallised (Eales, 1990). According to Eales (1990) this can be accounted for by "non-systematic additions and subtractions of cumulus phases", and potentially this problem can be proved by computation. By running "tests" on the Mixer Programme, the "composition of SiO_2-depleted sample at 49% crystallised may be precisely simulated by addition of 3.6% titanomagnetite and 1.9% pigeonite, and subtraction of olivine and augite", from the estimated liquid BR40 (Eales, 1990). The sample in question has almost double the amount of V, 512 ppm compared to the normal range of 215-240 ppm, which can be interpreted as a result of localised oxidation of the liquid (Eales, 1990).

Table 7. Input and Output data of Mixer Programme. From Eales (1990).

	Initial	BR10	BR20		BR30		BR40		BR50		BR60		BR70	
SiO_2	52,13	52,35	52,58	(0,00)	52,95	(–0,01)	53,41	(+0,02)	54,13	(+0,01)	54,93	(0,00)	56,20	(+0,01)
TiO_2	1,01	1,08	1,22	(–0,04)	1,36	(–0,02)	1,62	(–0,04)	1,80	(+0,02)	2,15	(–0,03)	2,29	(0,00)
Al_2O_3	15,05	15,67	16,58	(–0,01)	16,79	(0,00)	16,50	(–0,03)	15,76	(0,00)	14,52	(+0,01)	13,01	(0,00)
FeO	9,27	9,46	9,74	(–0,01)	10,34	(+0,01)	11,21	(–0,05)	12,22	(–0,01)	13,57	(+0,01)	14,73	(+0,01)
MgO	7,27	6,52	5,36	(+0,01)	4,45	(0,00)	3,59	(0,00)	2,89	(0,00)	2,23	(–0,01)	1,52	(–0,05)
CaO	11,72	11,32	10,72	(+0,01)	10,12	(+0,01)	9,42	(–0,03)	8,62	(–0,01)	7,61	(0,00)	6,40	(0,00)
Na_2O	2,53	2,56	2,63	(+0,13)	2,68	(+0,05)	2,75	(+0,01)	2,84	(–0,05)	2,86	(–0,03)	2,95	(–0,17)
K_2O	0,61	0,68	0,76	(0,00)	0,86	(+0,01)	1,00	(+0,02)	1,20	(–0,02)	1,49	(–0,02)	2,03	(–0,13)
P_2O_5	0,17	0,19	0,21	(0,00)	0,24	(0,00)	0,28	(+0,01)	0,34	(0,00)	0,43	(0,00)	0,66	(–0,10)
Average diff.			(0,022)		(0,011)		(0,022)		(0,014)		(0,011)		(0,052)	
Olivine			Fo_{81}		Fo_{81}		Fo_{76}		Fo_{74}		Fo_{65}		–	
%			1,14		1,04		0,94		0,65		0,24		–	
Plagioclase			An_{71}		An_{64}		An_{64}		An_{64}		An_{61}		An_{54}	
%			2,18		5,03		6,94		6,33		6,81		5,99	
Augite			$Ca_{40}Mg_{47}$		$Ca_{40}Mg_{47}$		$Ca_{35}Mg_{45}$		$Ca_{35}Mg_{45}$		$Ca_{35}Mg_{41}$		$Ca_{35}Mg_{41}$	
%			6,60		4,59		4,14		2,75		2,02		1,61	
Pigeonite			–		–		–		–		$Ca_{11}Mg_{55}$		$Ca_{15}Mg_{45}$	
%			–		–		–		–		0,86		1,08	
Titanomagnetite			–		$Mt_{26}Usp_{74}$		–		$Mt_{26}Usp_{74}$		$Mt_{26}Usp_{74}$		$Mt_{26}Usp_{74}$	
%			–		0,10		–		0,14		0,16		0,52	
Total Crystal Extract (%)			9,92		10,76		12,02		9,87		10,09		9,20	

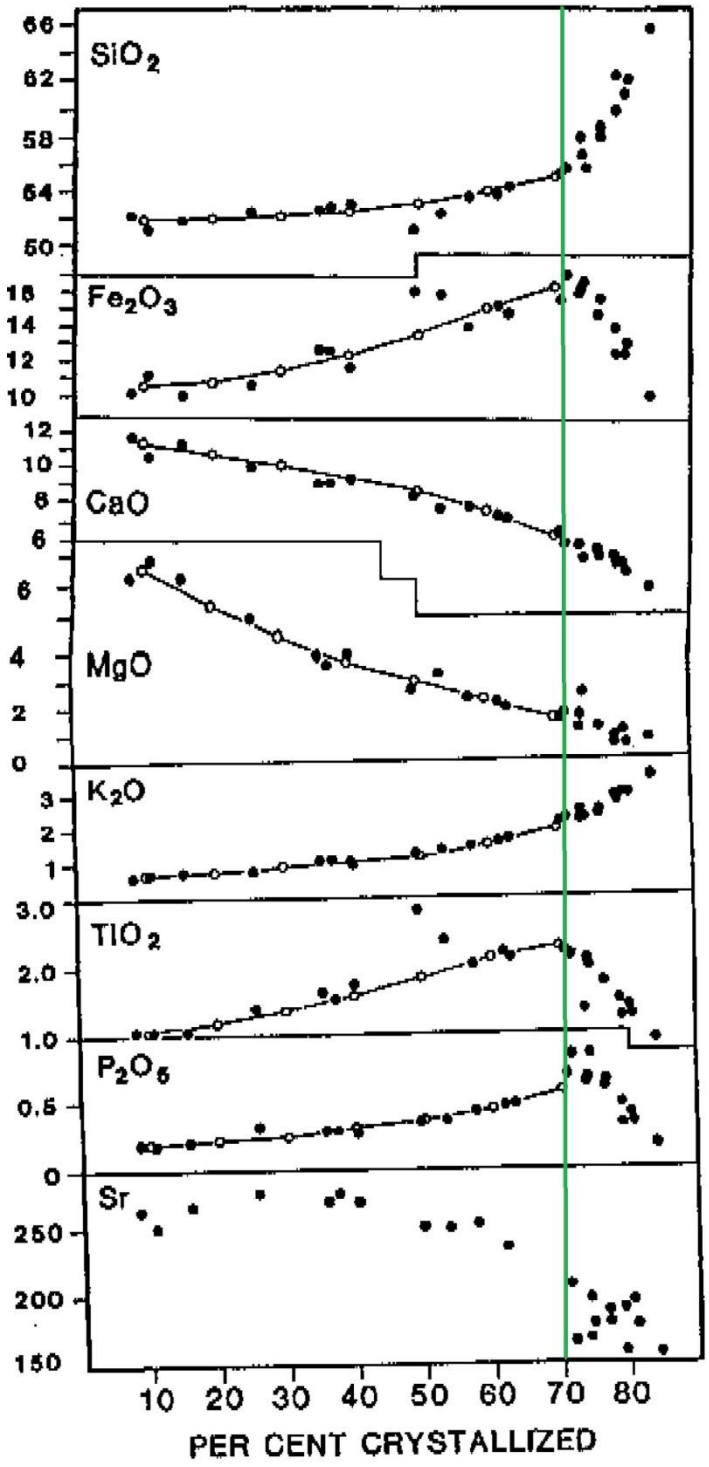

Figure 14. Analyses of 24 Birds River samples (filled circles) plotted against the degrees of crystallization. Empty circles connected by lines are the computed values for the Birds River rocks up to 70% crystallised (green line). Computed by the method shown in Table 3. Modified from Eales (1990).

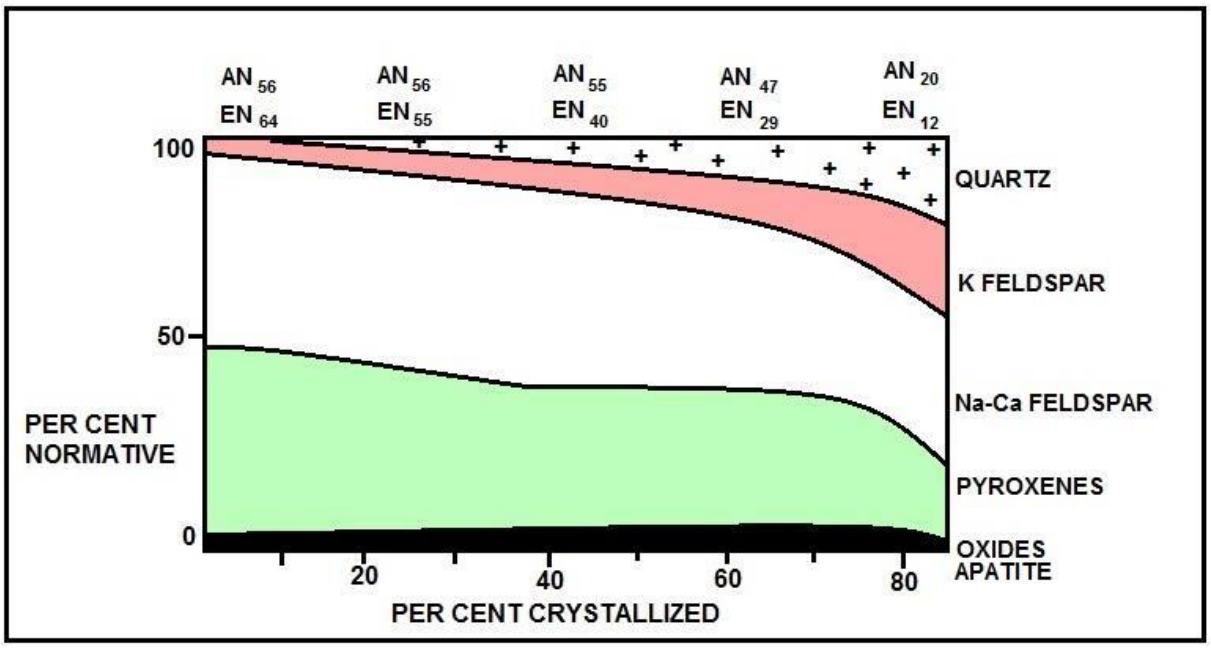

Figure 15. Normative composition plotted against the per cent crystallised. Normative composition of plagioclase and orthopyroxene are given at the top of the diagram. Calculations assume a uniform FeO:Fe_2O_3 of 10. Modified from Eales (1990).

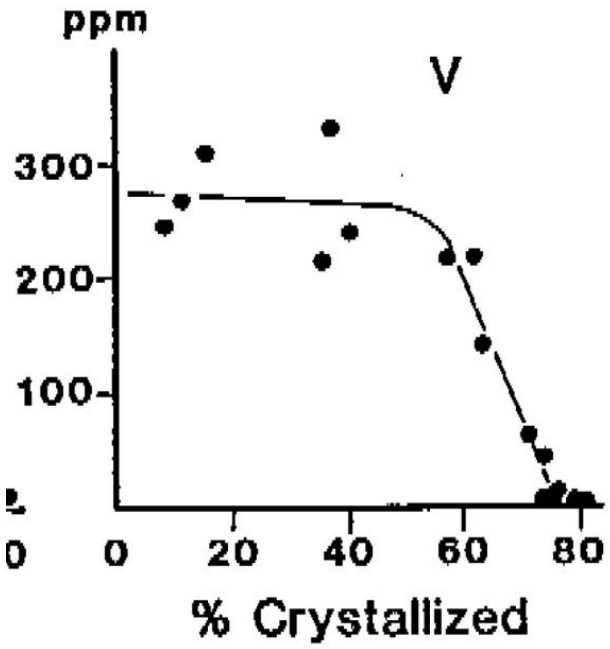

Figure 16. Depletion of V is deferred until significant magnetite is nucleated after 60% crystallization. From Eales (1990).

3.8 Trace Element Variation

Eales and Robey (1976) embarked on sampling the Denwood Kloof, the kloof that cuts through the ferrotholeiites in the south-western portion of the Birds River Complex (POINT B in Figure 11). As previously mentioned, the kloof provides excellent exposure, not only of the ferrotholeiites; but also of the metasomatic granophyres; the gabbros and gabbro pegmatites; and of the surrounding country rock. In other words, it provides a first-rate location for performing an analytical traverse through the interested section of the complex. Eales and Robey (1976) analysed for K and trace elements Rb, Sr, Y and Zr (Fig.17).

Moving from the left to the right of the diagram, left representing the contact between the Stormberg Group sediments and the Birds River Complex, there is a minor break in composition for K, Rb, Sr and Zr at the middle of the gabbros. Based on field evidence, Eales and Robey (1976) advocated that several separate gabbroic pulses intruded after the initial release of magma to the current position. At the contact between the gabbros and the intersertal ferrotholeiites, there is once again a marked change in concentration levels for K and Rb, Y and Zr. This represents the only marked change in concentration for Y. Sr levels dip significantly at the boundary between the gabbros and the intersertal ferrotholeiites.

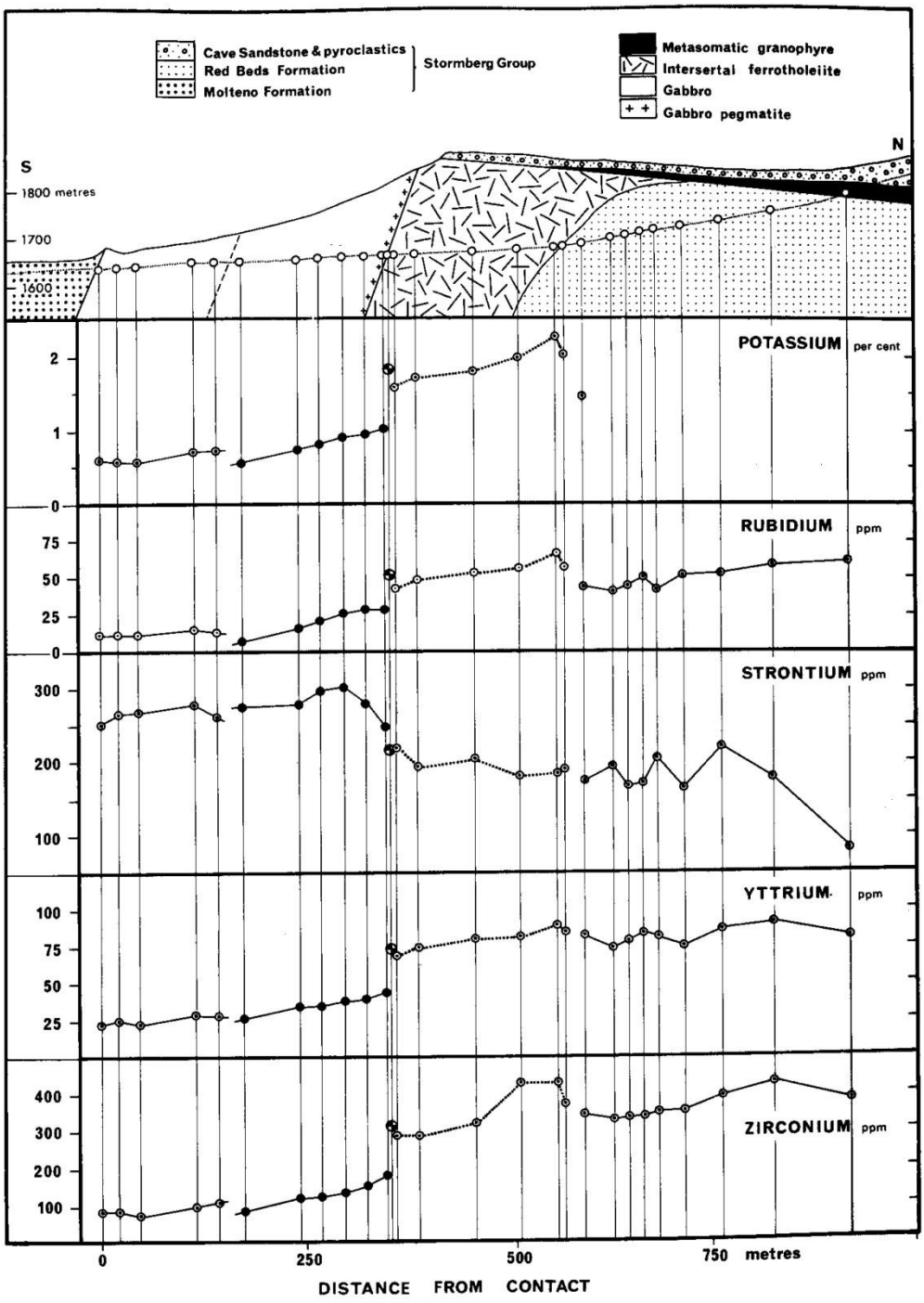

Figure 17. A cross section of the south-western margin of Birds River, displaying how potassium and trace elements vary across the complex. The cross section runs along a deeply eroded stream course. Half-filled circles represent a pegmatitic facies. The intrusives are in the centre, country rock on the left and xenolithic fragments on the right. From Eales and Robey (1976).

3.9 Discussion

3.9.1 Evolution of the Birds River Complex

These ferrogabbros, or ferrotholeiites, supposedly represent the most differentiated portion of the Birds River Complex. Originally belonging to a deeper seated gabbroic intrusion, they were emplaced when the roof of the cauldron collapsed and were forced out of the chamber (Eales and Robey, 1976). At first, the composition of these newly emplaced magmas was supposedly similar to that of an olivine gabbro (Eales and Robey, 1976). It just so happens that the gabbros adjacent to the ferrotholeiites are relatively akin to such rocks.

Eales and Robey (1976) advocate the possibility of *in situ* differentiation for the intruded gabbros, which lead to an accumulation of residual melt under a sedimentary cap. This makes sense, considering the gradual change in concentration for K and Rb, Sr, Y, Zr from left to right (Fig. 17). In this scenario, the gabbros on the left represent the “bottom” of the intrusion; and the intersertal ferrotholeiites the migrated and trapped residual melt. However, there is a problem with this interpretation.

That is the presence of a glassy groundmass between the contacts of the gabbros, metasediments and porphyritic ferrotholeiites (Eales and Robey, 1976). A glassy groundmass between these rock units represents rapid cooling at the respective contact. This presents a problem for the idea that the porphyritic ferrotholeiites formed from the migration of residuum, as it implies that the porphyritic ferrotholeiites were already intruded and started crystallising (or at the very least exhibited a difference in temperature between the two intrusive bodies) by the time the gabbros started intruding. Sr levels decrease significantly on the gabbro-side of the gabbro-ferrotholeiite contact. As Sr is an incompatible element with a soft spot for plagioclase, it is inevitably linked to its chemical and physical evolution. Plagioclase changes composition from An_{61} to An_{16} and also decreases in abundance from 50 to 33% (Eales and Robey, 1976). The concentration of Sr in the melt is subsequently dealt a blow once the cumulus plagioclase composition becomes more sodic (Eales and Robey, 1976). Distinct variations in K, Rb, and Zr

between the ferrotholeiites and the regular gabbros (Fig. 17) imply that the ferrotholeiites belong to an alternate pulse of magma. This supports the field evidence that more than one intrusive event took place during the emplacement of the gabbros (Eales and Robey, 1976).

Further problems exist for this view. Xenoliths from the porphyritic ferrotholeiites are present in the gabbros (Eales and Robey, 1976). Moreover, even though the gradual change in trace elements across the intrusion supports the idea, it is thwarted by the presence of sharp discontinuities in trace elements and K between the different rock types (Fig. 17). This provides enough physical and chemical evidence that the iron-enriched porphyritic ferrotholeiites intruded separately from the gabbros.

3.9.2 Birds River Liquid Line of Descent

The LLD for Birds River was first compiled by Eales and Booth (1974). The evolution of total iron in three rock types for Birds River Complex is shown in Figure 18. The trends from Birds River are compared to that of Skaergaard and calc-alkaline series rocks. It should be noted that the trend presented here for Skaergaard (Fenner trend) is from a single estimate, and should not be taken as the definitive estimate for Skaergaard liquid line of descent. It does, however, quite conveniently highlight the problem pertaining to the Skaergaard LLD, as the trend presented here for the Birds River ferrogabbros and tholeiites has since been published as a possible trend for Skaergaard.

Percentage crystallisation experiments performed by Eales (1990) indicate that a stark change in the evolution of the melt took place at ~70% crystallisation (Fig. 14). Crystallisation of Fe-Ti oxides correlates well with the expected behaviour of these elements at such time. The dramatic increase of SiO_2 and simultaneous drop of Fe_2O_3 and TiO_2, suggests that Fe-Ti oxides did in fact nucleate at ~70% crystallisation. The concurrent drop in P_2O_5 can only be attributed to the arrival of apatite on the cotectic and must thus have been present as a cumulus phase. Broken and terminated crystals of apatite in the groundmass imply that apatite formed as a cumulus phase within the original, deeper magma chamber, and prior to

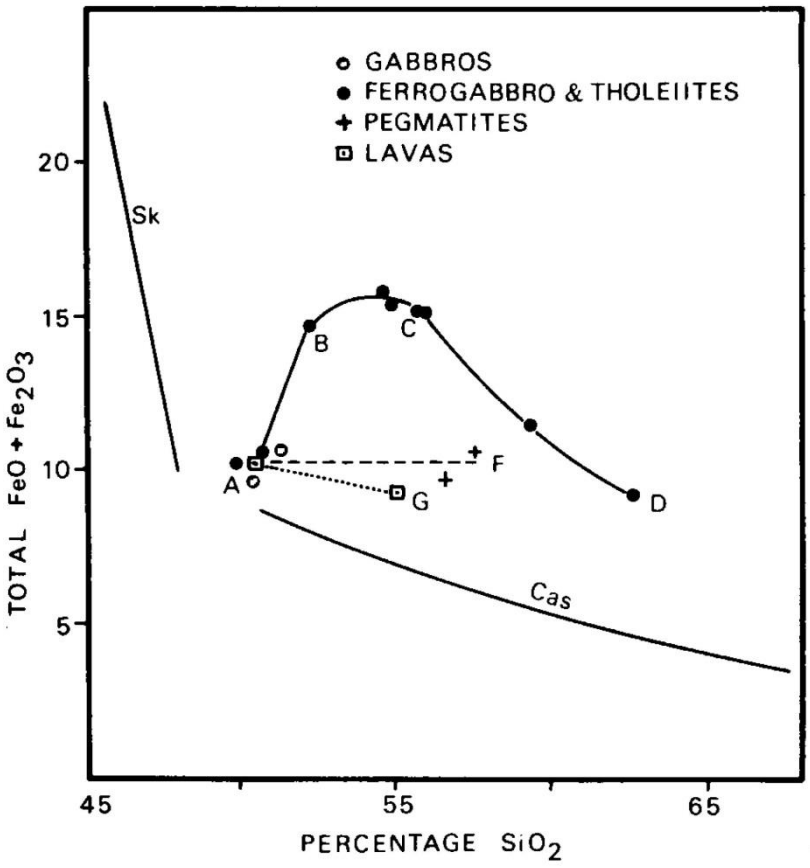

Figure 18. Plots of total iron (wt.%) against SiO_2 (wt.%) for Birds River rocks. Curves are also shown for the Skaergaard Intrusion (Sk) and a calc-alkaline series (Cas) after Osborn (1959). From Eales and Booth (1974).

emplacement of the supposed iron-rich residuum (Eales and Robey, 1976). These euhedral crystals would then have been forced, and subsequently extended into, the cooling viscous groundmass (Eales and Robey, 1976).

Compared to Skaergaard, where apatite became a cumulus phase once normative plagioclase reached An_{57}, Birds River apatite only reached cumulus status at An_{37} and peaked at $An_{32\text{-}23}$ (Wager and Brown, 1968; Eales and Robey, 1976).

What is also of interest in Figure 18, is the distinct difference in trends observed between the three rock series, namely the gabbro-ferrogabbros-ferrotholeiites (A-B-C-D); the gabbro-gabbro pegmatites (A-F); and the basalt-quartz basalt (A-G); that constitute the Birds River Complex. The latter two exhibit nearly no change in FeO_{total} vs. SiO_2, whereas the former represents the classical Bowen trend.

Presumably, the initial increase and subsequent decrease of FeO_{total} is related to the timing of magnetite crystallisation.

Evolutionary paths for rock type (A-F) and (A-G) both exhibit similar paths to the calc-alkaline series presented by Osborn (1959), albeit not perfectly so. This is also reflected in the graph for mafic index versus SiO_2 (not presented here; Fig. 7 in Eales and Booth, 1974). In both instances, the evolutionary path for the ferrogabbros and tholeiites is in stark contrast to the rest.

Ti is a good indicator for ilmenite-magnetite crystallisation. As an incompatible element, it is a good monitor for crystallisation in the residual liquid. It will only be reduced in the melt once a crystal phase, in which it is strongly partitioned, starts to crystallised. This forces the incompatible element into the crystal phase, which in this case, is ilmenite-magnetite, and thus provides a decent monitor for the timing of crystallisation of such phases. These Fe-Ti oxides have a marked effect on the evolution of the liquid in terms of iron-enrichment or depletion, so once they crystallise the liquid should decrease in relative iron and increase in silica, especially if the Fe-Ti oxides – which obviously do not remove any silica from the melt during crystallisation – are the only phases on the cotectic at that time.

There is no definitive initial liquid composition, as has previously been mentioned, which in this case means the starting liquid composition for the modelling of Birds River differentiation is a putative one. It was taken from computed data smoothed by regression analysis (Table 6) (Eales, 1990). The premise behind calculating the differentiation trend for Birds River, is based on covariance of incompatible elements. The fundamental idea is that incompatible elements, especially the likes of Zr and Nb, will not be partitioned into any cumulus phases during the initial stage of crystallisation. As previously mentioned, trace elements that plot distally (Fig. 12) characterise highly fractionated liquids (Eales, 1990). Eales (1990) cautions against using rocks with the lowest concentration of trace elements as the initial composition, as it may simply echo dilution of the liquid in those elements due to the enrichment of crystallising cumulus phases. This makes sense, especially for trace elements that are easily removed during the initial stages of crystallisation, but surely for a highly incompatible trace element the risk is much

lower. The knowledge of which minerals are present in the rock, combined with the likelihood of the trace elements' portioning into those minerals, by virtue of partition coefficients, it is certainly not ludicrous to assume it might represent initial concentrations. Especially if this knowledge is corroborated by field evidence, such as using the glassy margin or an assumed feeder dyke.

In the case of Birds River, granted, it is slightly more complicated, as there is strong evidence to support multiple intrusive events. On top of that, it is entirely possible that the highly fractionated portion could have undergone differentiation in the deeper original magma chamber prior to emplacement. However, the gabbros surrounding the fractionated portion are assumed to be of a similar composition to that of the original magma. The calculated initial magma composition is close enough to samples taken from normal gabbros and of marginal gabbroic glasses, with the calculated initial magma showing a little more CaO and less FeO_{total}. The higher Ca-content can be accounted for by initial crystallisation of anorthite which more than likely took place as the magma ascended.

Eales (1990) therefore used concentrations for initial liquid composition from somewhere in-between the proximal and distal data points. This assumption is immediately noticed when comparing the calculated liquid evolutionary composition to actual analysed rocks (Fig. 19 and 20). Figures 19 and 20 were constructed using data from literature for ferrogabbros and tholeiites; the calculated initial and subsequent liquid composition for Birds River; and a representative sample of rocks (Eales and Booth, 1974; Eales, 1990). It should be noted that the initial composition for the ferrogabbros and tholeiites, i.e. the lowest SiO_2 value, was taken from an average of all the sampled glassy margins and normal gabbros. This was done in order to demonstrate the potential evolution of the rocks, and for comparison purposes (Fig. 18) has an almost identical starting composition for the ferrogabbros and tholeiites). TiO_2 was modelled in order to compare the fractionation trend for iron, as both are a very useful tool in tracking the crystallisation of Fe-Ti oxides, such as magnetite and ilmenite.

Each of the red squares (calculated liquid) represents an increase in crystallisation percentage of the liquid by 10. Thus, the left-most square represents

the initial liquid composition, the one just to the right 10% and so on. The evolution in this case moves from an initial liquid composition of just above 52 wt.% SiO_2, and increases in SiO_2 without deviation back to a silica-poor liquid. In other words, it steadily increases in SiO_2 as crystallisation continues.

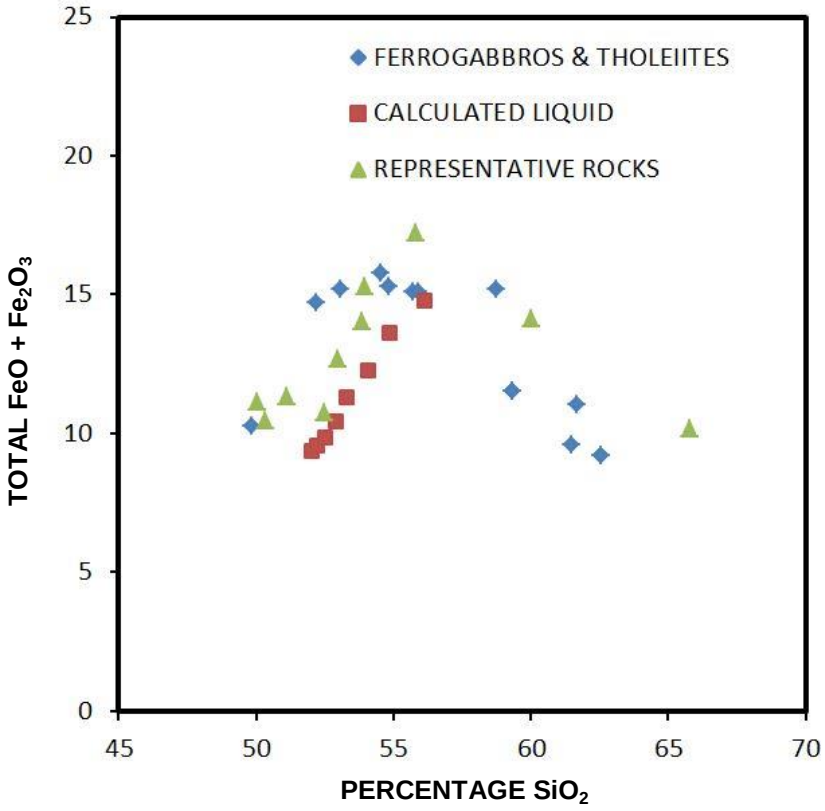

Figure 19. Plots for total iron (wt.%) against SiO_2 (wt.%) for Birds River rocks. Data from Eales (1990) and Eales and Booth (1974).

What should be noted, and this is a very important draw-back for this type of modelling, is that because of the inherent reliance on trace elements as a monitor for liquid evolution, the model can only accurately be used to estimate major element values up to 70% crystallisation. Many of the trace elements fall below detectable limits at ~80% crystallisation (Fig. 16). This means that for the final stages of crystallisation the model cannot be directly employed to analyse the evolutionary path. What Eales (1990) did was to compare the initial stage of evolution to measured values of actual rocks (Fig. 14). The green line in Figure 14 shows the point at which the model has failed to predict the compositional change in the melt. What is clear from the figure is that the major changes for SiO_2; Fe_2O_3; TiO_2 and P_2O_5 occur directly beyond this point. However, up to that point there is a reasonably

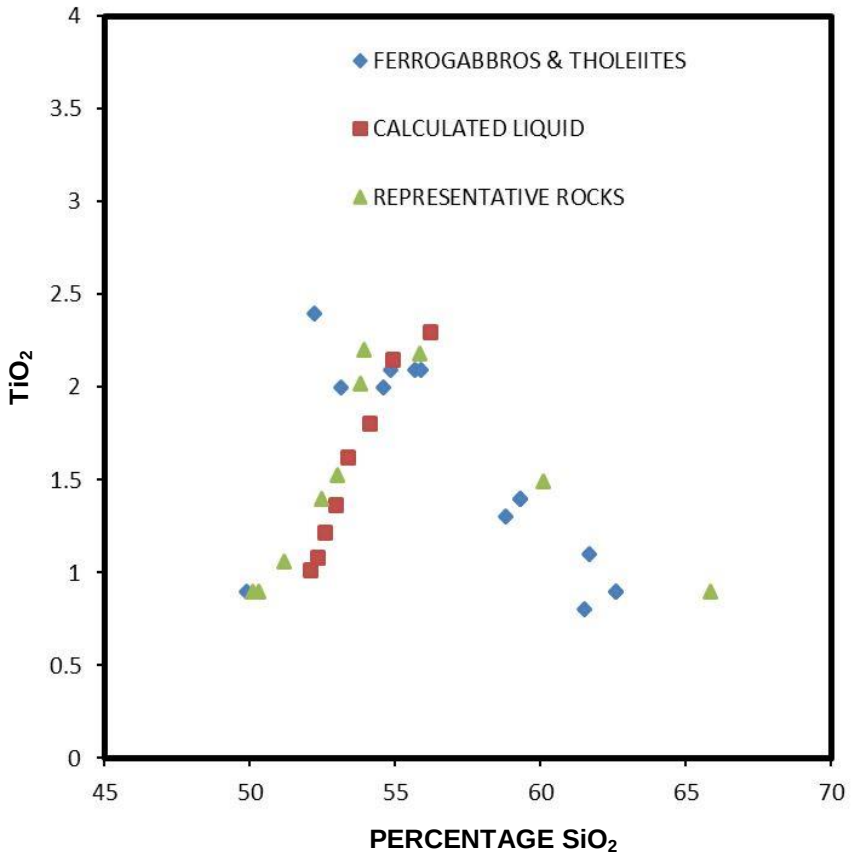

Figure 20. Plots for TiO_2 (wt.%) against SiO_2 (wt.%) for Birds River rocks. Data from Eales (1990) and Eales and Booth (1974).

good correlation between the actual measured values and the calculated ones, which gives a strong indication that the method can potentially be applied to good effect.

Another point is that the method is not beset by a host of assumptions that carry with them a potentially appreciable amount of uncertainties. It focusses on analytical data from actual rocks, albeit trace elements present in low concentrations.

A small discrepancy exists between the drop in V content at 60% crystallisation, and that of total iron and TiO_2 (Fig. 14 and 16). Vanadium has been shown to be heavily affected by magnetite crystallisation (e.g. Jang *et al.*, 2001), and will partition into the melt as soon as magnetite appears on the cumulus. However, the residual melt only shows depletion in total iron and TiO_2 at 70% crystallisation. It is possible that V absorption was buffered by oxygen fugacity or other factors. Just such a discrepancy exists in Skaergaard, where V content remains unchanged until the Middle Zone, but magnetite crystallisation already appears as a cumulus phase in the stratigraphic unit below it, the Lower Zone. Jang *et al.* (2001) attributes this to

the magnetite-rich liquid sinking down to lower levels after crystallising in the Middle Zone. A more or less 10% crystallisation gap also exists in the Skaergaard rocks, so clearly it warrants further investigation. In the case of Birds River, it would have been convenient had there been more analysis performed for V, as the statistical soundness of the trend line fitted to the data is slightly questionable. Had there been more data, it is not entirely implausible to suggest that the dip could in fact have taken place closer to 70% crystallisation. Eales and Robey (1976) account for this late drop in Fe_{total} and TiO_2 by proposing that oxygen fugacity in the deeper, original magma chamber, was such that precipitation of Fe-Ti oxides was postponed until after the roof-collapse.

A direct comparison between the calculated liquid and that of measured samples for ferrogabbros and tholeiites is shown in Figure 19 and 20 to better judge the possible evolutionary differences. In both instances the calculated initial liquid starts off much richer in SiO_2 than the other two suites. It also shows a very gradual slope and a much tighter data trend, although this is an inherent effect of the smoothing of the data - by regression analysis - that the modelling is based on.

Even though there is very good agreement between the initial 70% crystallisation of both the calculated liquid and measured samples, it is hard to reconcile with the fact that the model simply ceases to function after this point. This is in fact where most of the controversy lies for iron-rich intrusions, does the liquid become increasingly rich in iron or does it follow a trend of eventual depletion? The problem is that there is no real basis to continue projection beyond this point, and the inherent error values become too large due to low detectable concentration of trace elements.

4. Skaergaard Case Study

4.1 Geological History

Subsequent to its discovery and descriptions in the 1930's by Wager and Deer (1939) the Skaergaard layered intrusion has undergone a plethora of geochemical and petrologic studies. The intrusion is hallmarked as one of the prime examples of igneous differentiation and serves as the guinea pig for many new theoretical hypotheses and testing. The processes involved in its formation and evolution are well studied and understood thus making it an ideal candidate for theoretical testing. Though its original magma composition was estimated in by Wager (1960) by taking a sample from the chilled margin, it took another 30 odd years before Hoover (1989) questioned the validity of this sample as the source magma. During this time nearly all calculations involving the composition of Skaergaard used that sample as a starting liquid composition (McBirney, 1996). A thorough reworking and critical analysis of the chilled margin by Hoover (1989) led to a more reliable starting composition, which is notably different to the one estimated by Wager (1960) (McBirney, 1996).

Skaergaard intruded into the eastern coast of Greenland as part of a larger magmatic event associated with the opening of the North Atlantic at 55 Ma. (Deer, 1976; Brooks and Nielsen, 1982). Gabbros and syenites were emplaced and dyke swarms fed fissures which erupted flood basalts up to 4km in thickness (Wager and Deer, 1938; Nielsen, 1978). This volcanic event rests on up to 100 meters of Late Cretaceous to Paleocene arkoses and siltstones, with the rest on Archaean gneisses and amphibolites. The walls in the south and east of Skaergaard are composed of this volcanic sequence and the Precambrian rocks make up the walls of the lower two thirds (McBirney, 1996). The Skaergaard gabbros intruded into north-trending tholeiitic basalt dykes, and are themselves intruded by east-west striking dykes and sills of alkaline to tholeiitic basalts (Nielsen, 1978). One of the largest sills is the Basistoppen Sill which intruded into the upper part of Skaergaard, supposedly soon after solidification (Hughes, 1956; Douglas, 1961; Naslund, 1989). Its feeder dyke, the Vandfaldsdalen Macrodyke, cuts across the eastern margin of Skaergaard (White *et al.*, 1989). The central and upper parts were intruded by a swarm of small

granophyric dykes and sills, the largest of which, the Tinden Sill, intruded just short of the roof (Hirschmann, 1992). Exact age dating of Skaergaard has proved troublesome.

Low potassium contents and late-stage recrystallisation have proven to be an obstacle in reliably dating the gabbros. Estimates have been made by Brooks and Gleadow (1977) via fission-track measurements and by Hirschmann (1992) through Rb/Sr dating. Estimates for both attempts have delivered ages close to 55 Ma. If this proves to be accurate then Skaergaard is the youngest large intrusion in the area by ~15 million years (McBirney, 1996).

Skaergaard has three lithologically and structurally distinct major units: the Layered Series; Marginal Border Series; and the Upper Border Series (Fig. 21) The Layered Series is located at the bottom of the intrusion and is believed to have formed from ponded magma on the floor (McBirney, 1996). The Marginal Border Series, as the name suggests, formed during the crystallisation at the wall of the intrusion and the Upper Border Series crystallised adjacent to the roof (McBirney, 1996).

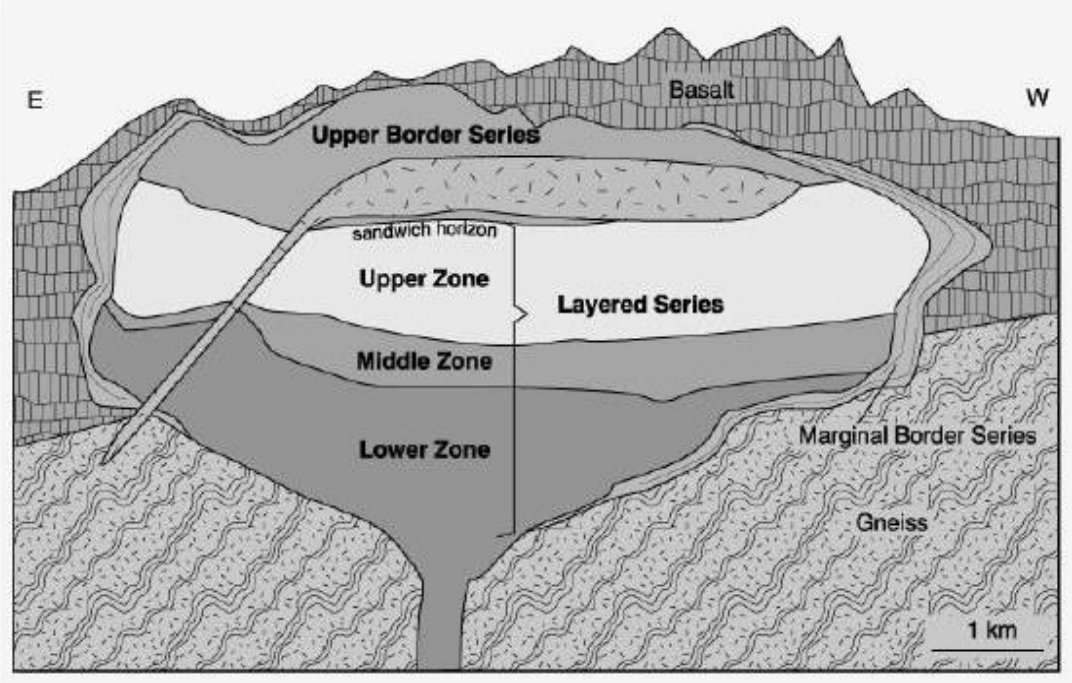

Figure 21. Emplacement and stratigraphy of the Skaergaard intrusion. From Hoover (1978).

4.1.1 The Layered Series

The Layered Series at the bottom of the intrusion is divided into three main zones, the Lower (LZ), Middle (MZ), and Upper Zones (UZ). This subdivision is marked by the lack of profuse primary olivine in the Middle Zone. It disappears at the bottom of the Middle Zone and reappears at the foot of the Upper Zone (Fig. 22). In the Middle Zone olivine presents itself as thin reaction products between pyroxene and Fe-Ti oxides and as intermittent grains (McBirney, 1996). The Lower Zone consists of three subzones, LZa, LZb, and LZc. They are divided by the presence of poikilitic pyroxene in LZa and the appearance of plentiful Fe-Ti oxides at the foot of the LZc. The Upper Zone is also subdivided into three zones, UZa, UZb, and UZc. At the bottom of UZb coarse apatite appears and UZc marks the arrival of inverted ferrobustamite (formerly ferrowollastonite) which exists in mosaic form (McBirney, 1996). Inverted pigeonite is present throughout the bottom of the intrusion, all the way up to the middle of UZa (McBirney, 1996). The Layered Series gabbros are medium to coarse grained and, like the rest of the intrusion, become increasingly mafic upward (McBirney, 1996). However, the average ratio of plagioclase to mafic minerals ranges somewhere between anorthosite and pyroxenite (McBirney, 1996). It should be noted that even rocks that appear homogenous vary in composition vertically and horizontally (McBirney, 1996).

4.1.2 The Upper Border Series

The Upper Border Series (UBS) was divided into three zones, UBSα, UBSβ, and UBSγ, by Wager (1960) and Douglas (1961) based on plagioclase compositions that correspond lithologically to the LZ, MZ, and UZ of the Layered Series. Naslund (1984) re-evaluated the position of these zones after more detailed mineral compositions were obtained, but their likeness to the Layered Series has remained unchanged. UBZα is comprised of coarse-grained gabbro containing plentiful plagioclase with lesser quantities primary olivine, Fe-Ti oxides and apatite (McBirney, 1996). Ca-rich pyroxene primocrysts (a crystal in equilibrium with the magma when primary crystallization occurred) is found in both UBZβ and UBZγ, but UBZγ contains primocrysts of olivine as well. Large apatite crystals can be found irregularly all through the intrusion with quartz present in small amounts (McBirney, 1996).

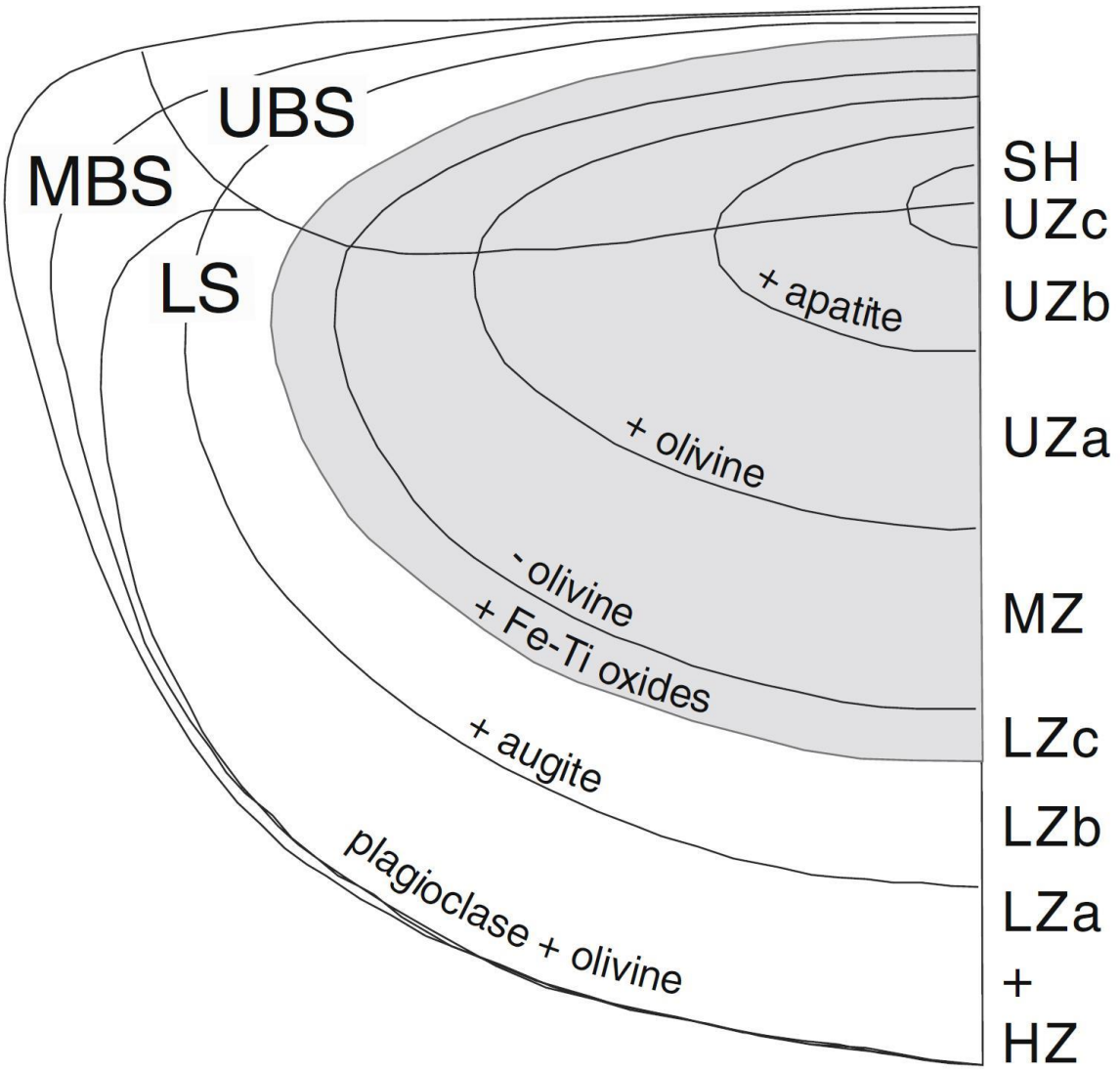

Figure 22. Stratigraphy of the Skaergaard Layered Intrusion. From Wager and Brown (1967).

4.1.3 The Marginal Border Series

The gabbros of the Marginal Border Series (MBS) were divided into the outer "Tranquil Division" and inner "Banded Division" by Wager and Brown (1968). These gabbros crystallised on the walls of the Skaergaard intrusion (Hoover, 1989).

During the cooling phase of the intrusion there was extensive hydrothermal activity, especially in the permeable basalts found in the roof and upper walls (McBirney, 1996). Oxygen isotopic ratios of the rocks were altered by these fluids to varying degrees (McBirney, 1996). Alteration was dependent on the temperatures and amount of water present (McBirney, 1996). Solidification of the entire intrusion

took about 130 000 years, but circulating hydrothermal fluids continued for another 370 000 years (Norton and Taylor, 1979; Bird *et al.*, 1988; Manning and Bird, 1991).

4.2 Wager (1960)

4.2.1 Introduction

The original work done on estimating the successive residual liquid compositions for the Skaergaard intrusion was by Wager and Deer (1939) and later by Wager and Mitchell (1951). The estimation was based on volume, which was approximated by mapping and petrological investigation, and assumed that Skaergaard was in fact a closed system. The composition of successive residual magmas was obtained in reverse order by summation of the different rock type's compositions with stratigraphic height (Wager, 1960). Hence, the composition of the liquid that led to the formation of the last rocks in the sequence was attained by averaging the compositions of these late-formed rocks (Wager, 1960). The next liquid composition, the liquid composition just younger than the last, is then calculated by using again the average composition of the rocks that formed from it, but also including the average composition of the later liquid (Wager, 1960). This is then applied repeatedly as far down the sequence as it is physically possible to attain samples and estimates of volume for. Wager (1960) is an attempt at improving on this by making use of a graphical method.

The three vital variables for this method is the volume of rock present, the bulk-rock composition and the composition of the original liquid. The original liquid is taken as the olivine gabbro chilled margin. The chosen sample is from near the southern boundary of the intrusion, about 3 ft away from the contact. Only one sample was chosen as the starting liquid composition, but apparently the average from all the starting liquid samples equals more or less that of the chosen sample (Wager, 1960). These values are given in Table 8. The original paper by Wager and Deer (1939) estimated by the overall volume by extrapolating the layered series both downward beyond outcrop and upwards, compensating for erosion. These estimates lead to a ratio of observable to hidden volume of about 3:2. Using this ratio some of the oxides in the HZ were reduced to zero. Therefore the HZ was assumed to be

more voluminous than expected, giving a ratio of 2:3. Problems again arose in the form of negative values for P_2O_5 in HZ. In the end chemical data was used instead of extrapolation, and is once again used here.

Table 8. Chilled Margin compositions for the three samples taken by Wager (1960) that serve as the starting composition for their LLD. From Wager (1960).

	4507	1724	1825	*Average*
SiO_2	48·08	47·83	48·01	47·97
Al_2O_3	17·22	18·62	19·11	18·32
Fe_2O_3	1·32	1·16	1·20	1·23
FeO	8·44	8·87	8·44	8·58
MgO	8·62	7·92	7·72	8·09
CaO	11·38	10·59	10·33	10·77
Na_2O	2·37	2·54	2·34	2·42
K_2O	0·25	0·20	0·17	0·21
H_2O^+	1·01*	0·27	0·55	0·61
H_2O^-	0·05	0·16	0·05	0·09
TiO_2	1·17	1·29	1·51	1·32
P_2O_5	0·10	0·06	0·07	0·08
MnO	0·16	0·09	0·12	0·12
TOTAL	100·17†	99·00	99·62	99·81

4507. Southern margin near coast on east side of Skaergaard Bay. Specimen 3 ft from contact with lavas. Anal.: E. A. Vincent and B. A. Collett. Various trace constituents have been determined (see Wager, Vincent, & Smales, 1957).
1724. Southern margin near coast on east side of Skaergaard Bay. Specimen 25 m from contact with lavas. Anal.: W. A. Deer.
1825. South-eastern margin at head of Udlöberen. Specimen 3 m from contact with lavas. Anal.: W. A. Deer.

4.2.2 Methodology

The new graphical method developed by Wager (1960) is explained with the use of Figure 23. Figure 23 illustrates the amount of TiO_2 crystallised against total volume of crystallisation for the intrusion. It is assumed that the volume for each unit is directly proportional to its thickness, thus the percentage crystallised is also proportional to the thickness (Wager, 1960). This excludes a half percent at the end of crystallisation to account for the intermediate and acidic rocks. Four figures are presented in Figure 23, each one depicting a different assumption with regards to the amount of intrusion crystallised at the bottom of the observable rocks. In Figure 23A it is assumed that 60% crystallisation had taken place at the bottom of the observable rocks, in Figure 23B it is 70% and in Figure 23C 80%. These graphs are then used to see which assumption produces the more probable outcome.

In Figure 23A the TiO_2 value drops to below zero before the actual start of crystallisation of the earliest layered rocks, which is impossible. Thus, other assumptions on the amount of crystallisation that had occurred in the lowest of the observable rocks were made and can be seen in Figure 23B. For 23B it is 70% and 80% for 23C. Assuming that 70% of the magma had crystallised at this point it gives a value of 0.6 % TiO_2, whereas the 80% crystallised assumption produces a TiO_2 percentage of 0.9 (Wager, 1960).

To plot the TiO_2 values against percentage of crystallisation of the intrusion, the average composition of TiO_2 is taken from Table 8. These values correspond to a certain lithological height, which in turn are directly associated with the percentage of crystallisation. The starting liquid composition in terms of TiO_2 is assumed to be 1.17 wt.%, taken from the TiO_2 value in Table 8. Wager (1960) states, that the total TiO_2 for the intrusion is equal to the area *oabc* (Fig. 23) The quantity of TiO_2 in the visible rock is proportional to the area between the abscissa and the curve *QRSTU*, thus the area *QRSTUCD*. It is important that the dashed line part of the curve extends to the left as this will give the TiO_2 values for the rocks of the HZ (Wager, 1960).

What happens before (to the left of) the curve moving away from the starting point (the first measured amount of TiO_2 in the observable rocks) is controlled by the statement that the area under the curve, *PQRSTU*, which is the total amount of TiO_2 in the intrusion, is proportionally equal to the rectangle *oabc* (Wager, 1960). The estimated portion of the graph (left of *Q*) is therefore controlled by the fact that it cannot exceed the maximum amount of TiO_2 which is defined by the area of *oabc*. The area *PQ* is therefore adjusted accordingly.

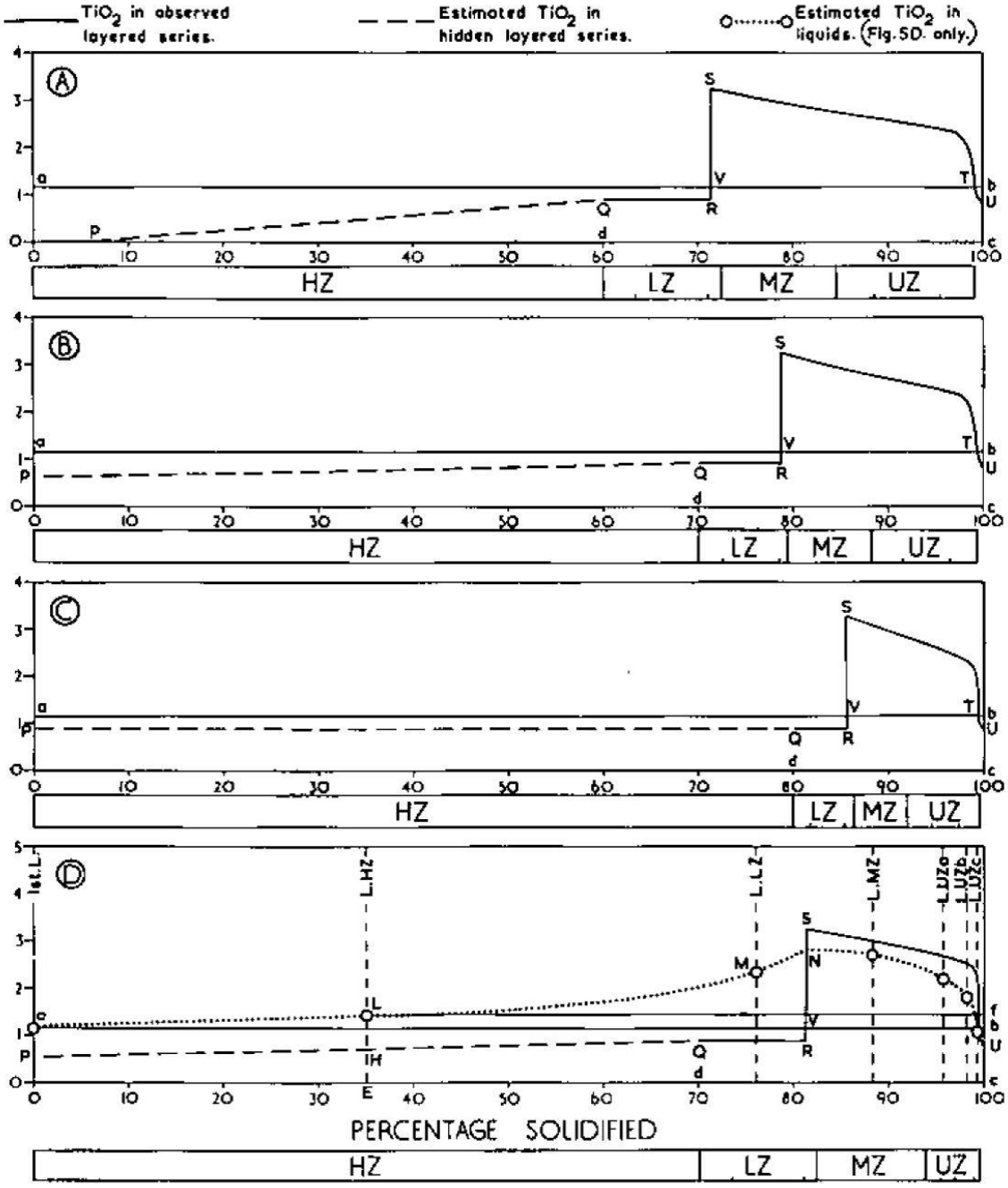

FIG. 5. The TiO_2 content of layered rocks, plotted against percentage solidified, with various assumptions about the relative volumes of the observed and hidden layered series, and deduction of TiO_2 composition of HZ rocks and of successive liquids (Fig. 5D only):

A, assuming lowest observed layered rock formed when 60 per cent of the intrusion was solidified.

B, assuming that the lowest layered rock formed at 70 per cent solidified.

C, assuming that the lowest layered rock formed at 80 per cent solidified.

D, the same as B with the additional assumption that the UZ rocks have, on the average, half the volume they would have had if the volume were proportional to thickness. On this graph the estimated composition of successive liquids is also shown.

Figure 23. The modelled LLDs produced by Wager 1960. From Wager (1960).

Calculating the composition of the successive residual magmas is done using the same method as described above. The example makes use of the amount of TiO_2. The starting liquid composition in terms of TiO_2 has been established as 1.17% from the chilled olivine gabbro margin. This is shown in Figure 23D as point *a*. At 35% solidified, which is the average for HZ, the point *L* indicates the amount of TiO_2. This point was determined because the amount of TiO_2 in the intrusion from 35 to 100% solidified is equal to the area *HQRSUcE*. The point L is then chosen as the point where the rectangle *LfcE* is equal to the area *HQRSUcE*. At the maximum point for TiO_2, which is *N*, the amount drops off due to titaniferous magnetite precipitation (Wager, 1960).

4.3 Hunter and Sparks (1987)

4.3.1 Introduction

Hunter and Sparks (1987) argue that the classic model for differentiation of Skaergaard, which involves iron-enrichment, is incorrect and consequently present a different model. The classic model doesn't involve any silica enrichment until c. 98% crystallisation (Hunter and Sparks, 1987). The model presented here shows iron-depletion and silica-enrichment, during which the liquid line of descent evolves from olivine basalt through to rhyolite. This type of evolution has been quantified in Iceland and a discussion on the liquid evolution as well as the coexisting cumulus phases is presented. This evolution is then compared to the Skaergaard intrusion.

4.3.2 Reasoning

McBirney and Nakamura (1974) and McBirney (1975) produced a comparable trend to Wager (1960), in that it represents a continual decrease in SiO_2 during differentiation until, at low temperatures, a liquid miscibility gap appears, at which point a silica-rich liquid segregates (Hunter and Sparks, 1987). To produce a representative universal intercumulus melt by remelting of Skaergaard rocks is a potentially inaccurate method for inferring a liquid line of descent, as post cumulus processes are complex and can produce varying compositions depending on factors such as re-equilibration, zoning, loss of intercumulus melt by compaction and melt circulation (Hunter and Sparks, 1987). Thus, Hunter and Sparks (1987) discards this

LLD on the basis that such an intercumulus melt represents a mixture of liquids formed by various processes during the final stages of crystallisation and cannot be assumed to be a representative example of the single intercumulus melt in existence at that time (Hunter and Sparks, 1987). The remelting of these rocks can therefore yield liquids that are not suitable for use in the modelling of the liquid line of descent (Hunter and Sparks, 1987).

The lack of similar rocks to the ones found in Skaergaard might suggest that the processes taking place during crystallisation were atypical, or that the liquids produced were too dense to erupt (Hunter and Sparks, 1987). The possibility that the liquids were too dense to erupt is a consequence of the extreme iron-enrichment proposed by Wager (1960) and McBirney (1975) and leads to some difficulty in understanding exactly how the physical processes that lead to the formation of layered suites work (Bottinga and Weill, 1970; McBirney and Noyes, 1979). The Skaergaard rocks are considered to be the “cumulus assemblages extracted during the evolution of the parental liquid” (Hunter and Sparks, 1987). In this case that involves evolution from “olivine basalt through ferrobasalt, basaltic andesite, tholeiitic andesite (icelandite) and dacite, to rhyolite (Hunter and Sparks, 1987). .

Hunter and Sparks (1987) propose that the Skaergaard magma started out as evolved tholeiitic basalt and followed a differentiation path from ferrobasalt in the Lower Zone; to icelandite in the Middle Zone up to the horizon where apatite appears as a cumulus phase in the Upper Zone; and to an iron-rich rhyolite in the Sandwich Horizon. Hunter and Sparks (1987) identify that difficulties exist in the constraints of all three parts of the reconstruction of the Skaergaard liquid line of descent, namely the residual liquid; the mineral extract and the parent liquid. The latter’s main issue is that chilled margins are often altered by assimilation and the samples chosen by Wager (1960) demonstrate variability. The unknown dimensions of the Hidden Zone make it extremely difficult and risky to model the entire evolution of the Skaergaard intrusion (Hunter and Sparks, 1987).

Hunter and Sparks (1987) propose that the reasonable constraints on the SiO_2-content of the residual liquid at the point of magnetite crystallization, the bulk composition of the Layered Series above and including LZc make it effectively

possible to calculate and model the liquid trends from this point onward. From the onset of magnetite crystallization in LZc the dissimilarity in SiO_2 content between the bulk-cumulus extract and residual liquid will be greatly enhanced (Hunter and Sparks, 1987). The residual liquid will evolve toward a rhyolitic composition and by comparison with evolved rhyolites from Iceland and Hebrides it is clear that these liquids are in equilibrium with iron-rich ferromagnesian silicates, Fe-Ti oxides and sodic plagioclase which are found in UZc and SHR (Hunter and Sparks, 1987).

4.3.3 Liquid Line of Descent

It is fairly obvious that the bulk composition of the ferrobasalt at the point of magnetite crystallization must be able to cater for all the phases formed from the base of LZc to the SHR at the top of UZc (Hunter and Sparks, 1987). The parent liquid can then be considered to lie on a tie-line that connects the rhyolite formed from the differentiation of the residual liquid to the bulk composition of the Layered Series above LZb (Hunter and Sparks, 1987). Considering the starting SiO_2 content of 50-52% for LZc and using the lever rule, compositions for parental liquids containing both 50% and 52% SiO_2 were calculated. These two compositions were calculated from the bulk composition of the cumulus extracts which was in turn calculated from estimated thicknesses and bulk-composition data for the main zones of Layered Series as proposed by Wager and Brown (1968), and from the Tinden Sill's composition. The Tindel Sill was chosen by Hunter and Sparks (1987) as a representative sample of the residual rhyolite. These calculated liquid lines of descent are shown in Figure 24, and the calculated compositions are shown in Table 9.

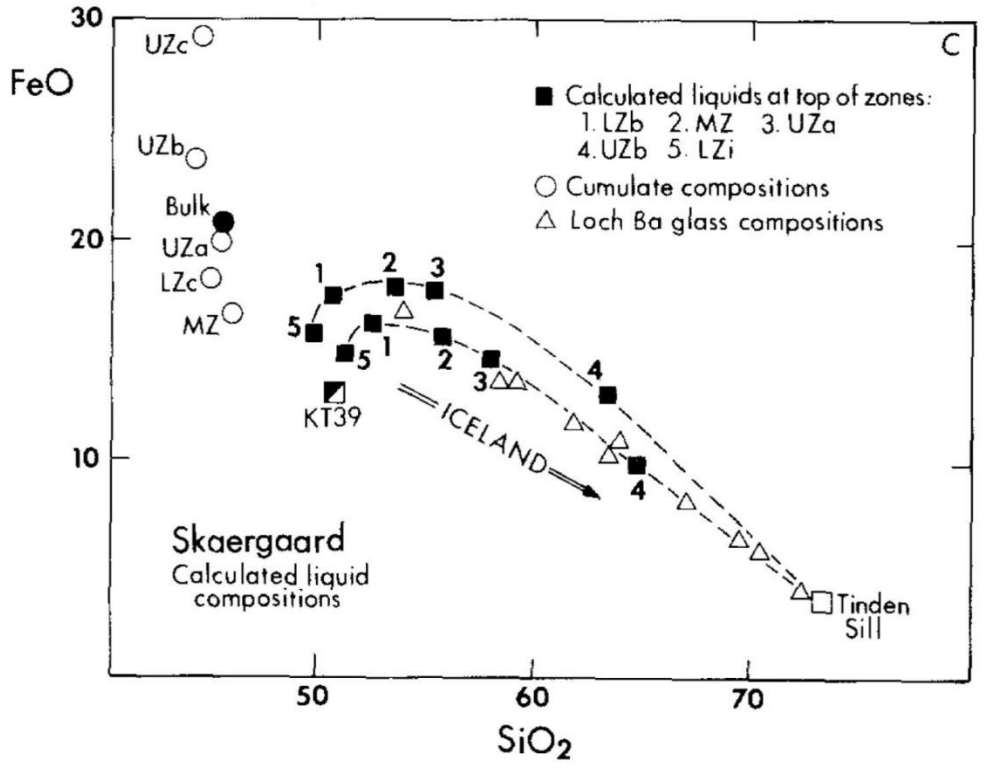

Figure 24. Total iron as FeO versus SiO_2 for Icelandic tholeiites and Skaergaard liquid compositions. Lower Zone liquid is calculated by addition of the LZ cumulate average to parental ferrobasalts. Black filled circle indicates Bulk, which represents the calculated composition for LZc + MZ + UZ. Cumulates are taken as the average for each zone measured by Wager and Brown (1968). KT 39 is the chilled margin composition taken by Hoover (1978). From Hunter and Sparks (1987).

Table 9. Calculated liquid compositions at the top of the main zones of Skaergaard using parent ferrobasalts with 50 and 52% SiO_2. From Hunter and Sparks (1987).

	Parent	MZ	UZa	UZb	UZc	LZi	Parent	MZ	UZa	UZb	UZc	LZi	KT39
SiO_2	50.0	53.1	54.8	62.8	73.2	49.2	52.0	55.9	57.9	65.9	73.2	50.7	50.1
TiO_2	2.31	1.90	1.72	1.11	0.46	1.94	2.16	1.75	1.56	1.00	0.46	1.83	2.64
Al_2O_3	13.1	11.7	11.3	11.4	13.2	13.9	13.1	12.0	11.7	12.1	13.2	14.0	13.4
Fe_2O_3	3.05	2.90	2.76	2.12	0.92	2.73	2.88	2.66	2.49	1.82	0.92	2.60	1.77
FeO	14.5	15.3	15.1	11.2	2.83	13.5	13.5	13.7	13.2	8.98	2.83	12.7	11.8
MnO	0.23	0.27	0.29	0.30	0.01	0.19	0.19	0.19	0.19	0.13	0.01	0.10	0.20
MgO	3.84	2.00	1.37	0.27	0.16	5.32	3.64	1.79	1.18	0.22	0.16	5.17	6.54
CaO	8.31	7.05	6.44	4.21	1.81	9.00	7.78	6.48	5.82	3.74	1.81	8.62	10.1
Na_2O	3.13	3.31	3.34	3.51	4.05	3.02	3.24	3.43	3.48	3.70	4.05	3.10	2.42
K_2O	0.82	1.20	1.41	2.22	3.28	0.68	0.88	1.24	1.43	2.07	3.28	0.72	0.57
P_2O_5	0.65	1.03	1.24	0.52	0.03	0.50	0.60	0.89	1.05	0.40	0.03	0.46	0.22
I[a]		40.0	18.3	42.9	35.7	−26.0		36.0	16.7	36.6	26.9	−26.0	
f[b]		0.60	0.49	0.28	0.18			0.64	0.53	0.34	0.25		

4.5 Toplis and Carrol (1995)

4.5.1 Introduction

Toplis and Carrol (1995) investigated the effect that Oxygen Fugacity has on Fe-Ti oxide stability, their phase relations and mineral-melt equilibria in Ferro-basaltic systems. It is known that differentiation of a sub-alkaline basalt under low-pressure produces a tholeiitic trend, becoming enriched in iron before the onset of Fe-Ti oxide precipitation. Toplis and Carrol (1995) attempt to constrain exactly what conditions, specifically the conditions surrounding oxygen fugacity, lead to the kind of extreme iron-enrichment supposedly evident in Skaergaard.

It is well documented that the liquid line of descent and phase equilibria is greatly affected by magnetite stability. Iron depletion in the melt is unavoidable after the arrival of magnetite crystallisation, assuming a fixed fO_2 (Osborne, 1959; Presnall, 1966). Iron enrichment beyond this point has been shown to be possible upon the occasion that fO_2 is low enough to suppress magnetite crystallisation, and/or in closed magnetite-saturated systems. It must be stressed that these experimental systems do not contain sodium or titanium therefore ignoring the important plagioclase solid solution series and all titanium-bearing minerals which have been shown to be very important in the Skaergaard Layered Series (Toplis and Carrol, 1995).

Toplis and Carrol (1995) attempt to provide: experimental phase relations applicable to Skaergaard; Fe-Ti oxide stabilities; melt compositions trends and mineral-melt partitioning of major elments. These experiments were all done, where applicable, over a range from 2 log units below to 1.5 log units above the fayalite-magnetite-quartz (FMQ) buffer. The aim is to determine whether previous work done by Osborn (1959) and Presnall (1966) is applicable to complex natural systems, especially concerning the effect of magnetite crystallisation on liquid lines of descent. Moreover, the aspects controlling saturation surfaces of Fe-Ti oxides in natural systems are assessed. The results of the study allow for estimation of the liquid lines of descent in systems that are open or closed to oxygen, but these results are published in Toplis (1994) and Toplis and Carrol (1996).

4.5.2 The experiment

The starting composition is a synthetic ferro-basalt with eight components (Si-Ti-Al-Fe-Ca-Mg-Na-K oxides). It parallels compositionally to the proposed parental magma for Skaergaard (basaltic dyke C of Brooks and Nielsen (1978)). There is no manganese in the basalt but this is not expected to have a noticeable effect on the outcome (Toplis and Carrol, 1995). The lack of phosphorous, however, which has a suppression effect on magnetite crystallisation is can be problematic but is not expected to influence the main conclusions reached in this study (Toplis and Carrol, 1995). fO_2 has a potentially massive influence on the Fe^{3+}/Fe^{2+} ratio and the range is therefore very important to get it as close to the actual values in the natural system as possible (Kennedy, 1948; Fudali, 1965; Sack *et al.*, 1980; Kilinc *et al.*, 1983). Assuming a static composition the Fe^{3+}/Fe^{2+} ratio of the melt phase is roughly constant along T- fO_2 paths that run parallel to the FMQ buffer (Fudali, 1965; Sato, 1978; Carmichael and Ghiorso, 1986). The chosen fO_2 of FMQ+1 to FMQ-2 falls within the range inferred for both plutonic and volcanic tholeiitic rocks (Williams, 1971; Frost *et al.*, 1988; Carmichael, 1991). This chosen range results in a starting composition atomic Fe^{3+}/Fe^{total} of ~0.21 at FMQ+1 to ~0.06 at FMQ-2, using the calculation outline provided by Kilinc *et al.* (1983).

The starting materials for these experiments were glass powders primed from reagent grade oxides, namely: SiO_2; TiO_2; Al_2O_3; Fe_2O_3; MgO; and carbonates $CaCO_3$; Na_2CO_3; K_2CO_3. Because of the difficulty in maintaining a large liquid proportion over a wide crystallisation period two starting compositions were used. The first, named SC1, was used in experiments that range from near liquidus to ~50% crystallised. The second, SC4, was synthesized to reflect as closely as possible the residual glass composition after ~40% crystallisation of SC1. For a full discussion on the sample preparation and experimental methods the reader is referred to Toplis and Carrol (1995). It is noted that oxygen fugacity was kept in check by making use of a CO-CO_2 gas mixture (Deines *et al.*, 1974). The appraisal was done by making use of an yttrium-stabilized zirconia probe that was calibrated against the Ni-NiO reaction (Huebner and Sato, 1970). The linear flow rate was 3mm/s which supposedly fixed fO_2 whilst reduced Na_2O loss (Tormey *et al.*, 1987).

4.5.3 Results

In all the tested conditions Fe-Ti oxides crystallise after the appearance of clinopyroxene, but in the case of magnetite and ilmenite are heavily dependent on oxygen fugacity conditions. SC1 liquidus is at ~1162 °C, at which point olivine and plagioclase start to crystallise. Plagioclase is a stable phase in all the studied experimental temperatures and oxygen fugacities. SC4 does not contain any olivine as it represents the liquid phase at ~40% crystallisation, i.e. at which point olivine had already ceased to crystallise. Ca-rich pyroxene crystallises third, also at all experimental conditions. Magnetite is the fourth phase to crystallise above the FMQ buffer, shadowed by ilmenite at lower temperatures, but is the inverse below the FMQ. Magnetite initially crystallises at ~1125°C during FMQ+1 conditions, and the liquidus drops by ~30°C per log unit decrease in oxygen fugacity. At negative FMQ conditions ilmenite's liquidus remains relatively constant. It is noted that there exists dissimilarity in the liquid products of SC4 and those found in the continued crystallisation of SC1, despite both being under virtually equilibrium conditions, due to the supposed fractionation and therefore removal of the solid phases.

TiO_2 content in the melt increase steadily during the initial crystallisation until Fe-Ti oxides are precipitated. At negative FMQ values TiO_2 content peaks at ~5-5.5 wt.% and ~1100°C, coinciding with the arrival of ilmenite on the liquidus, and drops off promptly with continued cooling. At positive FMQ values TiO_2 never surpasses 5 wt.% and is blissfully unaffected by magnetite crystallisation. Values start to drop once ilmenite crystallisation commences.

The iron in the melt acts in a very specific way: the total amount of iron, i.e. the maximum, increases with a decrease in fO_2 and simultaneously the temperature at which the maximum is attained will decrease. In other words, as the fO_2 goes down, more iron enrichment takes place in the melt as well as the temperature at which iron concentration peaks goes down, therefore giving more time for enrichment to occur. Toplis and Carrol (1995) provide the example: ~15 wt.% FeO at FMQ+1 and ~18.5 wt.% FeO at FMQ-2. At negative FMQ values, ilmenite is the first Fe-Ti oxide phase to crystallise. The maximum iron content in the melt is much broader at these low FMQ values, and it occurs on the low temperature side of ilmenite's solidus. It

seems that the appearance of ilmenite in the cumulus phase does not immediately halt iron enrichment, but it does start to restrict the enrichment and eventually lead to the conclusion of this event. Magnetite's appearance does however immediately terminate enrichment and leads to a steady decline in iron content. Magnetite emerges on the liquidus concurrently with the maximum iron content at conditions above FMQ.

Silica content initially lingers around its original value of ~48 wt.% during the opening periods of crystallisation but surges promptly under high fO_2 conditions as magnetite crystallises early. The melt composition, in terms of silica and iron, is heavily influenced by the variation in oxide minerals present, as shown in Figure 25.

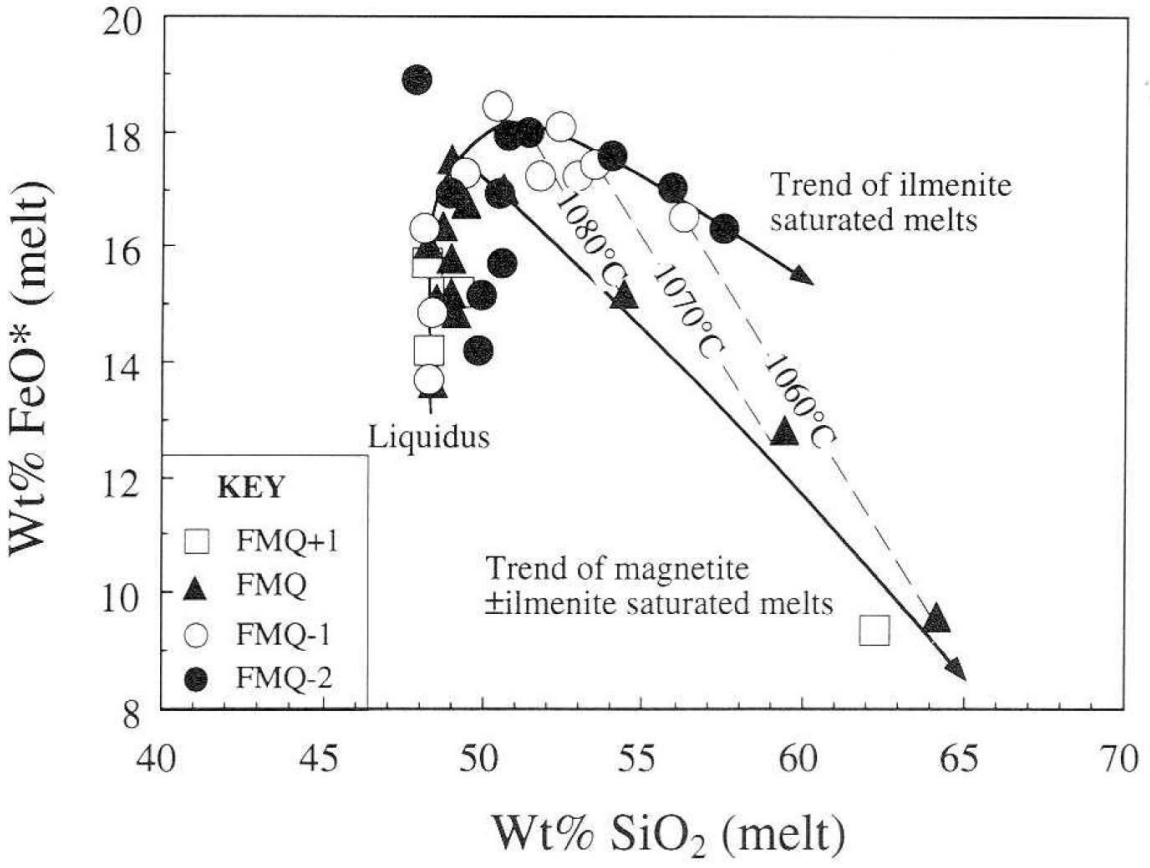

Figure 25. Figure demonstrates covariation in silica and iron (total iron as FeO) at varying fO_2. Dashed lines represent isotherms for ilmenite and magnetite (±ilmenite) for both magnetite- and ilmenite-saturated melts (solid lines). From Toplis and Carrol (1995).

Initial iron enrichment takes place at constant SiO_2 before Fe-Ti oxide saturation for all experiments (Fig. 25). The melts saturated in magnetite and

ilmenite respectively, diverge strongly from each other as cooling continues. At FMQ conditions, the melt is depleted in iron instantly, following magnetite-saturation. Both ilmenite- and magnetite-saturated melts produce an increase in silica content once Fe-Ti oxide crystallisation commences. However, at identical temperature, magnetite saturated melts lead to a superior increase in silica.

4.6 Tegner (1997)

4.6.1 Introduction

Most of the studies conducted in the 90s aimed at defining the liquid line of descent for tholeiitic basalts, are done by experimental modelling (eg. Snyder *et al.*, 1993; Toplis and Carrol, 1995), and they all conclude that the appearance of Fe-Ti oxides leads to the magma following the Bowen trend of evolution. However, Tegner (1997) analysed a ~950 m borehole drilled through the Upper Zone of the Skaergaard layered intrusion (Fig. 26), the zone associated with iron enrichment as it represents the most evolved liquids, and found that by modelling the evolution of the liquid by incremental bulk-rock summation the iron content increased from 20.1 to 26.5 wt.% FeO_T as did the silica content from 47.5 to 49.6 wt.% SiO_2, which is known as the Fenner trend.

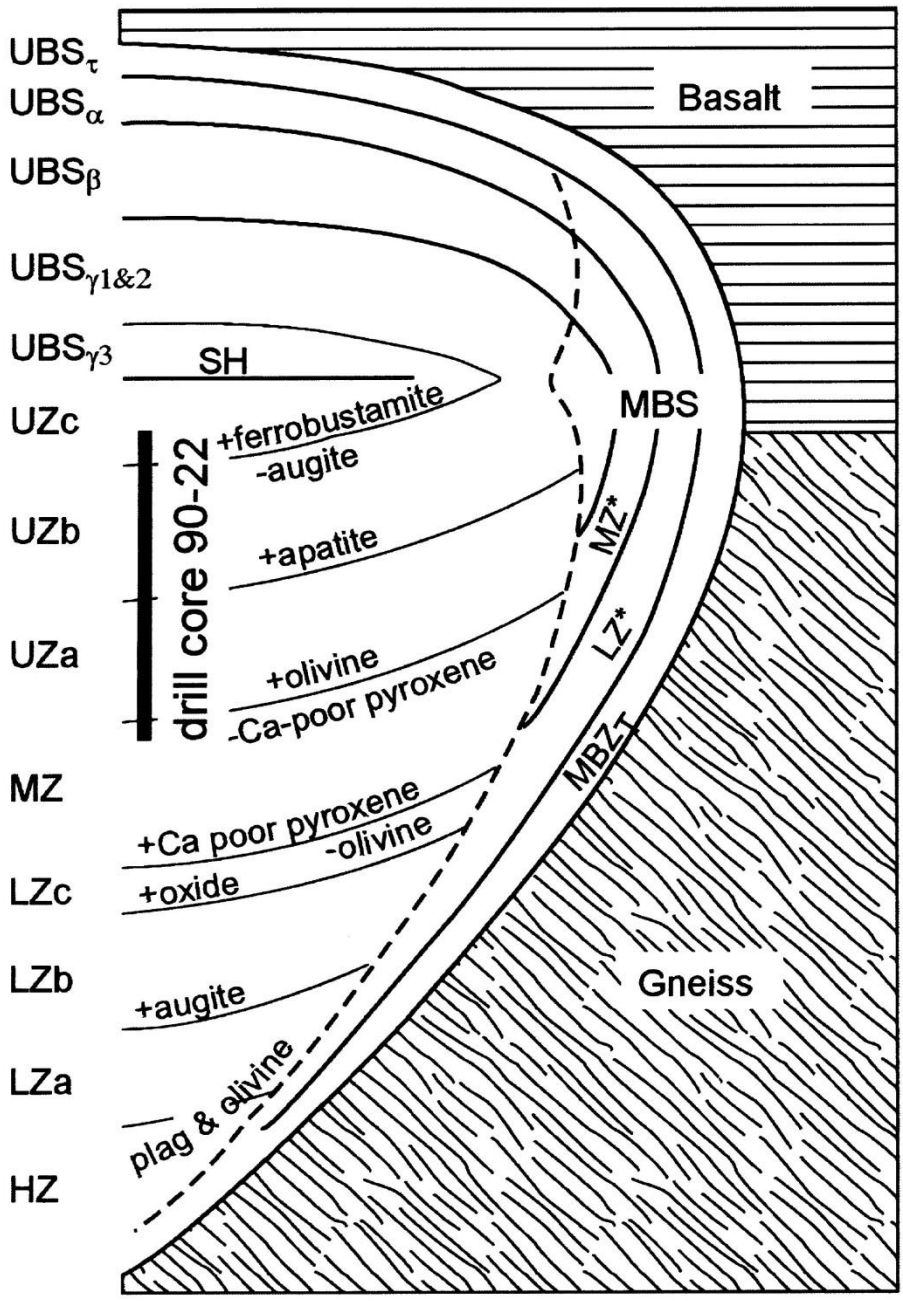

Figure 26. Stratigraphy of Skaergaard. From Tegner (1997).

Other studies concerned with obtaining the Skaergaard liquid line of descent have also come to similar conclusions, but they used different methods and these will be discussed later on. Tegner (1997) found a positive correlation between the modelled iron content of the magma and the measured iron content in the plagioclase, which is believed to confirm that iron enrichment is feasible. Tegner (1997) states the most obvious reason for this to occur in nature is when fractional crystallisation takes place with the system closed to oxygen exchange. Osborn

(1959) and Presnall (1966) show that oxygen fugacity and the crystallisation of magnetite strongly influences the liquid line of descent. If low oxygen fugacity conditions prevail, a Fenner trend arises, and conversely high oxygen fugacities lead to a Bowen trend (Tegner, 1997). Other authors to question whether iron enrichment is possible at all are: (Hunters and Sparks, 1987, 1990; Thy and Lofgren, 1994).

Skaergaard is a good testing ground for these two theories because it represents a highly differentiated igneous body that was supposedly a closed system (Tegner, 1997). Previous work has been the basis for assuming that Skaergaard is an example of iron enrichment, most notably by Wager (1960); Brooks and Nielsen (1978, 1990); McBirney and Naslund (1990); and Hanghøj *et al.* (1995) (Fig. 27). From a petrological point of view there is strong evidence that Skaergaard is an example of "extreme, closed-system fractional crystallisation of tholeiitic magma" (Wager and Brown, 1968; Naslund, 1984; Hoover, 1989; McBirney 1989, 1995). Larsen and Brooks (1994) believe that the presence of discordant gabbro pegmatites point to very little, if any, material was removed during solidification. McBirney (1975, 1989) backs up this statement citing pods of melanogranophyre which could be the result of liquid immiscibility. Estimated liquid compositions produced in this study are given in Table 10.

Table 10. The estimated liquid compositions produced by Tegner (1997). From Tegner (1997).

	This study	H&al[b]	B&N[b]	M&N[b]	W&B[b]	T&al[b]	H&S[b]
SiO_2	47.4	45.7	46.3	46.7	47.4	51.1	53.8
TiO_2	3.7	4.6	5.9	3.6	2.2	4.0	1.9
Al_2O_3	11.9	11.8	11.1	9.5	12.5	10.3	11.9
FeO_T	20.1	17.1	17.1	22.7	20.7	18.5	18.2
MnO	0.3	0.2	–	0.4	0.3	–	0.2
MgO	3.3	3.5	6.3	3.2	2.5	2.9	1.8
CaO	8.5	12.8	10.0	10.0	9.5	8.2	6.6
Na_2O	3.4	3.0	2.4	2.4	3.2	2.9	3.5
K_2O	0.6	0.4	0.9	0.5	0.6	0.9	1.3
P_2O_5	0.8	0.8	–	1.2	1.2	1.1	0.9

[a] Recalculated to 100% volatile free.
[b] H&al = Hanghøj et al. (1995); B&N = Brooks and Nielsen (1990); M&N = McBirney and Naslund (1990); W&B = Wager and Brown (1968); H&S = Hunter and Sparks (1987); T&al = Toplis et al. (1994).

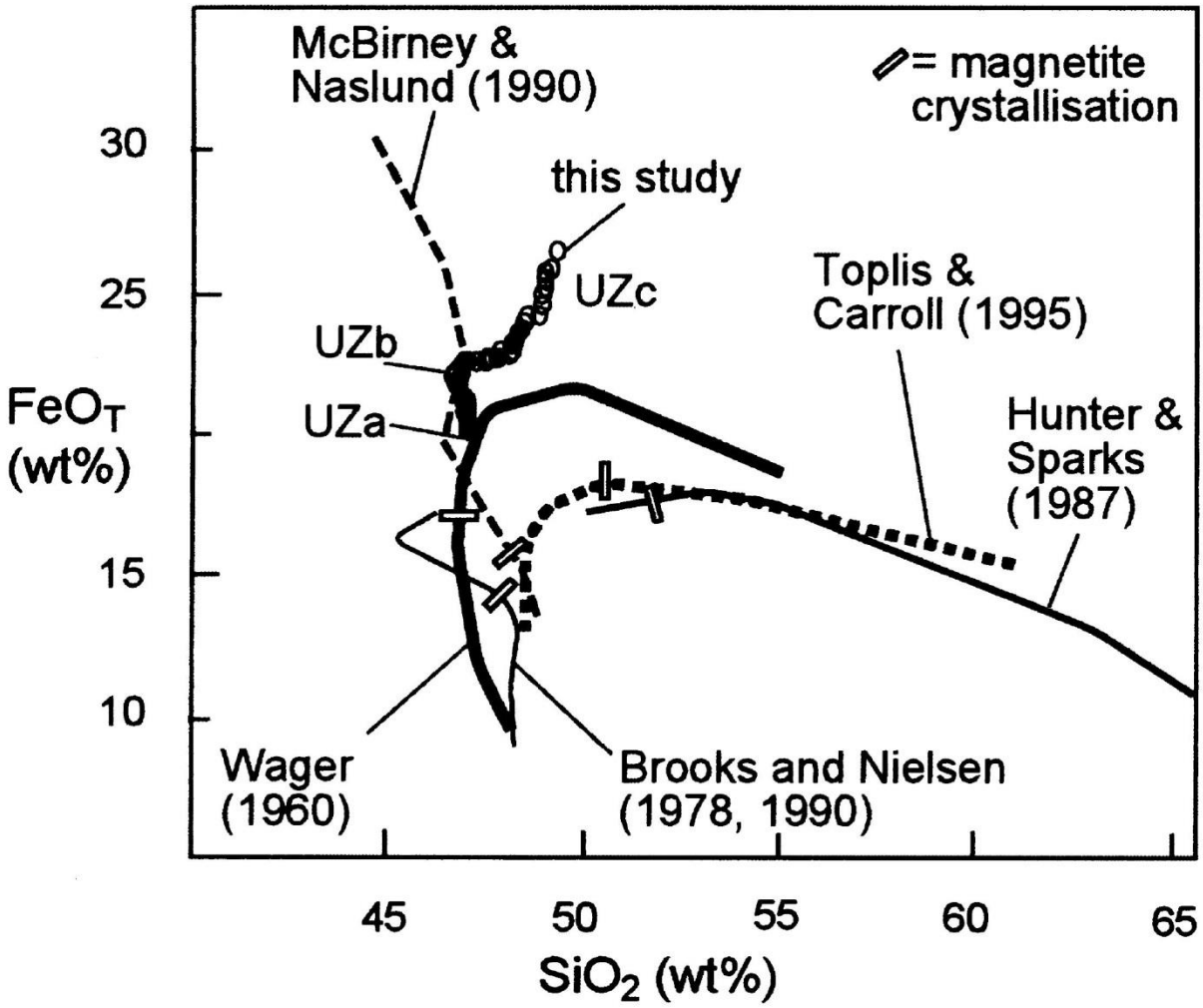

Figure 27. The diagram shows a collection of LLDs produced by various authors. From Tegner (1997).

4.6.2 Liquid Line of Descent

The smooth trend displayed by anorthite (Fig. 28) (An% = (Ca/(Ca + Na))), which decreases from An_{46-32} with increase in stratigraphic height also supports this (Tegner, 1997). Iron content in plagioclase (FeO_T plagioclase) shows in inverse relationship with An% and increases with stratigraphic height. Bulk SiO_2 stays relatively constant in the first half of the borehole and then decreases from ~45 wt.% to ~36 wt.% at ~400 m, after which it increases to ~45 wt.% at the top of the hole. The lower values of bulk SiO_2 corresponds to a melanocratic section in the lower portion of the UZb (Tegner, 1997).

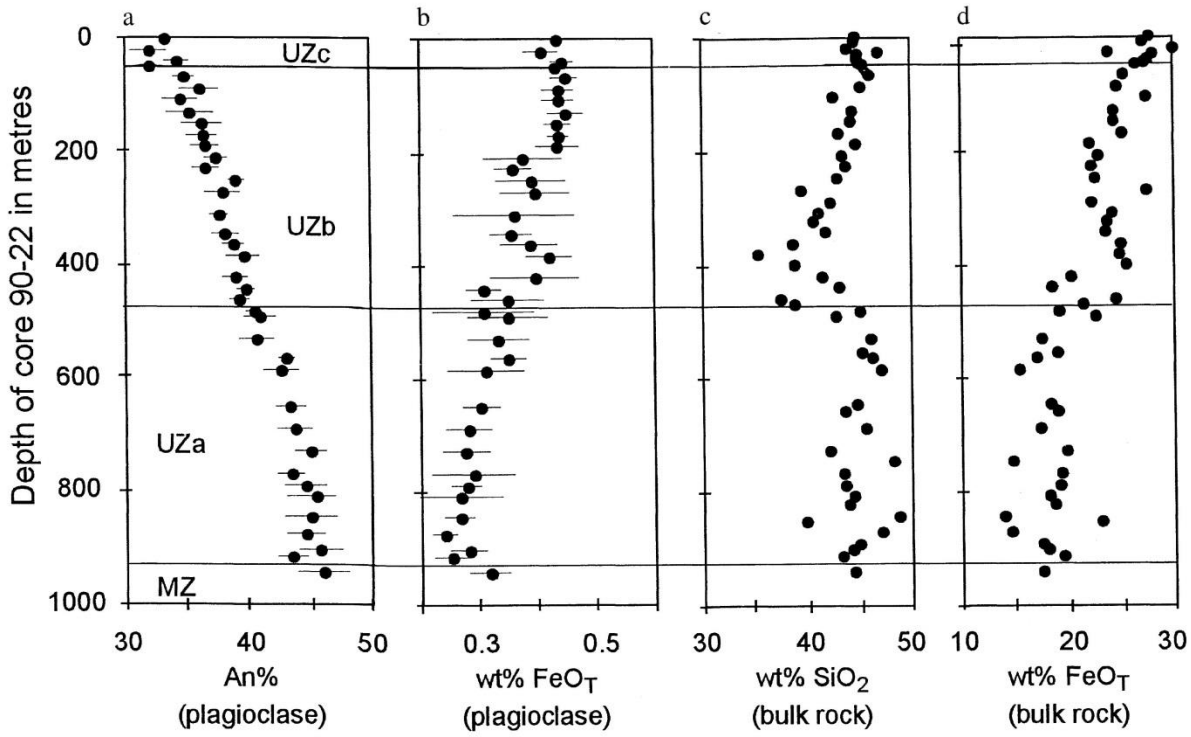

Figure 28. Analysed data plotted against depth of drill core 90-22. From Tegner (1997)

Bulk FeO_T follows a similar trend to that of FeO_T in plagioclase, but stays slightly more constant in the UZa portion (~18 wt.%), but increases to ~30 wt.% at the top of UZc. The borehole was drilled by Platinova Resources Ltd. and its ~950 m represents ~62% to 95% of the fractionation product (McBirney, 1975, 1979).

As previously stated, iron partitioning into plagioclase is highly dependent on the oxidation state of iron. Fe^{3+} and Fe^{2+} substitute into the tetrahedral T-sites of plagioclase and Fe^{2}+ into the interstitial M-sites. The partition coefficient of iron into plagioclase is determined by the equation: (D_{iron} = wt.% FeO_T in crystal/wt.% FeO_T in melt) for calcic plagioclase (>An_{75}) which show a 12-fold increase from ~0.030 at very low oxygen fugacities through ~0.044 at (FMQ) to ~0.36 in air (Phinney, 1992).

4.6.3 Oxygen Fugacity and Iron in Plagioclase

Previous work done on the determination of f_{O2}all conclude that the f_{O2} for Skaergaard magma in the Upper Zone was well below the FMQ buffer at the time of intrusion, and that the f_{O2}levels decreased by 2-3 log units below FMQ as fractionation continued toward the Sandwich Horizon (Williams, 1979; Morse *et al.*,

1980; Frost and Lindsley, 1992). Thus, with levels of f_{O2} dropping as fractionation continues, it would be impossible to achieve the results seen in measured FeO_T content, as a drop in FeO_T is to be expected, not the inverse (Bernstein *et al.,* 1992). In work done by Smith (1983) and Smith and Brown (1987) it is seen that iron content in plagioclase decreases with decreasing An%. This relates nicely to the stoichiometry of plagioclase, in that a decrease in albite ($CaAl_2Si_2O_8$) content and thus an increase in anorthite ($NaAlSi_3O_{8)}$ will give rise to more Si^{4+} ions occupying the T- and M-sites in anorthite, leaving less space for the Fe^{3+} and Fe^{2+} ions (Tegner, 1997). Thus, a change in major element crystal composition cannot account for the inverse relationship between FeO_T and An% (Tegner, 1997). The only alternative is that the iron content in plagioclase found in Skaergaard must be directly related to the iron content (predominantly Fe^{2+}) of the fractionating magma (Tegner, 1997).

4.6.4 Methodology

Tegner (1997) uses the bulk summation method to estimate liquid evolution. As Tegner (1997) rightly points out, the biggest issue with this type of modelling is with regards to the estimation of volume and composition. Cumulates were formed on the floor, roof and walls of the chamber (floor: floor of the LS; roof: UBS; walls: MBS). Unfortunately the borehole only cuts through the central part of the Upper Zone, thus not sampling the correct proportions of cumulate (Tegner, 1997). The calculation makes use of 50 samples, one every ~20 m (Tegner, 1997). Naslund (1984) and McBirney (1995) estimated the UBS to LS volumetric ratio to be 3:1. MBS cumulates are ignored in this study as Hoover (1989) determined their bulk-rock composition to lie somewhere between LS and UBS, plus they are volumetrically insignificant at this stratigraphic height (Tegner, 1997). The bulk composition of UBS is taken as an average between $UBS_{\gamma 1}$ and $UBS_{\gamma 2}$ (Naslund, 1984). A summary of the cumulate compositions used for the modelling is shown in Table 11. A notable obstacle is the existence of exsolved melanogranophyres (Tegner, 1997). Melanogranophyre quantities increase toward the Sandwich Horizon (Wager and Brown, 1968; McBirney, 1989). Within each section of the Upper Zone, UZa, UZb and UZc, it is estimated that 2, 8 and 15 volume% exsolved, respectively (Tegner, 1997). The ratios for LS to UBS to melanogranophyre read thus as 74:24:2 for UZa, 69:23:8 for UZb and 64:21:15 for UZc (Tegner, 1997).

Table 11. Average rock compositions for calculated liquids. From Tegner 1997.

Rock / Depth of Core 90-22 (m)	1[b]	2[b]	3[b]	UZa[c] 809.2	UZb[c] 249.2	UZc[c] 10.6
SiO_2	54.01	59.06	49.34	44.97	43.61	45.39
TiO_2	2.35	1.18	2.14	5.33	3.56	2.96
Al_2O_3	12.76	14.69	8.30	11.97	11.95	8.95
FeO_T	16.03	13.45	26.70	18.50	23.04	27.70
MnO	0.20	0.24	0.40	0.26	0.34	0.73
MgO	1.43	0.58	0.20	6.32	2.94	0.27
CaO	7.45	4.57	9.02	9.79	9.34	10.20
Na_2O	3.78	3.83	2.68	2.64	3.20	2.71
K_2O	1.16	2.05	0.66	0.17	0.29	0.24
P_2O_5	0.82	0.35	0.56	0.05	1.73	0.83

[a] Recalculated to 100% volatile free.
[b] 1 = average of $UBS_{\gamma 1}$ and $UBS_{\gamma 2}$ (Naslund 1984), 2 = average melanogranophyre (Wager and Brown 1968), 3 = average of UZc, $UBS_{\gamma 3}$ and Sandwich Horizon (Wager and Brown 1968; Naslund 1984; McBirney 1989).
[c] Representative bulk rock samples, this study.

4.6.5 Results

The results of modelled melt compositions are shown Figure 27 and Table 12. Both clearly indicate strong enrichment of iron and silica with increased fractionation in the Upper Zone, with the exception of a slight decrease in silica at the base of UZb.

Table 12. Skaergaard liquids calculated by bulk summation. From Tegner (1997).

Cumulate Zone / Depth of Core 90-22 (m)	Base UZa 914.2	Mid UZa 769.1	Base UZb 461.8	Mid UZb 270.3	Base UZc 46.2	Mid UZc 0.7
SiO_2	47.4	47.4	47.1	48.2	49.4	49.6
TiO_2	3.7	3.6	3.1	2.7	2.3	2.2
Al_2O_3	11.9	11.8	11.2	11.0	9.3	8.6
FeO_T	20.1	20.6	22.2	22.9	25.2	26.5
MnO	0.3	0.3	0.3	0.4	0.3	0.1
MgO	3.3	2.9	2.2	1.5	0.5	0.4
CaO	8.5	8.4	8.0	7.5	4.9	1.3
Na_2O	3.4	3.5	3.6	3.9	5.7	8.3
K_2O	0.6	0.7	0.8	0.9	1.6	2.5
P_2O_5	0.8	1.0	1.4	1.0	0.7	0.6

[a] Recalculated to 100% volatile free.

4.7 Discussion of the Skaergaard Liquid Line of Descent

4.7.1 Wager (1960)

It is important to note that the only requirements for constructing the graphical sequence of compositional changes are the proportions, compositions and sequences of the different portions of the intrusion.

According to Wager (1960), the earliest crystal phases that were produced under equilibrium conditions in Skaergaard were Fo_{81} and An_{77}. These observations were made from the gabbro picrites and the feldspar rock that can be found perpendicular to the marginal border group (Wager & Deer, 1939). Together with these minerals there is assumed to have been about 35% of trapped liquid, which is expected to have been similar in composition to the original liquid (Wager, 1960). The quantity of TiO_2 is controlled by the amount of trapped liquid, and according to these assumptions there must have been about 0.4% TiO_2 at the start of the hidden zone (Wager, 1960). Following this reasoning, 24B, which assumes 70% crystallisation, is the most appropriate choice. The same method was applied to the amount of P_2O_5 for the intrusion. It was found, however, that the amount of P_2O_5 projected for the intrusion was almost one and a half times more than the actual amount of P_2O_5 present. P_2O_5 is predominantly found in the UZ b and c, where apatite exists as a cumulus mineral. Wager (1960) proposes that the volume of the UZ is not directly proportional to its width as is the case in other layers for Skaergaard. It is therefore assumed that the volume of the UZ is half of that inferred from their thickness (Wager, 1960). Once this assumption is made the total amount of P_2O_5 for the earliest layered rocks is 0.4%.

The alteration of thickness for the data to better suit the proposed composition is a risky one. It does not allow for normal observational practice to take precedence. Most of Skaergaard's rocks are not exposed, so calculating an accurate LLD based on volumetric assumptions is very nearly impossible. At the time of publishing there was no real alternative, but unless the intrusion is completely exposed, or a good understanding of its size and shape has been established by alternative methods, such as drilling, proper volumetric estimations cannot be made and should be

avoided. It is not to say that it is a poor method, just that it should be used with great caution. To properly assess the potential variation in this method, the volume and initial composition should be varied using a statistical method, such as a Monte Caro type simulation. The effect that volumetric changes have on the model can then be quantified in terms of deviation, which should prove to be an interesting outcome.

4.7.2 Hunter and Sparks (1987)

It is pointed out that Wager (1960) may have been erroneous in selecting the marginal gabbros as a starting composition for the parental magma, as the marginal gabbros display variable composition (McBirney, 1975; Hoover, 1978) and experimental studies undertaken by Ford (1981) indicate that the chosen sample is an unlikely candidate to produce the observed mineral assemblages in the Skaergaard layered rocks. It also mentions that the presence of such a large "Hidden Zone" assumed by Wager (1960) has no realistic geophysical evidence to back it up (Blank and Gettings, 1973; McBirney, 1975).

A favourable aspect of these calculated estimates is that the volume for each layer or zone is not important at all and plays no part in the outcome. This is good because of the great uncertainty in the shape and volume, not only for each layer of the Layered Series but for the intrusion as a whole. The average composition of the Layered Series varies only slightly, that is 44-47% SiO_2, thus by the lever rule the subsequent liquid compositions in terms of SiO_2 can be deduced without any understanding or estimate of the proportions involved (Hunter and Sparks, 1987). However, it must be noted that the SiO_2 content of the final residual liquid must be known in order to use this technique. The FeO content is very weakly influenced by the relative proportions (Hunter and Sparks, 1987). On the other hand, elements such as P_2O_5 are strongly affected by the proportions of the zones (Hunter and Sparks, 1987).

There is no field evidence of any rhyolites ever erupting from the Skaergaard magmatic system. The isotopic composition of granophyres related to the Skaergaard intrusion are incompatible with direct differentiation from the magmas that produced the Layered Series, which clearly indicates that crustal contamination

and partial melting of country rock was involved during their formation (Leeman and Dasch, 1987; Kays *et al.*, 1987).

Hunter and Sparks (1987) admit that there are problems with the choice of the Tinden Sill as the compositional example of the most evolved rhyolitic portion of the residual liquid, such as the Tinden Sill having a higher Sr^{87}/Sr^{86} ratio than the Layered Series, but are adamant that the major element chemistry is similar to Icelandic rhyolites and Hebridean rhyolites. The granophyres in question contain isotopic signatures consistent with crustal contamination even though it is known that a sizeable fraction formed as a result of basaltic differentiation (Dicken *et al*., 1984). Hunter and Sparks (1987) maintain that if the calculated trend is correct, the majority of rhyolites formed from the extreme silica-enriched residual liquid of the Skaergaard Layered Series must have erupted, assuming an open system, or have since been eroded into distant memory. Iceland contains evidence of explosive eruptions of aphanitic andesite, dacites and rhyolites, specifically the Hekla and Askja systems which contain evidence of having formed from extreme differentiation of basaltic magmas, such as the presence of magnetite gabbros (Thorarinsson and Sigvaldason, 1972; Sigurdsson and Sparks, 1978; Hunter and Sparks, 1987). The lack of roof rocks in the Skaergaard intrusion make it impossible to unequivocally prove that rhyolites were present, but it also makes it impossible to unequivocally disprove it.

Research conducted by Wood (1978) and Macdonald *et al.* (1987) on major and trace element modelling of Icelandic rocks show that more or less 70-80% fractionation of a ferrobasalt is required to produce a rhyolite residue. An estimated thickness of 250m of rhyolite would have been produced above the UZc by the differentiation of the Layered Series (Hunter and Sparks, 1987). This estimation is based on the volume of magma in the differentiating body, i.e. the Layered Series, but is difficult to constrain as there is so much ambiguity around the actual shape and volume of the Skaergaard intrusion. It is also possible that, as in the case of Iceland, small periodic eruptions of evolved rhyolite lead to an evolving chamber which remains unaffected by the presence of rhyolitic liquid (Hunter and Sparks, 1987). Thus, the rocks remaining in the Layered Series predominantly consist of cumulate

compositions, therefore calculating and constructing the residual liquid by mass balance calculations will result in deceptive outcomes (Hunter and Sparks, 1987). However, this is only applies if the residual liquid did in fact differentiate to rhyolitic composition. Seeing as there is no field, or chemical evidence for such, it is hard to reconcile this model.

4.7.4 Toplis and Carrol (1995)

Toplis and Carrol (1995) present a very simplified argument around the influence of magnetite and ilmenite crystallisation on the composition of a melt, especially in terms of silica and iron content. Experiments were conducted to determine the behaviour of an Fe-Ti oxide-saturated melt under varying fO_2 conditions. The entire range of fO_2 investigated presents a stable environment for Fe-Ti oxides, with the appearance or disappearance of specific oxides being very sensitive to fO_2 conditions.

Toplis and Carrol (1995) show that ferric iron content in magnetite-saturated melts has an almost linear relationship with inverse temperature, thus independent of fO_2 (Toplis and Carrol, 1995). Toplis *et al.* (1994) identified a relationship, in phosphorous-saturated melts, between calculated ferric iron content of magnetite-saturated melts and P_2O_5. These phosphorous-saturated melts indicated that an increase in P_2O_5 invariably lead to an increase in ferric iron. Toplis and Carrol (1995) suggest that because a similar relationship exists between the ferric iron content of magnetite-saturated melts and inverse temperature in a similar study done by Juster *et al*. (1989), and is much more pronounced than the phosphorous-saturated melt saturated melts this kind of relationship could prove to be a useful method of predicting magnetite crystallisation in melts.

The idea that the Fe-Ti oxides are markedly affected by conditions open, or closed to oxygen, to the extent that large differences in oxide modes exist is simply not applicable. Oxygen fugacity has, without a shadow of a doubt, a great effect on the timing of Fe-Ti oxide crystallisation (Fig. 29). Experimental work by Thy *et al.* (2006) clearly show that Fe-Ti oxides are not drastically affected by conditions open, or closed to oxygen, but rather by the magnetite/ilmenite ratio (Fig. 30). Take for

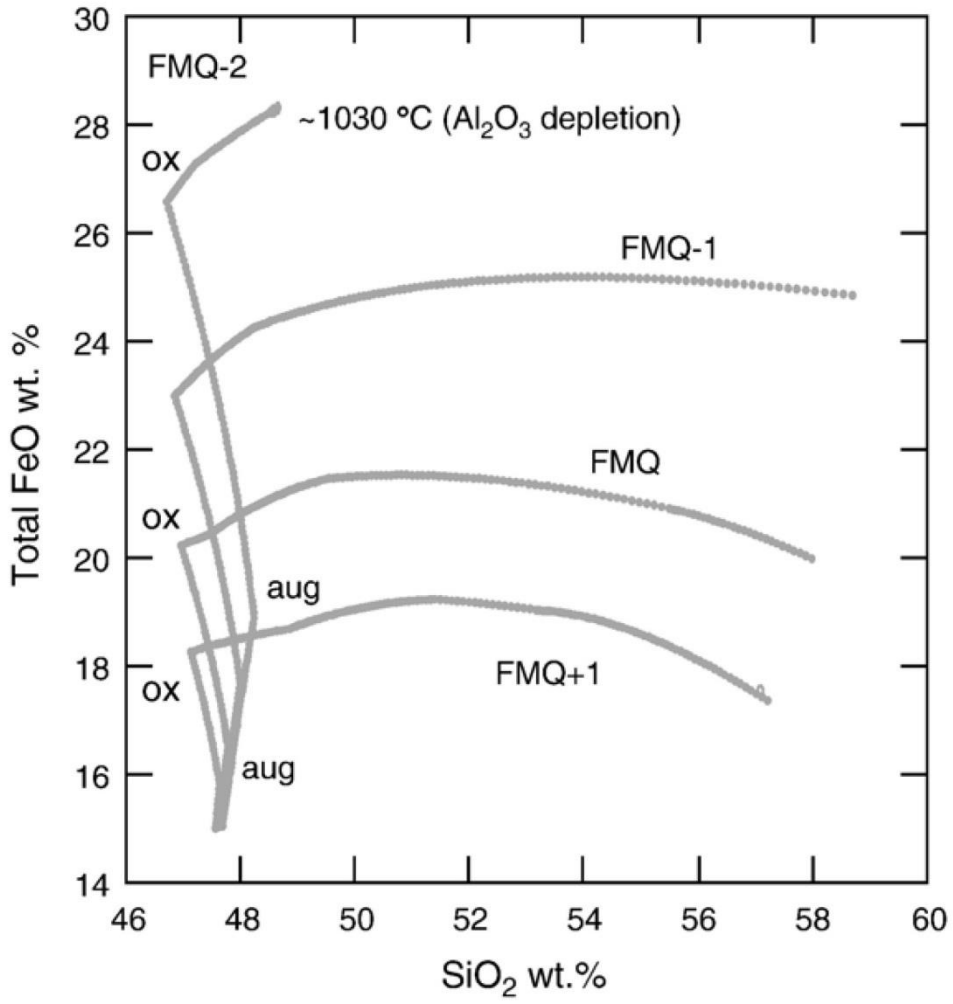

Figure 29. The effect of f_{O2} on fractional crystallisation. This experiment was conducted open with respect to oxygen. At FMQ-2 the suppression of oxide crystallisation causes depletion in Al_2O_3. Data from Toplis and Carrol (1995) and Thy *et al.* (2006). From Thy *et al.* (2006).

example the line in Figure 30 representing the magnetite/ilmenite ratio of 0.5. There is very little difference with respect to Fe_{total} values between conditions open or closed to oxygen. A much larger difference exists between the different oxide ratios and this is clearly a very important variable to consider.

Relative amount of magnetite to ilmenite also has a marked effect on oxygen fugacity of the system. More Fe^{3+} is partitioned into magnetite than ilmenite, therefore the change in f_{O2} with respect to the FMQ buffer will hinge on the amount of magnetite crystallising (Thy *et al.*, 2006). Only once very high modal proportions

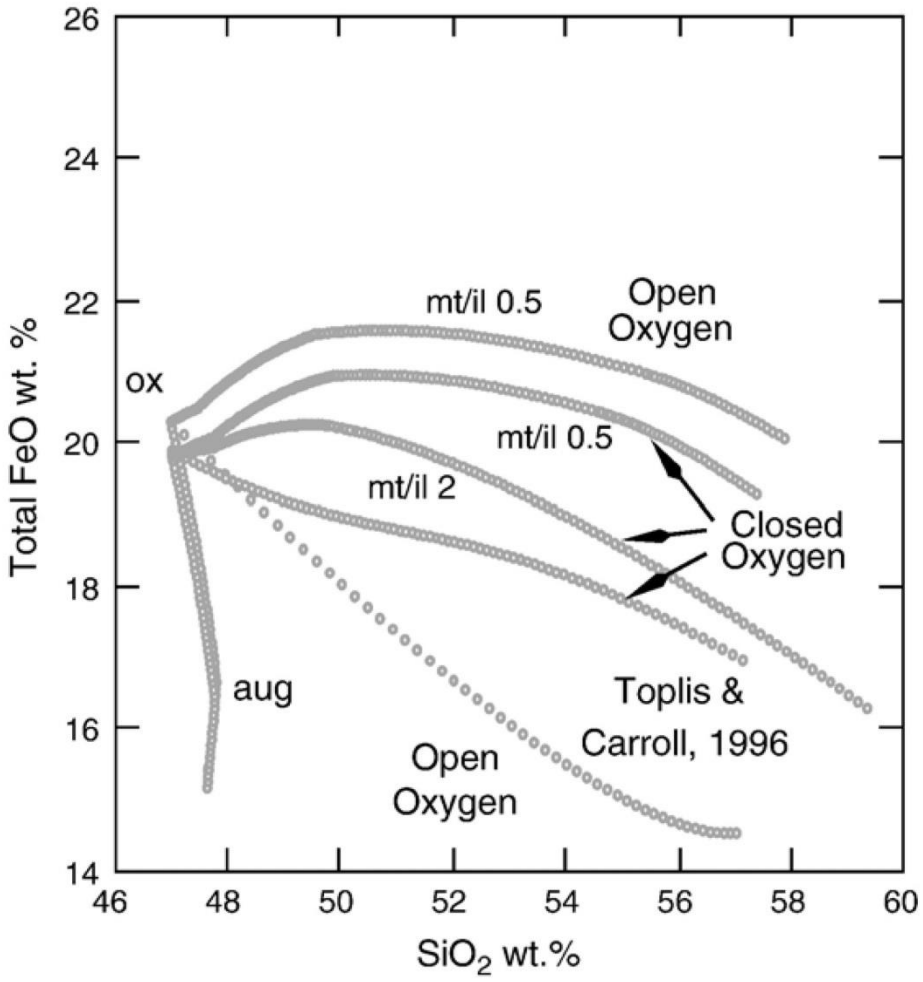

Figure 30. Fractional crystallisation open and closed with respect to oxygen. Oxygen fugacity values are compared to the FMQ buffer. Magnetite/ilmenite ratios are given as mt/il. The Toplis & Carrol, 1996 shows the data determined by their experimental works. For further discussion on the experimental parameters the reader is referred to Thy *et al.* (2006). From Thy *et al.* (2006).

of magnetite are used will it have a marked effect on the change in f_{O2} conditions (Toplis and Carrol, 1995, 1996).

4.7.5 Tegner (1997)

The LLD proposed by Tegner (1997) shows enrichment in iron as well as silica, i.e. a Fenner trend. A slight decrease in silica in UZb is very likely due to the presence of the aforementioned melanogranophyre in UZb. Tegner (1997) ascribes its presence to crystallisation kinetics rather than a substantial change in magma composition, and does not feel it is an important part of the Upper Zone. Tegner

(1997) further backs his modelled compositions by citing his composition of UZa to be in good agreement with most published estimations Table 10, barring those by Hunter and Sparks (1987) and Toplis *et al.* (1994). The fact that there is a reasonable correlation between measured FeO_T content in plagioclase and FeO_T of the modelled liquid is encouraging (Tegner, 1997). Furthermore, Tegner (1997) goes so far as to say that the result Toplis and Carrol (1996) acquired from their modelling of the Skaergaard liquid line of descent, which strongly emphasizes a Bowen trend, is most probably due to their overzealous weighting of magnetite content (~43 wt.% in the open system and ~26 wt.% in the closed system at FMQ), which will almost definitely deplete any liquid of iron following the onset of magnetite crystallisation.

What is important to note is that Tegner (1997) apparently calculated the effects of large volumetric changes for the UBS and melanogranophyres, and even up to ~50% did not meaningfully modify the outcome.

There are some assumptions associated with the bulk summation method. It is assumed that the volume is directly proportional to the depth, i.e. it is viewed as a cylinder. The starting composition is assumed to be the average of UZc, Sandwich Horizon and $UBS_{\gamma 3}$, as taken to be the top 40 m of the core. It is assumed that crystallisation of the portion in question crystallised in a closed system. Isotopic evidence backs up this assumption as there is very little variation to suggest that assimilation of country rock or new magma injections took place in any of the rocks younger than LZb (Stewart and DePaolo, 1990; McBirney 1995). McBirney (1995) showed that late-stage migration of interstitial magma was significant for highly incompatible elements, but it is assumed that this was not the case for major elements. Jang *et al.* (2001) studied the variation in trace elements with change in stratigraphic height for Skaergaard. A case exists for the downward migration of heavy, late stage iron-rich liquids to a lower portion of the intrusion. Variations in especially the content of V back up this statement. The Marginal Border Series was ignored by Tegner (1997) and did not form part of the calculations. This is by no means a small portion of the intrusion and also contains a much more silica-rich portion than most of the Skaergaard intrusion, and goes some way to explain the relative lack of silica-enrichment for this version of Skaergaard's LLD.

However, the assumption that iron content in the residual liquid can be monitored in plagioclase is still under some scrutiny. It is by no means a proven science, and while it is a potential alternative method for analysing the evolution of a magma chamber, it is just that, an alternative, and should probably only be used as such. Having said that, a reasonable correlation between the work done by Tegner (1997) and newer modelled data exists, so there is doubtless some potential to the for the method, as long as partitioning coefficients for Fe^{3+} can be strictly determined for each change in stratigraphic height. It can thus be a good companion to more traditional modelling techniques, but has too many unknown variables to be the only method for assessing a layered intrusion.

5. Investigating the effect of fO_2 and H_2O using AlphaMELTS

5.1 Introduction

The MELTS program is a powerful thermodynamic modelling software used to examine the behaviour of melts during crystallisation in natural basaltic systems. Various versions of the MELTS program exist and are applied to specific problems, depending on their inherent capabilities and/or limitations. MELTS is the original version developed by Ghiorso and Sack (1995) which focuses on the crystallisation of shallow-seated, predominantly basaltic melts (pressure <3 Gpa). The other versions later developed include: pMELTS, which, as the name suggests is applied to high-pressure melts, predominantly the behaviour of peridotite in mantle conditions (Ghiorso *et al.,* 2001); Rhyolite-MELTS, developed to better constrain silicic systems (Gualda *et al.,* 2012); and AlphaMELTS (formerly Adiabat_1ph), used to determine equilibrium assemblages along a user-defined thermodynamic path (Smith and Asimow, 2005).

AlphaMELTS is a text-menu driven program used in command prompt (for Windows) and is compatible with all the main operating systems such as Linux and Mac. It uses the thermodynamic models for MELTS (Ghiorso and Sack, 1995) and pMELTS (Ghiorso *et al.*, 2002) to predict the behaviour and distribution of major and trace elements during crystallisation. The program delivers step-for-step liquid and solid composition for the crystallising melt. It provides simple text-format output files which can be converted into Excel tables for graphing and analysis, but require a fair amount of “cleaning” prior to conversion. AlphaMELTS is capable of modelling the evolution of basaltic melts under the effect of fractional crystallisation, but more importantly for this study, can incorporate the effect of fO_2 and aH_2O on the crystallising melt.

It is for this reason that AlphaMELTS was employed to perform isobaric fractional crystallisation modelling of pre-existing starting liquid compositions for the Birds River and Skaergaard intrusions at various FMQ and aH_2O conditions, in order to appreciate their potential effect on liquid evolution. Starting liquid compositions were taken from literature (Wager, 1960; Hunter and Sparks, 1987; Toplis and

Carrol, 1995; Tegner, 1997) and the resultant LLDs from this study are compared to those findings. This approach has never before been applied to the Birds River rocks and should provide a valuable alternative to the work done by Eales (1990). The original MELTS algorithm has been employed by Toplis and Carrol (1996) to perform similar calculations for Skaergaard rocks, also at various FMQ conditions, but neglected the combined effect of aH_2O.

5.2 Methodology

The simulation was executed using the alphaMELTS program version 1.4. The conditions at which iterations were executed and combinations of fO_2 and H_2O used can be found in Table 13. In keeping with literature, Skaergaard's oxidised conditions are limited to FMQ+2. 96 iterations were performed for Birds River and 151 for Skaergaard. The fractionation text files and MELTS files used for these iterations are given in the appendix. All the results produced and input files in AlphaMELTS are attached as a digital appendix.

The thermodynamic models from MELTS and pMELTS make use of bulk compositions in the systems SiO_2-TiO_2-Al_2O_3-Fe_2O_3-Cr_2O_3-FeO-MnO-MgO-NiO-CoO-CaO-Na_2O-K_2O-P_2O_5-H_2O and SiO_2-TiO_2-Al_2O_3-Fe_2O_3-Cr_2O_3-FeO-MgO-CaO-Na_2O-K_2O-P_2O_5-H_2O with maximum pressure conditions of 3 Gpa and 4 Gpa respectively (Smith and Asimow, 2005). It is not recommended to use the program outside of these conditions (Smith and Asimow, 2005).

The algorithm treats H_2O as an oxide, thus it can partition into: melt; hydrous minerals; or exist as pure vapour (Smith and Asimow, 2005). The vapour phase standard state properties for MELTS are applied from the Haar equation of state (Haar *et al.,* 1984), while pMELTS makes use of the Pitzer and Sterner equation of state for higher pressures (Pitzer and Sterner, 1994). An update to AlphaMELTS on H_2O behaviour was given in Antoshechkina *et al.* (2010).

Starting compositions were taken from literature and are given below in Table 14. Iterations were analysed and the resulting data for major elements were graphed. It should be noted that AlphaMELTS requires input conditions for temperature as degrees Celsius (°C), but output is in degrees Kelvin (K). Pressure

conditions are always given in bars. When performing a batch calculation prior to executing the simulation at superliquidus, as was the case for every simulation performed here, AlphaMELTS automatically determines the appropriate value for Fe_2O_3 by distributing FeO* = FeO + 0.9 Fe_2O_3.

Table 13. A summary of the parameters used in the iterations are presented here. Many more H_2O intervals were used in the Birds River analysis, but are omitted here for the sake of brevity. Whenever an inflection point was sought, more H_2O intervals than are presented here were used, but those are mentioned elsewhere. The compositions referred to here can be found in Table 14.

	Comp	ΔT	P (bar)	fO_2	H_2O	H_2O	H_2O	H_2O	H_2O	H_2O
BR	E	1	500	FMQ+3	0	0.01	0.05	0.1	0.5	1
	E	1	500	FMQ+2	0	0.01	0.05	0.1	0.5	1
	E	1	500	FMQ+1	0	0.01	0.05	0.1	0.5	1
	E	1	500	FMQ	0	0.01	0.05	0.1	0.5	1
	E	1	500	FMQ-1	0	0.01	0.05	0.1	0.5	1
	E	1	500	FMQ-2	0	0.01	0.05	0.1	0.5	1
S	W	1	2000	FMQ+2	0	0.01	0.05	0.1	0.5	1
	W	1	2000	FMQ+1	0	0.01	0.05	0.1	0.5	1
	W	1	2000	FMQ	0	0.01	0.05	0.1	0.5	1
	W	1	2000	FMQ-1	0	0.01	0.05	0.1	0.5	1
	W	1	2000	FMQ-2	0	0.01	0.05	0.1	0.5	1
	H&S	1	2000	FMQ+2	0	0.01	0.05	0.1	0.5	1
	H&S	1	2000	FMQ+1	0	0.01	0.05	0.1	0.5	1
	H&S	1	2000	FMQ	0	0.01	0.05	0.1	0.5	1
	H&S	1	2000	FMQ-1	0	0.01	0.05	0.1	0.5	1
	H&S	1	2000	FMQ-2	0	0.01	0.05	0.1	0.5	1
	T&C	1	2000	FMQ+2	0	0.01	0.05	0.1	0.5	1
	T&C	1	2000	FMQ+1	0	0.01	0.05	0.1	0.5	1
	T&C	1	2000	FMQ	0	0.01	0.05	0.1	0.5	1
	T&C	1	2000	FMQ-1	0	0.01	0.05	0.1	0.5	1
	T&C	1	2000	FMQ-2	0	0.01	0.05	0.1	0.5	1
	T	1	2000	FMQ+2	0	0.01	0.05	0.1	0.5	1
	T	1	2000	FMQ+1	0	0.01	0.05	0.1	0.5	1
	T	1	2000	FMQ	0	0.01	0.05	0.1	0.5	1
	T	1	2000	FMQ-1	0	0.01	0.05	0.1	0.5	1
	T	1	2000	FMQ-2	0	0.01	0.05	0.1	0.5	1

Table 14. Starting liquid compositions for Birds River (BR) and Skaergaard (S) from literature (E – Eales, 1990; W – Wager, 1960; H&S – Hunter and Sparks, 1987; T&C – Toplis and Carrol, 1995; and T – Tegner, 1997). Wherever FeO values are denoted by an asterisk *, FeO values are given as total iron = (FeO + Fe2O3).

	BR	S			
	E	W	H&S	T&C	T
SiO_2	52.13	47.97	53.8	48.8	47.4
TiO_2	1.01	1.32	1.9	2.9	3.7
Al_2O_3	15.05	18.32	11.9	14.9	11.9
FeO	9.27*	8.58	18.2*	13.1*	20.1
Fe_2O_3	-	1.23	-	-	-
MnO	-	0.12	0.2	-	0.3
MgO	7.27	8.09	1.8	6.5	3.3
CaO	11.72	10.77	6.6	10.9	8.5
Na_2O	2.53	2.42	3.5	2.7	3.4
K_2O	0.61	0.21	1.3	0.3	0.6
P_2O_5	0.17	0.08	0.9	-	0.8
Total	**99.76**	**99.11**	**100.10**	**100.10**	**100.00**

5.2.1 Birds River

Isobaric conditions were chosen at 500 bar and starting temperature at 1473.15 K. Birds River intruded at very shallow depth, so the 500 bar pressure condition seems reasonable. No estimations of pressure conditions exist for Birds River in the literature. Some of the iterations were performed at 1000 bar for random testing without significant variation. The temperature was chosen based on first phase appearance at 1471.15 K, so performing calculations considerably above that is pointless.

5.2.2 Skaergaard

Isobaric conditions were chosen at 2000 bar and starting temperature at 1493.15 K. The pressure conditions were taken from literature as an accepted value for the UZ (Larsen and Tegner, 2006). The temperature was chosen based on first phase appearance at 1489.15K. As previously mentioned, the oxidising conditions

for Skaergaard are limited to FMQ+2. This is in keeping with what has been presented in literature (e.g. Toplis and Carrol, 1995).

5.3 Results

5.3.1 Birds River

Given here are all the graphs produced in accordance with the description given above. One feature that arose from these simulations is the presence of gaps within the output data. The potential exists for such gaps to be prodigious and can complicate analysis of the data. It is assumed that these gaps are produced by the presence of peritectic reactions, where the complexity of the phases coming in and phases going out wreak havoc within the thermodynamic model of AlphaMELTS. This is especially true for oxidising conditions (FMQ+1 to FMQ+3). Just such an example is given below in Figure 31A. As for reducing conditions, such as in Figure 32, the effect is negligible.

In order to minimise such gaps in data, the fractionation intervals were changed from 1 to 0.01 °C. An interval of 0.1 °C made little impact. These simulations were performed using the liquid composition of the last point prior to the formation of the gap (39.4% in Fig. 31A). The starting temperature was 1 °C above the chosen liquid composition's temperature to allow for overlap of data, and likewise terminated at 1 °C below the required corresponding crystallisation value (39.2% in Fig. 31A). The result of one such simulation is given in Figure 31B. It should be noted that not all of these types of simulations were successful. Some did not produce the desired result even at 0.01 °C. Intervals of 0.001°C were then attempted with poor results. The latter simulations were extremely time-consuming proved to be an ineffective solution. All of these simulations were compared to graphs where a line was fitted to the original 1 °C interval data, and it proved to be almost identical in outcome. Wherever such a gap appeared, it appears that the composition changed in an

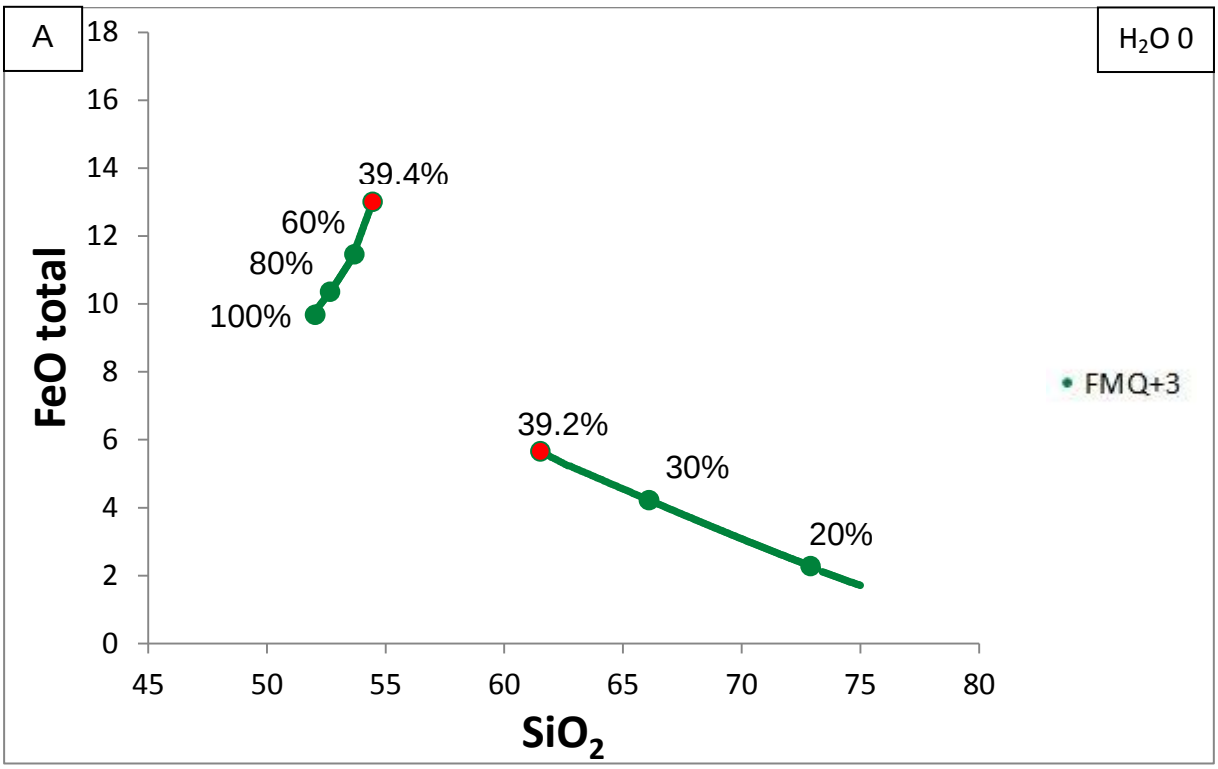

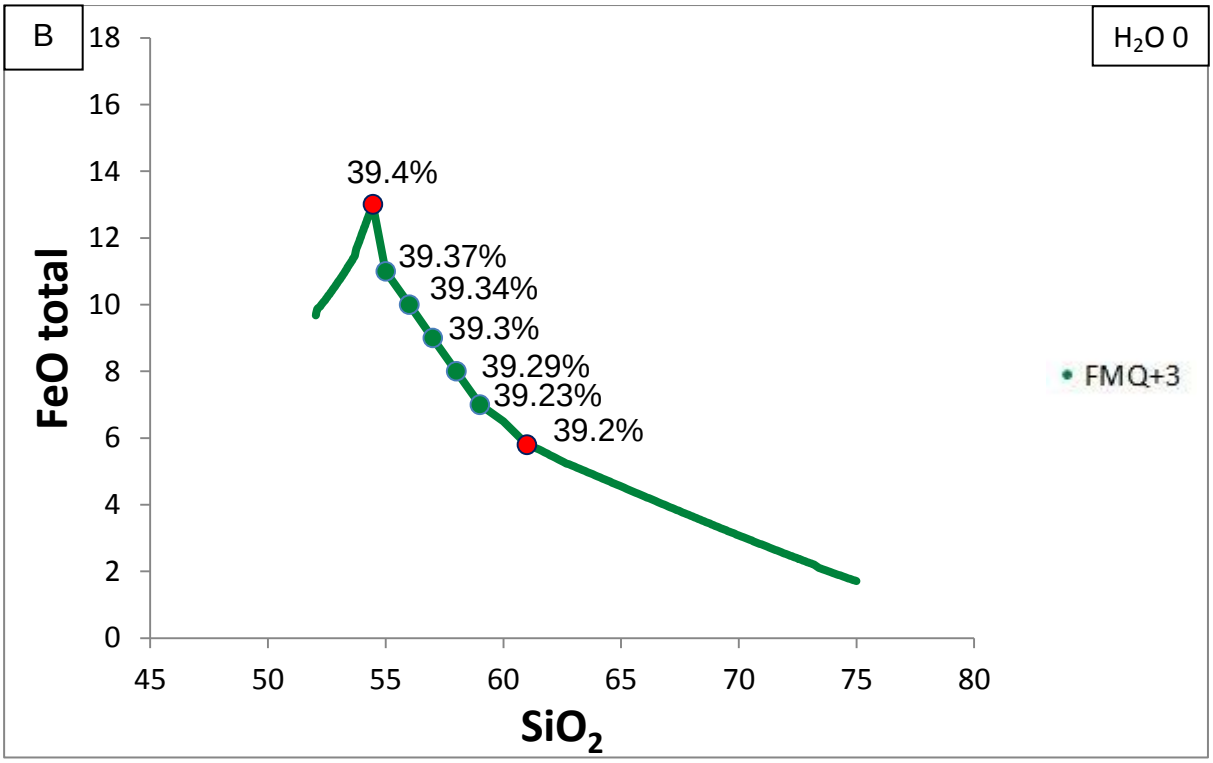

Figure 31. A plot of total iron (FeO + Fe_2O_3) against silica in the liquid for Birds River in wt.%. Red circles indicate the major jump in composition over a very short crystallisation period Birds River FMQ+3 and H_2O = 0. Data from Eales (1990).

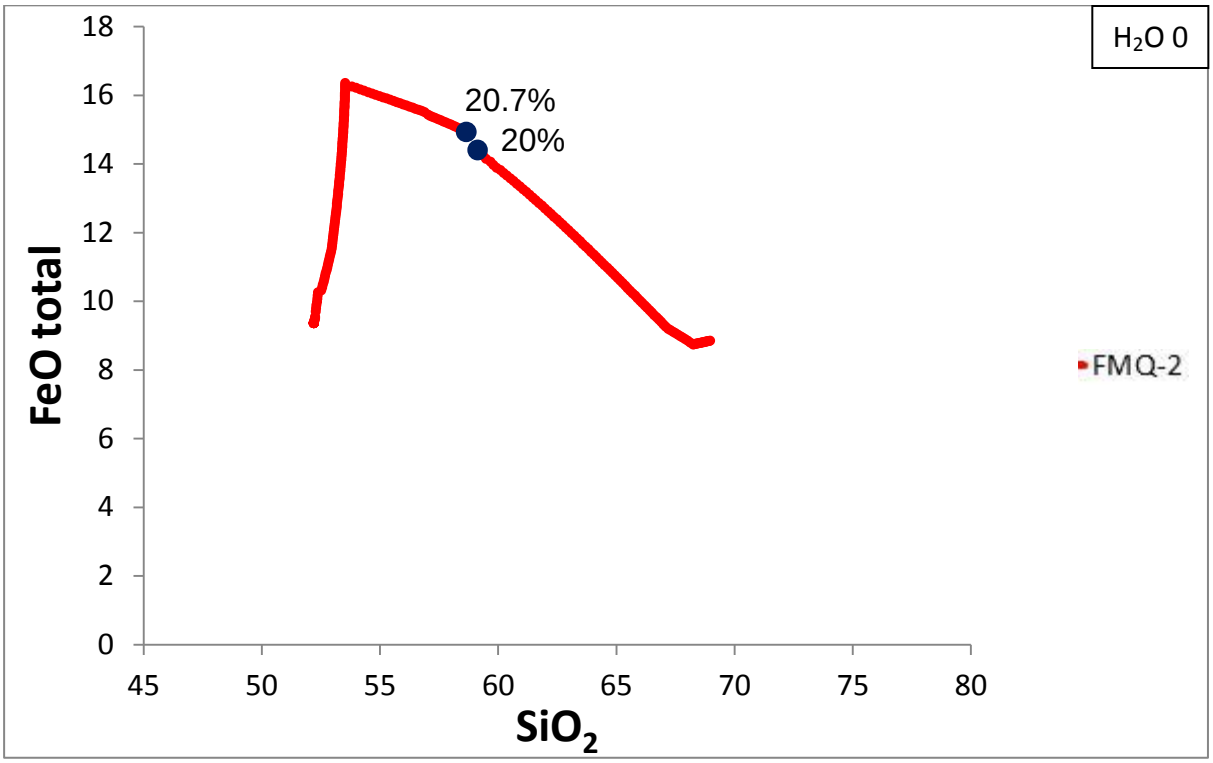

Figure 32. A plot of total iron (FeO + Fe_2O_3) against silica in the liquid for Birds River in wt.%. No line has been fitted to data. Blue circles indicate points prior to and post the jump in composition. Percentages are indication of % liquid remaining. Note the almost negligible change in composition across the gap. FMQ-2 at H_2O = 0. Data from Eales (1990).

almost linear fashion from the point prior to the gap, to after it. Thus, in most of the graphs, a line was fitted to the data for the sake of continuity.

Initial simulations for Birds River were performed at oxidising (FMQ+2) and reducing (FMQ-2) conditions with varying H_2O content (Fig. 33A and B). The whole spectrum of FMQ and H_2O conditions were simulated, but often very little variation was found, so only the major alterations in H_2O content is plotted here, namely 0; 0.1; 0.5; and 1.0 at FMQ+2 and FMQ-2. Whenever a large variation was found, minor alterations were included in order to determine the exact conditions of the inflection point. The behaviour of anhydrous and hydrous liquids at varying FMQ conditions for Birds River are given in Figure 34A and B. Once again very little variation was found in the intermediate simulations.

Results show initial iron-enrichment in the liquid, up to about 40-30% liquid (60-70% crystallisation) with little enrichment in SiO_2, followed by an unmistakeable drop in iron and enrichment in SiO_2 (Fig. 33A and B; Fig. 34A and B). Every

inflection point coincided with the arrival of spinel and was categorically followed by silica-enrichment and iron-depletion (Figure 33A). Iron-enrichment was slightly more pronounced in reduced conditions (FMQ-2 to FMQ) and a drop in maximum iron is clearly evident in oxidised conditions (FMQ+1 to FMQ+3), regardless of water content (Fig. 34A and B).

Water content had a major influence on the behaviour of melts. Increasing water content forced much lower levels of iron-enrichment than the anhydrous counterparts (Fig. 33A and B).

5.3.2 Skaergaard

Simulations for Skaergaard liquids yielded a lot more variability. This is mainly due to the differences in starting liquid compositions used. A host of simulations were performed wherever extreme iron-enrichment took place in order to ascertain the exact conditions at which the liquid continued along its iron-enrichment trend, or reached an inflection point and swung toward a silica-rich end. Just one such example is given in Figure 35A.

Simulations were conducted for four of the so-called “classic” LLDs, namely Wager (1960); Hunter and Sparks (1987); Toplis and Carrol (1995); and Tegner (1997). They are given here in chronological order. As with Birds River, plots of total iron ($FeO + Fe_2O_3$) versus silica in wt.% of the liquid are given here. Plots are given for oxidised (FMQ+2 or FMQ+1) and reduced (FMQ-2) conditions with varying H_2O content, as well as a standard plot of anhydrous ($H_2O = 0$) and/or hydrous liquid ($H_2O = 1$) with varying FMQ conditions. Sometimes one or more of the plots are omitted when it fails to show significant variation. This is done for all four starting liquids as given in Table 14.

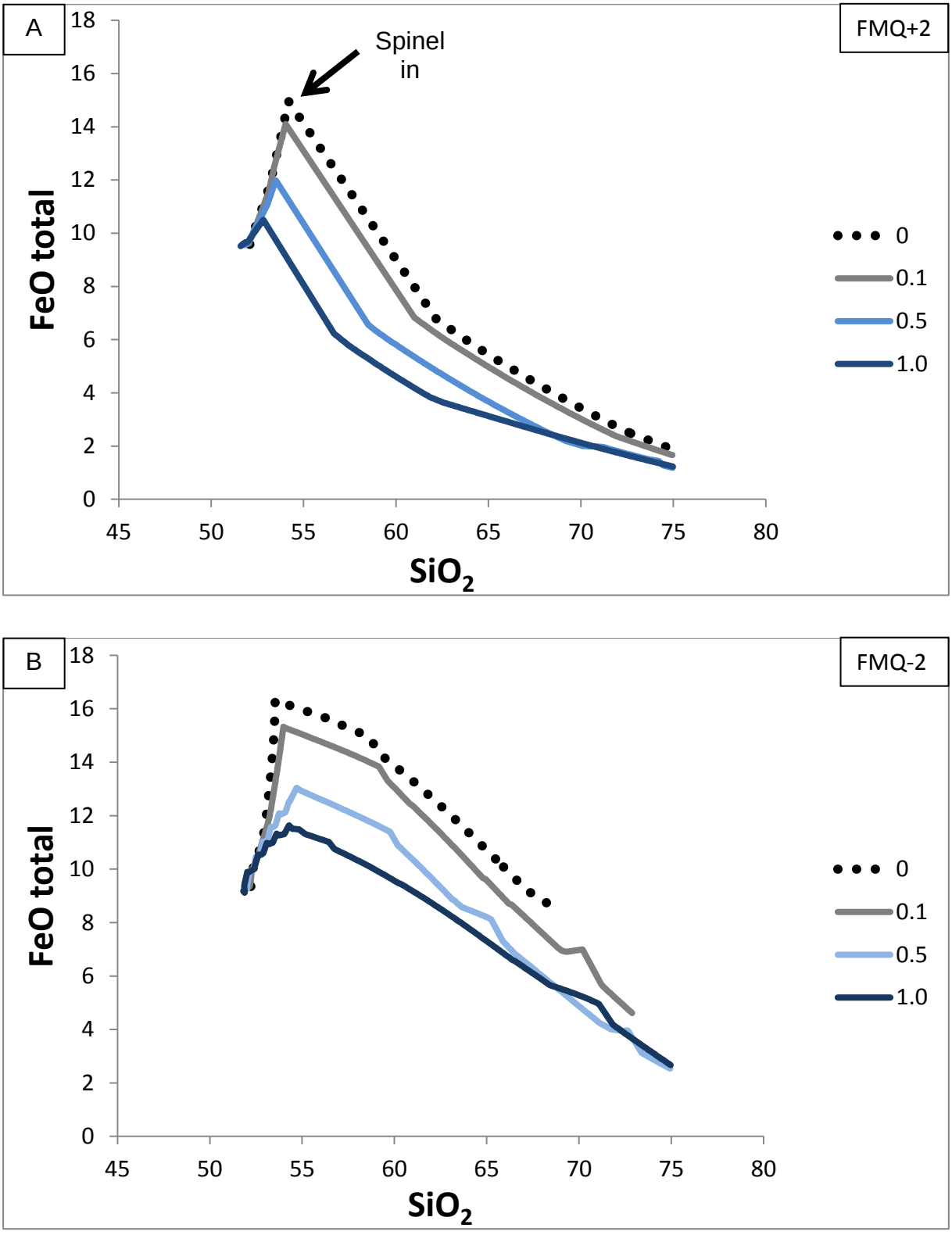

Figure 33. A plot of total iron (FeO + Fe_2O_3) against silica in the liquid for Birds River in wt.%. Arrow indicates the arrival (in) of spinel. A) FMQ+2 with varying H_2O content. B) FMQ-2 with varying H_2O content. Data from Eales (1990).

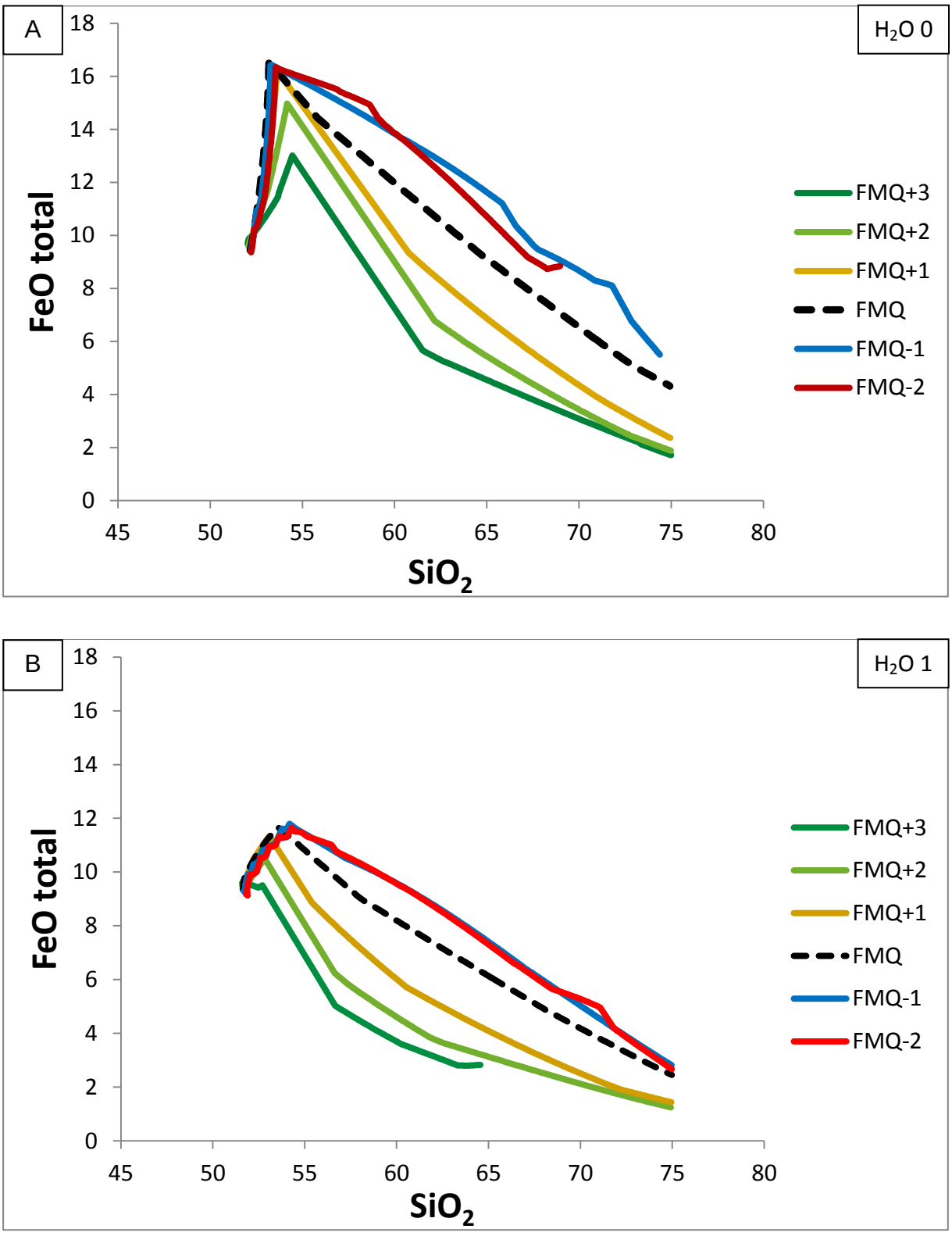

Figure 34. A plot of total iron ($FeO + Fe_2O_3$) against silica in the liquid for Birds River in wt.%. A) $H_2O = 0$ with varying FMQ conditions. B) $H_2O = 1$ with varying FMQ conditions. Data from Eales (1990).

Simulations for the starting liquid proposed by Wager (1960) lead to extreme iron-enrichment under higher fO_2 conditions (FMQ+1 and +2) (Fig. 35A and 36). Also, fO_2 has an opposite effect to that described in simulations performed for Birds River.

Water content once again buffered iron-enrichment (Fig. 35A and B). Under hydrous conditions (H_2O =1) very little iron enrichment takes place, regardless of fO_2 conditions (Fig. 35A and B). In fact, LLDs for hydrous melts are almost identical with varying fO_2. The extreme iron-enrichment that takes place at FMQ+2 (~49 wt.% FeO total) under anhydrous conditions was closely investigated to determine under what conditions spinel would appear (in terms of water content) (Fig. 35A). It was found that below H_2O = 0.125 spinel never appears and that the drop in FeO total was due to oxide phases appearing and disappearing (Fig. 35A). Somewhere between H_2O = 0.15 and H_2O = 0.125 spinel appears and causes the sharp decline in FeO total normally associated with its arrival.

In the case of Hunter and Sparks (1987), many of the simulations terminated before any meaningful amount of liquid had crystallised, thus no trend was visible. All of the graphs plotted in a similar fashion to Figure 37, that is to say, with little to no iron-enrichment following a silica-enrichment trend.

Only one graph was produced for the data from Hunter and Sparks (1987), because of a close similarity between all of the tested conditions, as well as high failure rates for the simulations. Many of the simulations terminated at very low crystallisation levels, thus the data produced from those are useless. It is unclear why these simulations failed. It is possible that because of the chosen starting composition, which is a hotly debated topic (McBirney and Naslund, 1990), the composition is too felsic (low amounts of Al_2O_3, MgO, CaO and high amounts of K_2O, Na_2O) for the AlphaMELTS version of MELTS to successfully model, as it was specifically designed for modelling unevolved basaltic melts. The Rhyolite-MELTS version would probably be a better choice to model such a melt.

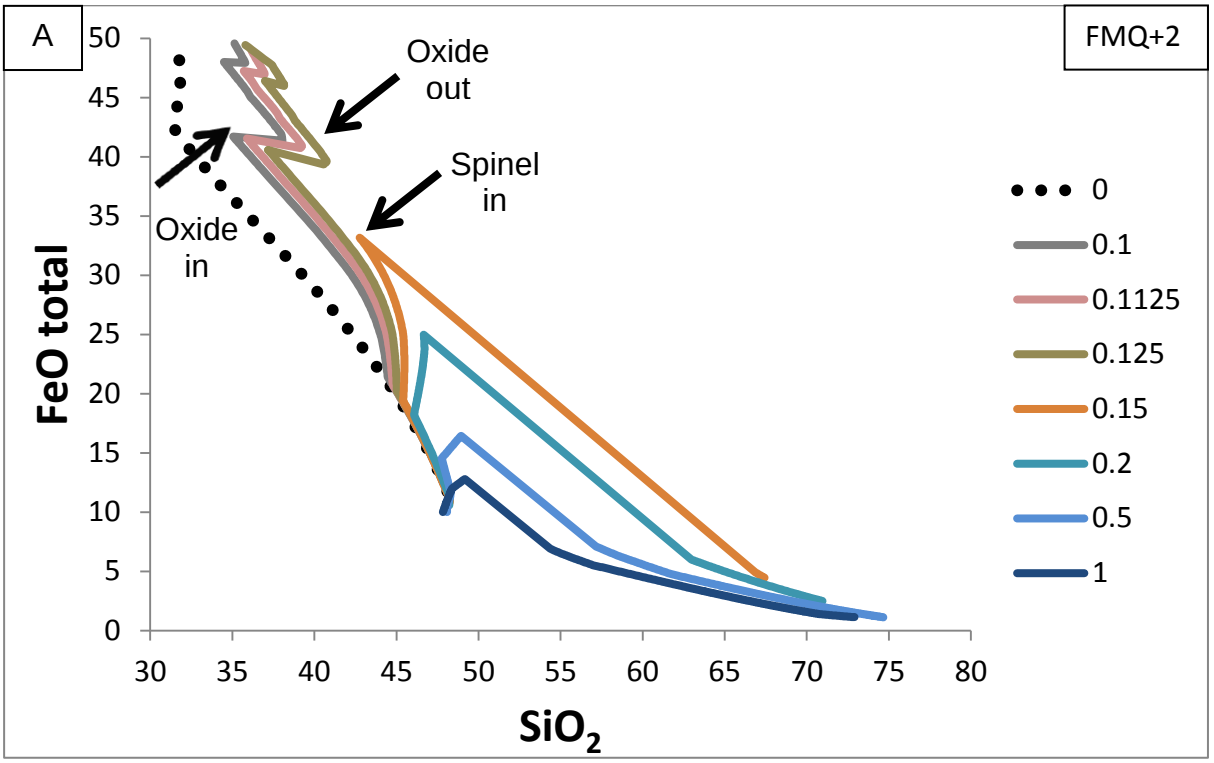

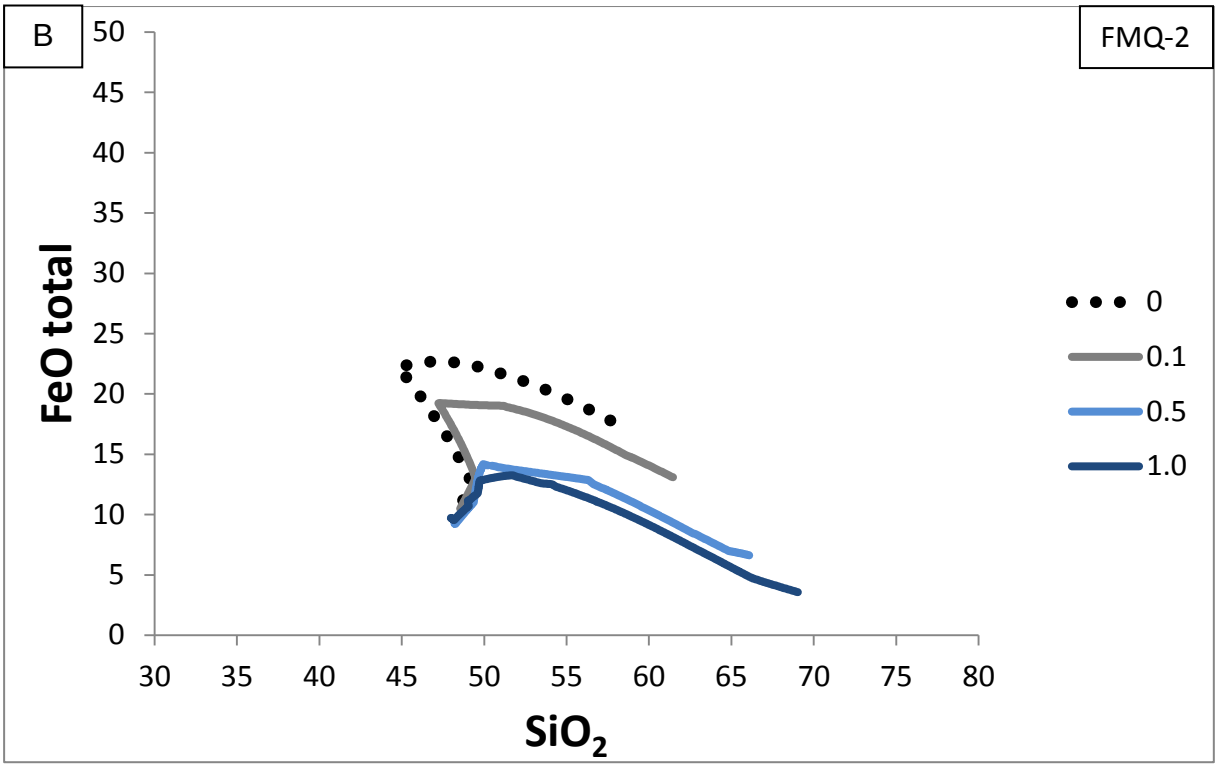

Figure 35. A plot of total iron (FeO + Fe_2O_3) against silica in the liquid for Skaergaard in wt.%. A) FMQ+2 with varying H_2O content. Arrows indicate arrival (in) and removal (out) of spinel and oxide. Note the inflection point for iron-rich, to iron-poor somewhere between H_2O = 0.15 and 0.125. B) FMQ -2 with varying H_2O content. Data from Wager (1960).

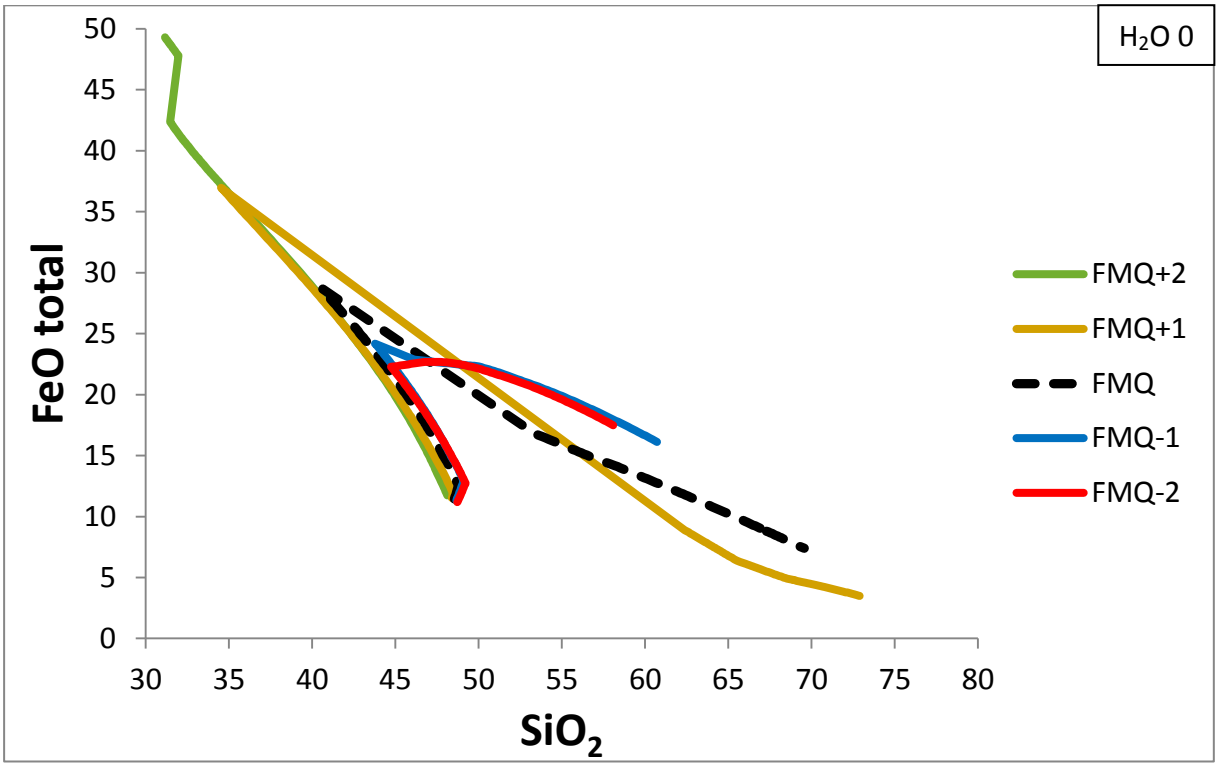

Figure 36. A plot of total iron (FeO + Fe_2O_3) against silica in the liquid for Skaergaard in wt.%. H_2O = 0 with varying FMQ conditions. Data from Wager (1960).

A plot of anhydrous liquid with varying fO_2 conditions is given in Figure 37. It shows no noteworthy iron-enrichment and becomes immediately enriched in silica, as is expected from the chosen starting composition. Almost no variability was shown in the data between hydrous and anhydrous, oxidising or reducing, or any combination of those. They all show a sharp decline in iron toward a silica-rich end. However, what is noteworthy is the return to "expected" behaviour of fO_2 conditions, thus a drop in fO_2 results in a larger iron maximum than for oxidising conditions. Spinel enters the systems almost instantly in all cases. The LLD produced in literature is most closely likened to FMQ-2 at anhydrous conditions (Fig. 37).

A reversal in "expected" fO_2 influence on iron-enrichment is once again present here for the starting composition proposed by Toplis and Carrol (1995) (Fig. 38A and B; Fig. 39). More oxidising fO_2 conditions inhibit spinel crystallisation and promote iron- enrichment. At anhydrous conditions, and higher fO_2 values (FMQ+1 and +2), extreme iron-enrichment takes place (~37 and ~40 wt.% FeO total respectively). At these conditions FMQ+2 does eventually return to a silica-rich end

once spinel arrives at ~95% crystallisation. This could be the case for FMQ+1, but the simulation terminated at ~89% crystallisation. The fact that anhydrous FMQ+2 returned to a silica-rich end at such a high crystallisation level is almost irrelevant, as the bulk of the melt has already crystallised.

An increase in water content severely hampers any form of iron-enrichment (Fig. 38A and B). Hydrous liquid doesn't become enriched in iron past 15 wt.% FeO total, regardless of fO_2 conditions. At FMQ+1 the inflection point for iron-rich to iron-poor was investigated by decreasing the value of H_2O as close to 0 as possible. The result of this is found in Figure 38B. The inflection point is somewhere between H_2O = 0.01 and 0. Spinel entered the system here at ~9% crystallisation. At FMQ+1 the appearance of oxides had a marked effect on the liquid evolution, moving from a highly iron-enriching liquid, to a silica-enriching one. The first oxide phase appeared at ~30% crystallisation.

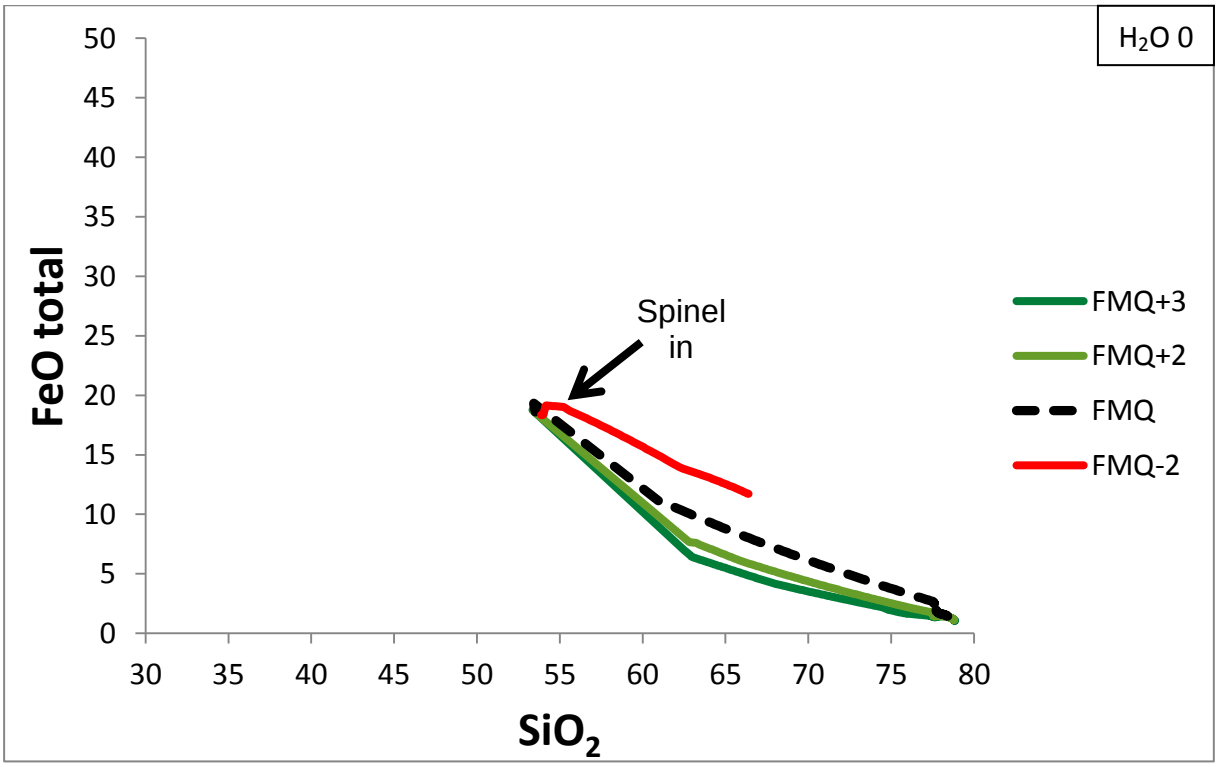

Figure 37. A plot of total iron (FeO + Fe_2O_3) against silica in the liquid for Skaergaard in wt.%. Arrow indicates the arrival (in) of spinel. H_2O = 0 with varying FMQ conditions. Data from Hunter and Sparks (1987).

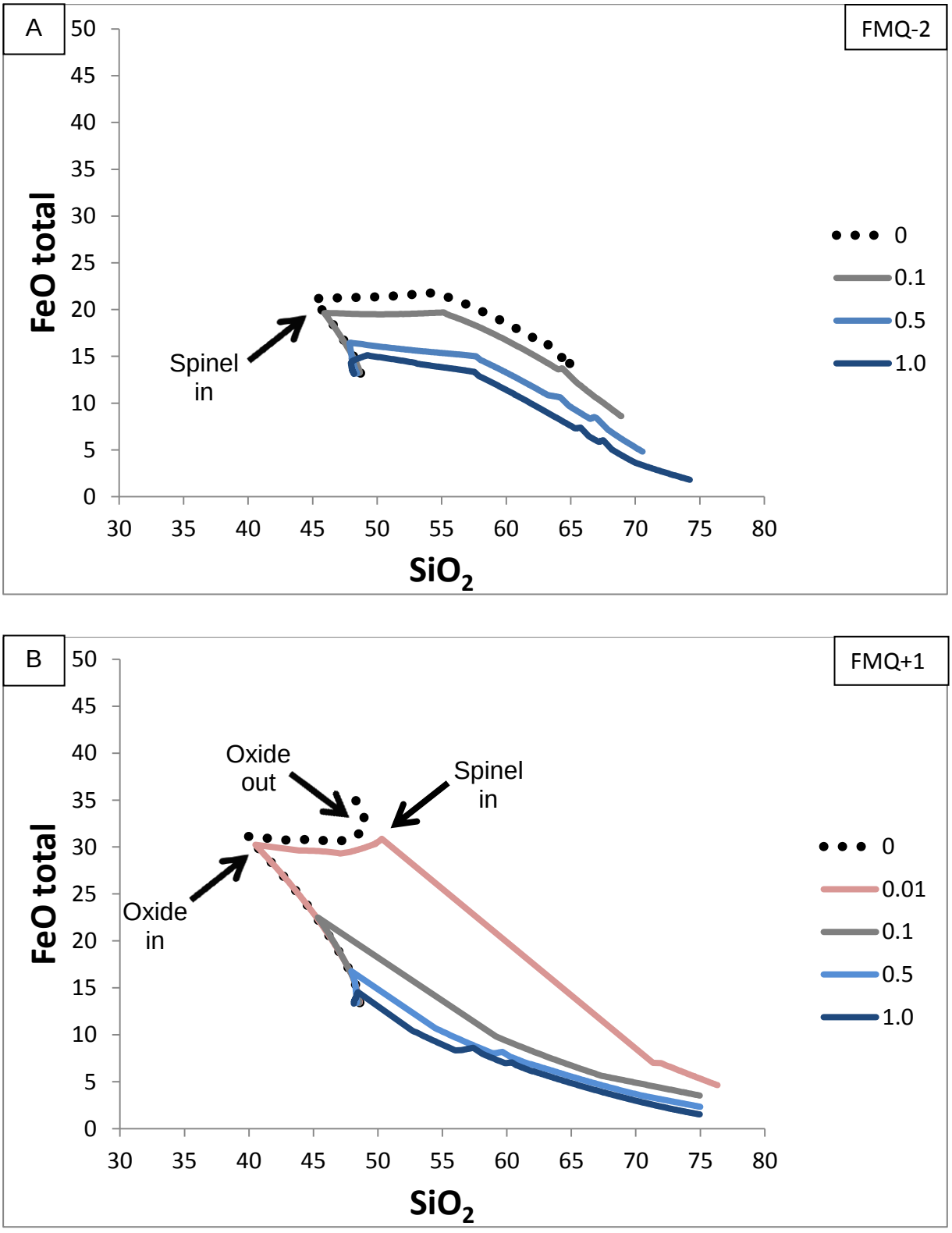

Figure 38. A plot of total iron ($FeO + Fe_2O_3$) against silica in the liquid for Skaergaard in wt.%. Arrows indicate the arrival (in) and removal (out) of spinel and oxides. A) FMQ-2 with varying H_2O content. B) FMQ+1 with varying H_2O content. Data from Toplis and Carrol (1995).

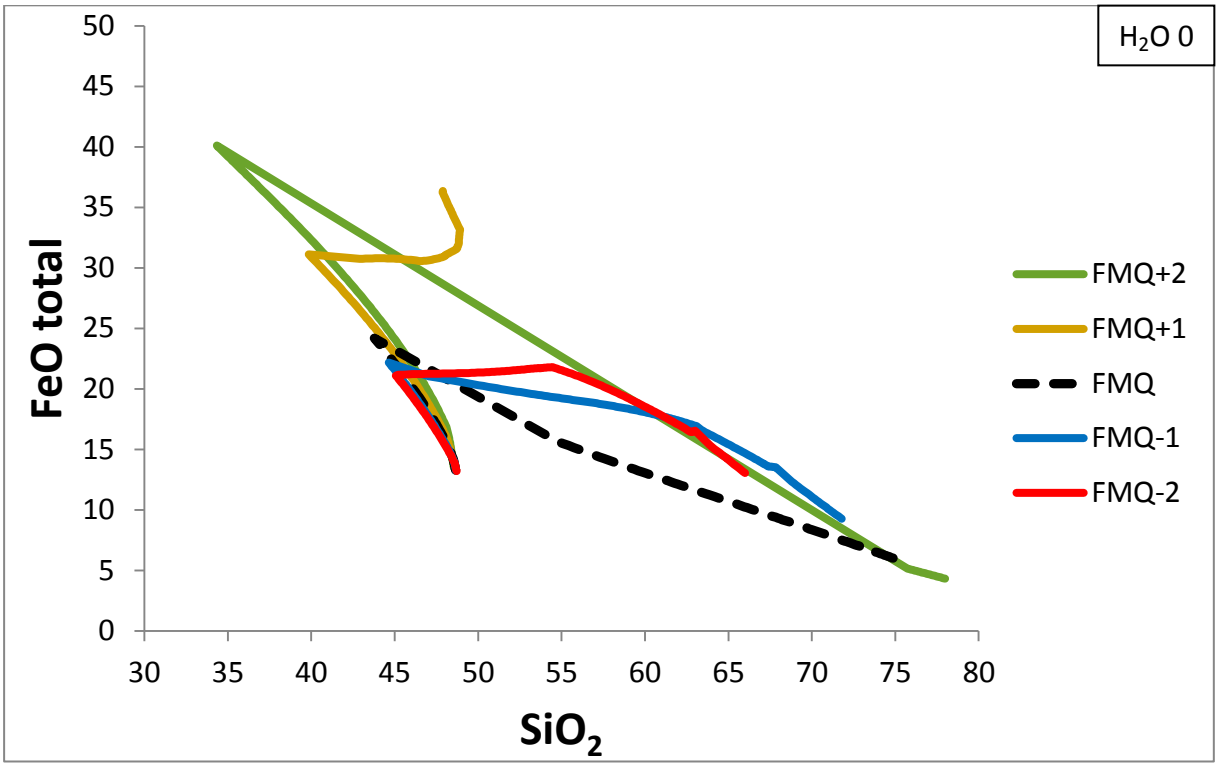

Figure 39. A plot of total iron (FeO + Fe_2O_3) against silica in the liquid for Skaergaard in wt.%. H_2O = 0 with varying FMQ conditions. Data from Toplis and Carrol (1995).

For iterations performed based on starting liquid composition proposed by Tegner (1997), all simulations that exhibited extreme iron-enrichment at H_2O = 0 terminated at ~60% crystallisation. In each case the liquids ran out of Al_2O_3, as shown in Figure 41. Once more higher fO_2 values promote iron-enrichment, and lower values promote silica-enrichment (Fig. 40 and 41). Extreme iron-enrichment took place for FMQ+1 and+2 (~37; ~42 wt.% FeO total respectively) at H_2O = 0. At lower FMQ conditions there is a slight initial increase in iron content until spinel enters the system at ~20% crystallisation and then follows a silica-enrichment trend.

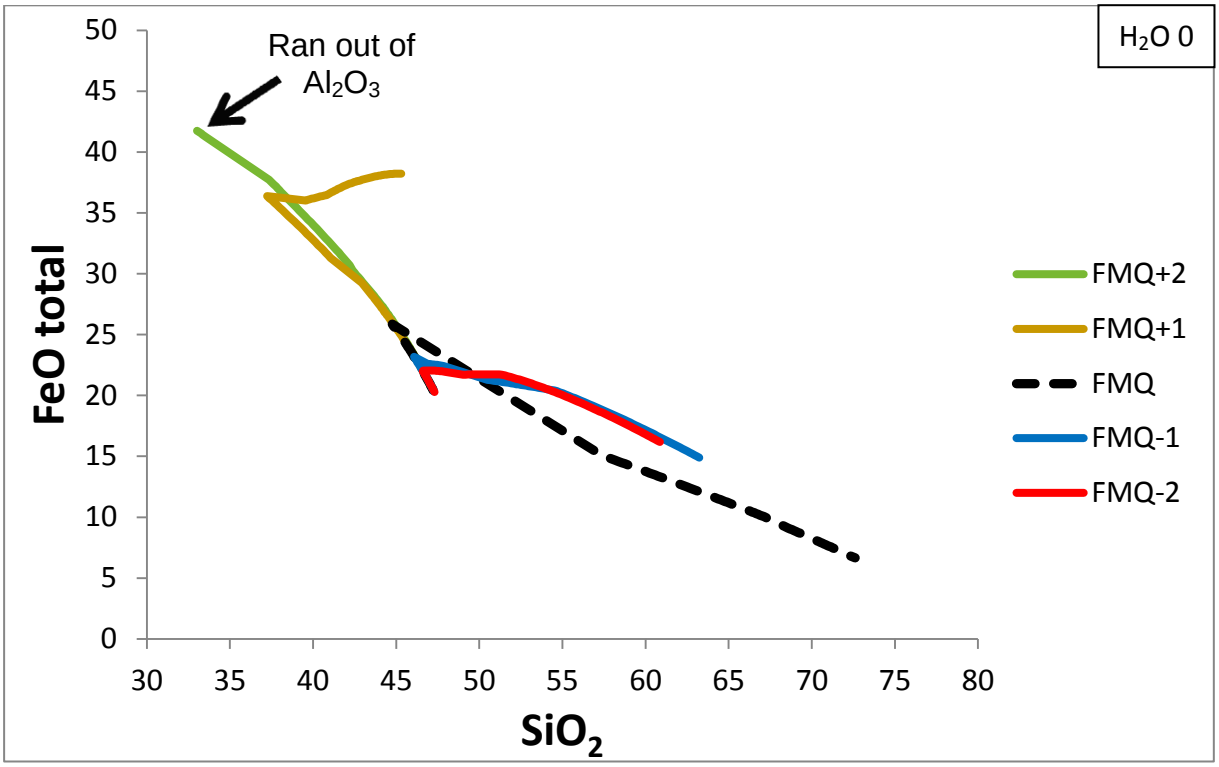

Figure 40. A plot of total iron (FeO + Fe_2O_3) against silica in the liquid for Skaergaard in wt.%. H_2O = 0 with varying FMQ conditions. It should be noted that the severely iron-rich liquid for FMQ+2 ends at only 44% liquid. Data from Tegner (1997).

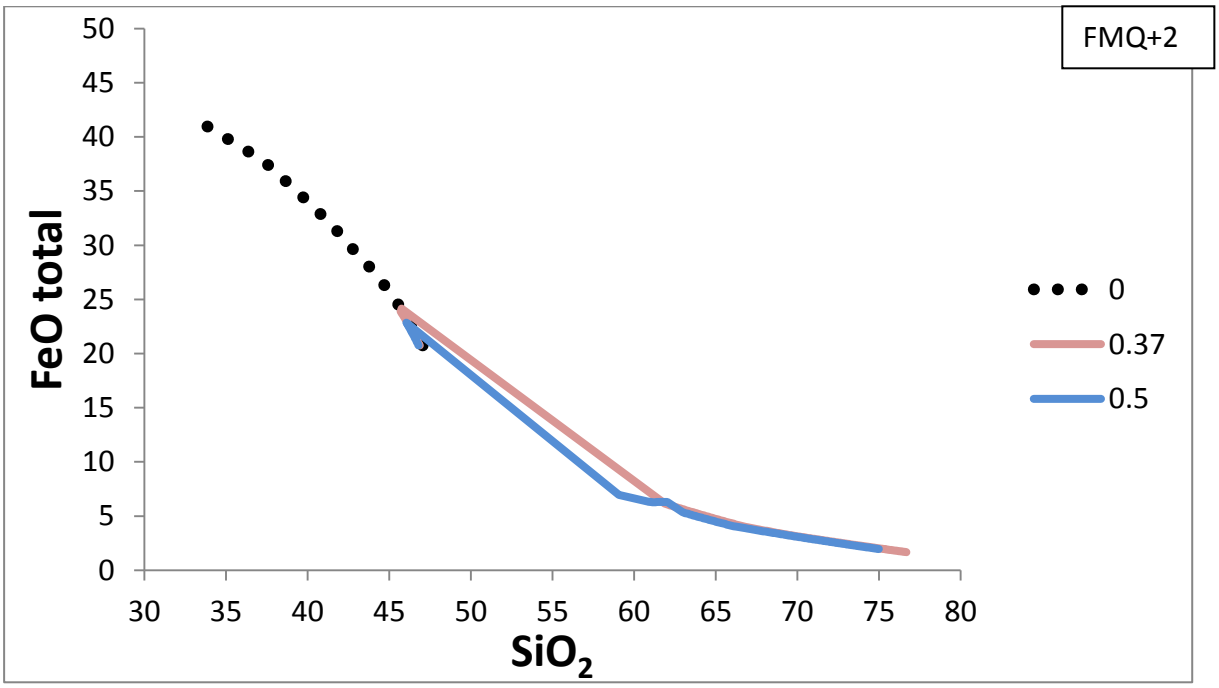

Figure 41. A plot of total iron (FeO + Fe_2O_3) against silica in the liquid for Skaergaard in wt.%. FMQ+2 with varying H_2O content. It should be noted that H_2O = 0 calculation ends at 44% liquid. Data from Tegner 1997.

5.4 Discussion

5.4.1 Birds River

Liquid evolution simulations for Birds River produce results very similar to that obtained by Eales (1990). The modelling shows initial iron-enrichment in the liquid, up to about 40-30% liquid (60-70% crystallisation) with little enrichment in SiO_2, followed by an unmistakeable drop in iron and enrichment in SiO_2. This observation is very much in keeping with results from Eales (1990) where iron-depletion and silica-enrichment occurred at 70% crystallisation (Fig. 14). These previous results are obtained from actual measured rock samples that supposedly represent the evolution of the iron-rich liquid. This was the case for all of the 96 simulations performed for Birds River.

Reducing conditions produced slightly higher maximum iron content compared to oxidising conditions. Thus, lower fO_2 conditions favour iron-enrichment, but buffers iron-enrichment at higher fO_2conditions. This is in keeping with the work done by Toplis and Carrol (1995) (Fig. 29).

Water content had a marked effect on iron-enrichment. An inverse relationship exists, where an increase in water content lead to a distinct drop in maximum iron reached compared to anhydrous conditions. However, regardless of water content the LLD always followed the same trend, one of initial iron-enrichment, the arrival of spinel, and then a drop in iron and simultaneous silica-enrichment. It should be noted that there was little discrepancy between maximum iron in FMQ-2 to FMQ conditions, for either anhydrous or hydrous conditions, but the effect of fO_2 became obvious under more oxidising conditions. This is in line with work done by Toplis and Carrol (1995) and Botcharnikov *et al.* (2008).

5.4.2 Skaergaard

Unlike simulations for Birds River, Skaergaard produced a great variety of results. This is to be expected with the range of starting liquid compositions. The original, and often quoted LLDs produced by Wager (1960); Hunter and Sparks (1987); Toplis and Carrol (1995); and Tegner (1997) are shown in Figure 42. The

first starting composition was from Wager (1960) (Table 14). It shows a trend of initial iron-enrichment, up to ~21 wt.% FeO total, followed by depletion in iron and enrichment in silica (Fig. 42). Magnetite crystallisation does not trigger a "land-slide" effect on iron in Figure 42, but rather a continued increase in iron followed by a slow change toward a silica-rich end. This was not the case in any of the simulations performed here for the starting composition proposed by Wager (1960); Hunter and Sparks (1987); Toplis and Carrol (1995); and Tegner (1997).

Two things stand out in the LLDs produced for starting compositions from Wager (1960); Toplis and Carrol (1995); and Tegner (1997): extreme iron-enrichment occurs under higher fO_2 conditions; and fO_2 has an opposite effect to that described in simulations performed for Birds River. These two things are not in keeping with literature, where higher fO_2 conditions (FMQ+2) buffer iron-enrichment and force magnetite to enter the system much earlier than under lower fO_2 conditions (FMQ-2), leading to a drop and/or cessation in iron-enrichment (Toplis and Carrol, 1995). In this case fO_2 seems to inhibit spinel crystallisation at higher FMQ values.

It is not understood why this is the case. In tholeiites with 4-5 wt.% TiO_2 and 17-18 wt.% FeO the magnetite liquidus is independent of fO_2 (Ariskin and Barmina, 1999). Furthermore, an addition of 1 mol% of P_2O_5 to a melt of basaltic composition will lead to a decrease in magnetite crystallisation temperature of 20 °C (Ariskin 1998). However, the liquids in question (Table 14) are nowhere near that in terms of composition. The simulations terminated at ~1050 °C, well below the expected crystallisation temperature of magnetite (~1100 °C).

An interesting point is that such extreme iron-enrichment only took place under anhydrous conditions. Once H_2O was present, even in small quantities, iron-enrichment was almost negligible. H_2O had the usual effect of buffering iron-enrichment and the effect became more pronounced with an increase in water content. This was especially evident for the simulations from Tegner (1997) which showed very little iron-enrichment, except for anhydrous melts under oxidising conditions. To highlight the stark difference between the LLDs produced here and those from literature, the LLDs produced here that best fit those presented in literature (Fig. 42) are plotted below in Figure 43.

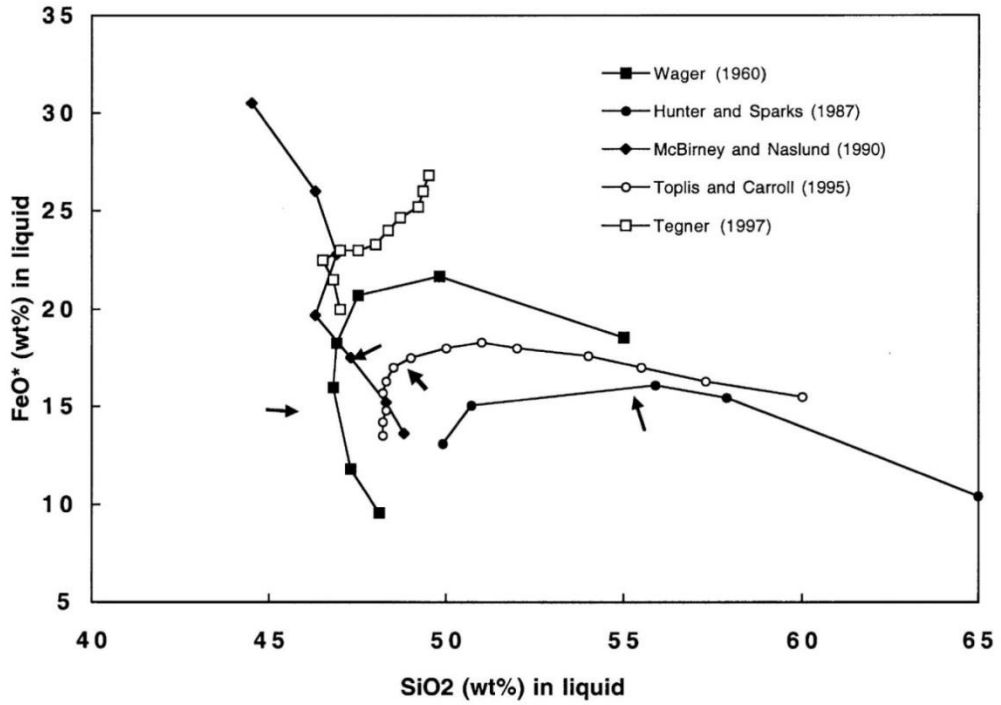

Figure 42. The five main proposed liquid lines of descent for the Skaergaard Intrusion, Greenland. Note the relatively similar initial trends below 50 wt.% SiO_2. Arrows indicate timing of magnetite crystallisation. From Jang *et al.* (2001).

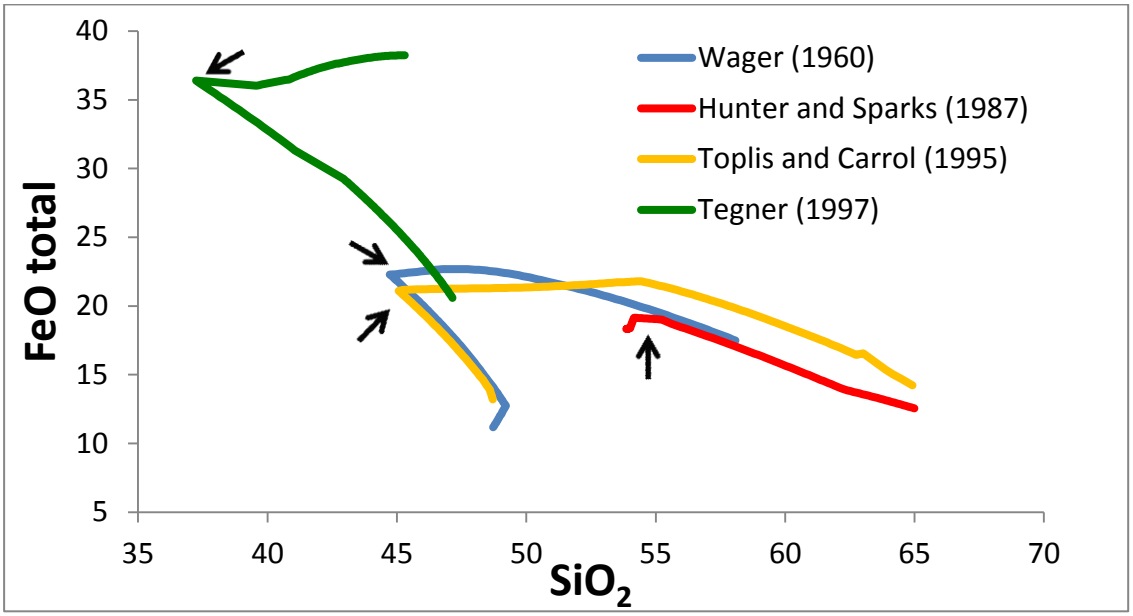

Figure 43. A plot of total iron (FeO + Fe_2O_3) against silica in the liquid for Skaergaard in wt.%. Presented here are four of the five main LLDs proposed for Skaergaard. Arrows indicate timing of magnetite crystallisation. This graph is a summary of the LLDs produced in this study that most like those from literature (Fig. 42). Note the axis had to be altered slightly because of higher iron enrichment present here.

6. Conclusion

Assumptions of any kind in the construction of a LLD are vitally important. For example, the assumption of size and volume for Skaergaard is a major problem, as it has not yet been perfectly determined, although geophysical estimates do exist. Thus, such estimations based on bulk summation should be avoided wherever possible. The inherent assumptions made during the construction of an LLD based on bulk summation calculations controls the outcome, if the size and proportions are not correctly ascertained.

The model produced by Eales (1990) for the Birds River LLD is based on modelling trace element behaviour in the melt. It is a potentially viable option, as it has been shown to follow a very similar trend to early measured behaviour of trace and major elements during the early stages of magma evolution. After ~70% crystallisation however, it does stop functioning as the trace elements that form the basis for the model have by that time decreased to below detectable limits. Even though very good correlation does exist prior to that point, it is difficult to reconcile modelling absolutely blind without any way to test or check the model. Jang *et al.* (2001) corroborate the importance of the evaluation of trace element behaviour, and highlight its use alongside petrological evidence.

Wager (1960); Hunter and Sparks (1987); and Tegner (1997) all based their LLD calculations on mass-balance equations. The chief difference between these three is while Wager (1960) and Tegner (1997) both produced liquids that become increasingly rich in iron, even beyond magnetite saturation, Hunter and Sparks (1987) depletes the moment magnetite appears on the liquidus. The fact that the former ultimately decreases in iron in the top-most portion of the Layered Series comes down to the assumption that the most evolved portion of Skaergaard is represented by a granophyre, although the model put forward by Tegner (1997) does show predominant iron-enrichment throughout most of the evolution of the Layered Series. This continued enrichment by Tegner (1997) might be because the Marginal Border Series was ignored during the calculation, which represents a much more silica-rich portion of the intrusion and could potentially drag the model toward a more silica-rich and iron-poor end. Hunter and Sparks (1987) assumed that the liquid

would follow a differentiation trend similar to primitive Icelandic magmas, thus a silica-enrichment trend, and chose the Tinden sill as the residual melt. Inherent in these assumptions is the undeniable fact that the liquids must ultimately become enriched in silica. Therefore, these models do not allow for anything other than silica enrichment.

Furthermore, Hunter and Sparks (1987) reject initial liquid compositions of anywhere below ~50% SiO_2, which is again based on the assumption that the Tinden sill represents the most fractionated portion of Skaergaard. It has been shown that small changes in the starting composition of differentiation melts can have drastic effects on the eventual outcome of forward liquid modelling (Ariskin, 2003; Thy *et al.*, 2006).

Not enough trials have been run for the method put forward by Tegner (1997) to concretely state that the measure of Fe^{3+} in plagioclase is a definite monitor for the behaviour of iron in the residual melt. It has only been used in two intrusions, namely Skaergaard; and the Bushveld Igneous Complex in South Africa. These two intrusions hardly represent the easiest and most straightforward petrological modelling sites in the world. It would be ideal to apply this model to an intrusion that has been a little better constrained and is a wee less ambiguous.

Toplis and Carrol (1995) produced experimental liquids that advocate a very strong correlation between magnetite crystallisation and the onset of iron-depletion and silica-enrichment, from a liquid undergoing iron-enrichment at the time of crystallisation. More than one author has questioned the validity of these results, pointing to the absurdly high quantity of magnetite present during fractionation in these experiments (e.g. Tegner (1997); Thy *et al.*, 2009;).

Very little petrological modelling software exists that is more powerful than AlphaMELTS. It is made especially powerful because of its ability to predict the effect of fO_2 and H_2O on the composition of a crystallising liquid. Isobaric calculations for Birds River and Skaergaard starting liquid compositions were performed at varying FMQ and H_2O conditions.

Simulations for Birds River produced results which are in good agreement to those modelled by Eales (1990). The sudden increase in SiO_2 with simultaneous drop in FeO total also took place at ~70% crystallisation, which is in accordance with actual rock samples taken for Birds River (Eales, 1990). A decrease in iron-enrichment was immediately preceded by spinel arrival. Increasing H_2O lowered the maximum iron content considerably, and seemed to be the most influential factor. A shift from reducing to oxidising conditions also decreased the maximum iron content, but to a lesser extent than H_2O. This is in line with what literature predicts.

Simulations for Skaergaard produced much more varied results, as is expected from the range of initial compositions. An inverse relationship exists between fO_2 and maximum iron content for 3 of the four LLDs (Wager, 1960; Toplis and Carrol, 1995; and Tegner, 1997). This translates into higher iron-enrichment at more oxidising conditions, which is not in agreement with literature. Extreme iron-enrichment takes place at anhydrous and oxidising conditions. It should be noted that at hydrous conditons (even slightly so) very little iron enrichment is observed and the LLD follows a path of silica-enrichment. Whenever iron-enrichment was terminated in favour of silica-enrichment it coincided with the arrival of spinel. However, in the cases where iron enrichment continued into the final stages of crystallisation spinel never appeared. A summary of the maximum and minimum iron-enrichment levels are summarised here in Table 15.

Table 15. A summary of the fO_2 and H_2O conditions at which maximum and minimum iron-enrichment was achieved. FeOt = FeO + Fe_2O_3.

	Initial FeOt	Conditions of max FeOt			Conditions of min FeOt		
Comp		**fO_2**	**H_2O**	**Max FeOt**	**fO_2**	**H_2O**	**Min FeOt**
E	9.27	FMQ-2	0	~17	FMQ+2	1.0	~9.5
W	9.81	FMQ+2	0	~48	FMQ-2	1.0	~12.5
H&S	18.2	FMQ	0	~19.5	FMQ+2	1.0	~18.3
T&C	13.1	FMQ+2	0	~40	FMQ-2	1.0	~13
T	20.1	FMQ+2	0	~42	FMQ-2	1.0	~20

Some of the iterations experienced problems whenever a peritectic was reached. The thermodynamic model seemingly struggles with the presence of simultaneous phases, so complex phase calculations are not possible when too many variables are applied. However, for the most part the thermodynamic model proved to be reliable.

Based on the results from this analysis, the importance of a good starting liquid composition cannot be stressed enough, as this has a major impact on the final LLD. The results for Birds River are nicely correlated to that in found literature, but the inverse relationship experienced between fO_2 and iron-enrichment in some of the starting compositions for Skaergaard cannot be explained. The fact that H_2O has a constant influence is some justifications that the thermodynamic model behind AlphaMELTS is functioning correctly, and that some LLDs were produced that do match that of literature. Further investigation is required.

7. Acknowledgements

The most important person I would like to thank is Dr. James Roberts for his unwavering support, words of encouragement and understanding. He always made himself available for discussions, a hasty debrief or a nice beer. I would like to thank the NRF, for without their support this project would never have been possible. Special thanks to the de Bruyn family for providing a place to call my own, and to Gert and Ina, if it wasn't for you I would in all likelihood never have gotten this far. Last, but not least, to my loving and simply marvellous fiancé Amanda.

8. References

Abu El-Ela, F.F. (1996). The petrology of the Abu Zawal gabbroic intrusion, Eastern Desert, Egypt: an example of an island-arc setting. *Journal of African Earth Sciences*, **22** (2), 147-157.

Allegre, C.J., Treuil, M., Minster, J.F., Minster, B. and Albarède, F. (1977). Systematic use of trace elements in igneous processes. *Contr. Mineral. Petrol.,* **60**, 57-75.

Antoshechkina, P. M., P. D. Asimow, E. H. Hauri, and P. I. Luffi (2010), Effect of water on mantle melting and magma differentiation, as modeled using alphaMELTS 3.0, Abstract V53C-2264 presented at 2010 Fall Meeting, AGU, San Francisco, Calif., 13-17 Dec.

Ariskin, A.A. (1998). Calculation of Titanomagnetite Stability on the Liquidus of Basalts and Andesites with Special Reference to Tholeiitic Magma Differentiation. *Geochemistry International,* **36** (1), 15-23.

Ariskin, A.A. (2003). Modeling of the Equilibrium Crystallization of Ultramafic Rocks with Application to the Problems of Formation of Phase Layering in the Dovyren Pluton, Northern Baikal Region, Russia. *Geochemistry International*, **41** (2), 107-129.

Ariskin, A.A. and Barmina, G.S. (1999). An empirical model for the calculation of spinel-melt equilibria in mafic igneous systems at atmospheric pressure: 2. Fe-Ti oxides. *Contributions to Mineralogy and Petrology,* **134** (2-3), 251-263.

Barnes, S-J. and Lightfoot, P.C. (2005). *Formation of magmatic nickel-sulfide ore deposits and processses affecting their copper and platinum-group element contents.* In: Hedenquist, J.W., Thompson, J.F.H., Goldfarb, R.J. and Richards, J.P. (eds.) Economic Geology 100th Anniversary Volume, p. 179-213.

Beattie, P., Drake, M.J., Jones, J., Leeman, W., Longhi, J., McKay, G., Nielsen, R., Palme, H., Shaw, D., Takahashi, E. and Watson, B. (1993). Terminology for trace-element partitioning. *Geochim. Cosmochim. Acta,* **57**, 1605-1606.

Bernstein, S., Rosing, M.T., Brooks, C.K. and Bird, D.K. (1992). An ocean ridge type magma chamber at a passive Volcanic, continental margin: the Kap Edvard Holm, layered gabbro complex, East Greenland. *Gol. Mag.,* **129**, 437-456.

Bird, D.K., Manning, C.E., & Rose, N.M., 1988. Hydrothermal alteration of Tertiary layered gabbros, East Greenland. *Am. J. Sci.,* **288**, 405-57.

Blank, H.R. and Gettings, M.E. (1973). Subsurface form and extent of the Skaergaard intrusion, East Greenland. *Trans Am Geophys Union (EOS)*, **54**, 507.

Bogaerts, M. and Schmidt, M.W. (2006). Experiments on silicate melt immiscibility in the system Fe_2SiO_4-$KAlSi_3O_8$-SiO_2-CaO-MgO-TiO_2-P_2O_5 and implications for natural magmas. *Contributions to Mineralogy and Petrology,* **152**, 257-274.

Botcharnikov, R.E., Koepke, J., Holtz, F., McCammon, C., and Wilke, M. (2008). The effect of water activity on the oxidation and structural state of Fe in a Ferro-basaltic melt. *Geochim. Cosmo. Acta,* **69**, 5071-5085.

Bottinga, Y. and Weill. D.F. (1970). Densities of liquid silicate systems calculated from partial molar volumes of oxide components. *Am. J. Sci.*, **269**, 169-182.

Bowen, N.L. (1928). *The evolution of Igneous Rocks*, Dover, New York. -334pp.

Brooks, C.K., & Gleadow, A.J.W., 1977. A fission-track age for the Skaergaard Intrusion and the age of the East Greenland basalts. *Geology,* **5**, 539-40.

Brooks, C.K., & Nielsen, T.F.D., 1978. Early stages in the differentiation of the Skaergaard magma as revealed by a closely related suite of dyke rocks. *Lithos,* **11**, 1-14.

Brooks, C.K. and Nielsen, T.F.D. (1990). The differentiation of the Skaergaard intrusion. Discussion of Hunter and Sparks (*Contrib. Mineral. Petrol*., **95**, 451-461.). *Contrib. Mineral. Petrol.,* **104**, 244-247.

Burnham, C.W. (1975). Water and magmas; a mixing model. *Geochim. Cosmo. Acta*, **39**, 1077-1084.

Cawthorn, R.G., Boudreau, A.E., Barnes, S.J., Mallitch, K. and Ballhaus, C. (2005). PGE, Cr, and V mineralization in igneous rocks: *Economic Geology 100th Anniversary Volume*, p. 000.

Charlier, B. and Grove, T.L. (2012). Experiments on liquid immiscibility along tholeiitic liquid lines of descent. *Contrib. Mineral Petrol.*, **164**, 27-44.

Clowe, C.A., Popp, R.K., and Fritz, S.J. (1988) Experimental investigation of the effect of oxygen fugacity on ferric-ferrous ratios and unit-cell parameters of four natural clinoamphiboles. Am Mineral, **73**, 487-499.

Carmichael, I.S.E. (1991). The redox states of basic and silicic magmas: a reflection of their source region? *Contributions to Mineralogy and Petrology,* **106**, 129-141.

Carmichael, I.S.E. and Ghiorso, M.S. (1986). Oxidation-reduction relations in basic magma: a case for homogeneous equilibria. *Earth and Planetary Science Letters,* **78**, 200-210.

Daly, R.A. (1914). *Igneous Rocks and their Origin.* New York: McGraw-Hill.

De, A. (1974). Silicate liquid immiscibility in the Deccan Traps and its petrogenetic significance. *Geological Society of America Bulletin*, **85**, 471-474.

Deer, W.A., 1976. Tertiary igneous rocks between Scoresby Sund and Kap Gustov Holm, East Greenland. In: A. Escher and W.S. Watt, (Editors) *Geology of Greenland.* Gronlands Geologiske Undersogelse, 405-429.

Deines, P., Hafzinger, R.H., Ulmer, G.C. and Woermann, E. (1974). Temperature-oxygen fugacity tables for selected gas mixtures in the system C-H-O at one atmosphere total pressure. *Bulletin of the Earth and Mineral Sciences Experiment Station, Pennsylvania State University*, **88**, 128.

Delaney, J.S., Dyar, M.D., Sutton, S.R. and Bajt, S. (1998). Redox ratios with relevant resolution: Solving an old problem by using the synchrotron microXanes probe. *The Geological Society of America*, **26** (2), 139-142.

Dicken, A.P., Brown, J.L., Thompson, R.N., Halliday, A.N. and Morrison, M.A. (1984). Crustal contamination and the granite problem in the British Tertiary Volcanic Province. *Philos. Trans. R. Soc. London*, **310**, 317-339.

Dickenson, M.P. and Hess, P.C. (1981). Redox equilibria and the structural role of iron in alumino-silicate melts. *Contrib. Mineral. Petrol.,* **78**, 352-357.

Dickenson, M.P. and Hess, P.C. (1986). The structural role and homogeneous redox equilibria of iron in peraluminous, metaluminous and peralkaline silicate melts. *Contrib. Mineral. Petrol.*, **92**, 207-217.

Dixon, S. and Rutherford, M.J. (1979). Plagiogranites as late-stage immiscible liquids in ophiolite and mid-ocean ridge suites: an experimental study. *Earth and Planetary Science Letters,* **45**, 45-60.

Dostal, J., Dupuy, C., Carron, J.P., Kerneizon, M. and Maury, R.C. (1983). Partition coefficients of trace elements: application to volcanic rocks of St. Vincent, West Indies. *Geochim. Cosmochim. Acta,* **47**, 525-533.

Douglas, J.A.V., 1961. Geologic investigations in East Greenland: Part VII. The Basistoppen sheet, a differentiated basic intrusion into the upper part of the Skaergaard Complex, East Greenland. *Meddr. Gronland* **164**, 1-66.

Du Toit, A.L. (1920). The Karroo dolerites of South Africa. *Transactions of the Geological Society of South Africa,* **23**, 1-42.

Du Toit, A.L. (1905). Geological survey of Glen Gray and parts of Queenstown and Wodehouse. *Tenth annual Rep., Cape Geological Commision*, 97-140.

Dyar, M.D., Delaney, J.S., and Sutton, S.R. (2001). Fe XANES spectra of iron-rich micas. *European J. Mineral.,* **13** (6), 1079-1098.

Eales, H.V. (1990). The Birds River Intrusion – a quantitative model for Karoo Central Province basalt fractionation. *South African Journal of Geology*, **93** (5-6), 717-728.

Eales, H.V. and Booth, P.W.K. (1974). The Birds River gabbro complex, Dordrecht District. *Transactions of the Geological Society of South Africa*, **77**, 1-15.

Eales, H.V. and Reynolds, I.M. (1983). Factors influencing the composition of chromite and magnetite in some southern African rocks. *Spec. Publ. Geol. Soc. S. Afr.,* **7**, 5-20.

Eales, H.V. and Robey, A. (1976). Differentiation of Tholeiitic Karroo Magma at Birds River, South Africa. *Contributions to Mineralogy and Petrology*, **56**, 101-117.

Fenner, C.N. (1929). The crystallization of basalts, *Am. Jour. Sc.,* 105, 225-253

Frost, B.R. (1991) Introduction to oxygen fugacity and its petrologic importance. *Revs. Mineral*., **25**, 1-9.

Frost, B.R. and Lindsley, D.H. (1992). Equilibria among FeTi oxides, pyroxenes, olivines, and quartz: Part II. Application. *Am. Mineral.*, **77**, 1004-1020.

Frost, B.R., Lindsley, D.H. and Anderson, D.J. (1988). Fe-Ti oxide-silicate equilibria: assemblages with fayalitic olivine. *American Mineralogist*, **73**, 727-740.

Fudali, R.F. (1965). Oxygen fugacities of basaltic and andesitic magmas. *Geochimica et Cosmochimica Acta*, **29**, 1063-1075.

Ghiorso, M.S., and Sack, R.O. (1995). Chemical Mass-Transfer in Magmatic Processes IV. A Revised and Internally Consistent Thermodynamic Model for the Interpolation and Extrapolation of Liquid-Solid Equilibria in Magmatic Systems at Elevated-Temperatures and Pressures. *Contributions to Mineralogy and Petrology*, **119** (2-3), 197-212.

Ghiorso, M.S., Hirschmann, M.M., Reiners, P.W. and Kress, V.C. (2002). The pMELTS: A revision of MELTS for improved calculation of phase relations and major element partitioning related to partial melting of the mantle to 3 GPa. *Geochem. Geophys. Geosyst.,* **3** (5), 1030.

Giehl, C., Marks, M. and Nowak, M. (2012). Phase relations and liquid lines of descent of an iron-rich peralkaline phonolitic melt: an experimental study. *Contrib Mineral Petrol,* **165** (2), 283-304.

Greig, J.W. (1927). Immiscibility in silicate melts. *American Journal of Science*, **13**, 133-154.

Grove, T.L. and Baker, M.B. (1984). Phase equilibrium controls on the tholeiitic versus calc-alkaline differentiation trends. *Journal of Geophysical Research*, **89**, 3253-3274.

Grove, T.L., Baker, M.B. and Kinzler, R.J. (1984). Coupled CaAl-NaSi diffusion in plagioclase feldspar: experiments and application to cooling rate speedometry. *Geochim. Cosmichim. Acta*, **48**, 2113-2121.

Gualda, G.A.R., Ghiorso, M.S., Lemons, R.V. and Carley, T.L. (2012). Rhyolite-MELTS: a Modified Calibration of MELTS Optimized for Silica-rich, Fluid-bearing Magmatic Systems. *Journal of Petrology,* **53** (5), 875-890.

Haar, L.J., Gallagher, J.S. and Kell, G.S. (1984). *NBS/NRC Steam Tables*. Taylor and Francis, Philadelphia, Pa.

Hanghøj, K., Rosing, M.T. and Brooks, C.K. (1995). Evolution of the Skaergaard magma: evidence from crystallized melt inclusions. *Contrib. Mineral. Petrol.,* **120**, 265-269.

Hamilton, D.L. and Anderson, G.M. (1967). Effects of water and oxygen pressure on the crystallization of basaltic magmas, 445-479. In: H.H. Hess, (Editor), *Basalts*. Interscience Publishers.

Hill, R. and Roeder, P. (1974). The crystallization of spinel from basaltic liquid as a function of oxygen fugacity. *Journal of Geology*, **82**, 709-729.

Hirschmann, M., 1992. Origin of the transgressive granophyres from the Layered Series of the Skaergaard Intrusion, East Greenland. J. *Volc. Geoth. Res.* 52, 185Hoover, J.D., 1989. The contact gabbro and initial liquid composition of the Skaergaard Intrusion. *J. Petrology,* **30**, 441-76.

Hofmeister, A.M. and Rossman, G.R. (1984). Determination of Fe^{3+} and Fe^{2+} concentrations in feldspar by optical absorption and EPR spectroscopy. *Physics and Chemistry of Minerals*, **11**, 213-224.

Huebner, S.J. (1971). Buffering Techniques for Hydrostatic Systems at Elevated Pressures. Research Techniques for High Pressure and High Temperature. In: G.C. Ulmer (Editors), *Research Techniques for High Pressure and High Temperature.* Springer-Verlag, New York, pp.123-177.

Huebner, J.S. and Sato, M. (1970). The oxygen fugacity-temperature relationships of manganese and nickel oxides buffers. *American Mineralogist*, **55**, 934-952.

Hughes, C.J., 1956. Geological investigations in East Greenland, Part VI. A differentiated basic sill enclosed in the Skaergaard Intrusion, East Greenland, and related sills injecting the lavas. Meddr. Gron., **137**, 1-27.

Hunter, R.H. and Sparks, R.S.J. (1987). The differentiation of the Skaergaard intrusion. *Contrib. Mineral. Petrol.,* **95**, 451-461.

Hunter, R.H. and Sparks, R.S.J. (1990). The differentiation of the SKaergaard intrusion. Replies to A.R. McBirney and H.R. Naslund, S.A. Morse, C.K. Brooks and T.F.D. Nielsen. *Contrib. Mineral. Petrol.*, **104**, 248-254.

Jakobsen, J.K., Veksler, I.V., Tegner, C and Brooks, C.K. (2005). Immiscible iron- and silica-rich melts in basalt petrogeneis documented in the Skaergaard intrusion. *Geology*, **33**, 885-888.

Jakobsen, J.K., Veksler, I.V., Tegner, C. and Brooks, C.K. (2011). Crystallization of the Skaergaard Intrusion from an Emulsion of Immiscible Iron- and Silica-rich Liquids: Evidence from Melt Inclusions in Plagioclase. *Journal of Petrology,* **52** (2), 345-373.

Jang, Y.D., Naslund, H.R. and McBirney, A.R. (2001). The differentiation trend of the Skaergaard intrusion and the timing of magnetite crystallization: iron enrichment revisited. *Earth and Planetary Science Letters,* **189**, 189-196.

Juster, T.C., Grove, T.L. and Perfit, M.R. (1989). Experimental constraints on the generation of Fe-Ti basalts, andesites, and rhyodacites at the Galapagos spreading centre, 85°W and 95°W. *Journal of Geophysical Research*, **94**, 9251-9274.

Kays, M.A., McBirney, A.R. and Goles, G.G. (1981). Xenoliths of gneisses and the conformable, clot-like granophyres in the marginal Border Group, Skaergaard intrusion, East Greenland. *Contrib. Mineral Petrol.*, **76**, 265-284.

Kennedy, G.C. (1984). Equilibrium between volatiles and iron oxides in igneous rocks. *American Journal of Science*, **246**, 529-549.

Kilinc, A., Carmicheal I.S.E., Rivers M.L., and Sack R.O. (1983) The ferric-ferrous ratio of natural silicate liquids equilibrated in air. *Contrib. Mineral Petrol*., **83**, 136-140.

King, P.L., Hervig, R.L., Holloway, J.R., Delaney, J.S., and Dyar, M.D. (2000) partitioning of Fe3+/Fetotal between amphibole and basanitic melt as a function of oxygen fugacity. *Earth and Planetary Science Letters*, **178**, 97-112.

Kohn, S.C. and Schofield, P.F. (1994). The implication of melt composition in controlling trace-element behaviour: an experimental study of Mn and Zn partitioning between forsterite and silicate melts. *Chem. Geol.,* **117**, 73-87.

Kress, V.C. and Carmichael S.E. (1988). Stiochiometry of the iron oxidation reaction in silicate melts. *Am. Mineral*, **73**, 1267-1274.

Kress, V.C. and Carmichael, S.E. (1989). The lime-iron-silicate melt system: redox and volume systematics. *Geochim. Cosmo. Acta*, **53**, 2883-2892.

Kress, V.C. and Carrmichael S.E. (1991). The Compressibility of Silicate Liquids containing Fe2O3 and the Effect of Composition, Temperature, Oxygen Fugacity, and Pressure on Their Redox States. *Contrib. Mineral. Petrol.*, **108**, 82-92.

Lac, D. (2009). *Using the oxidation state of iron in plagioclase to evaluate magma oxygen fugacity: a micro-XANES study.* MSc. Thesis (unpublished), University of Massachusetts Amherst, Massachusetts, United States of America, 80pp.

Larsen, R.B. and Tegner, C. (2006). Pressure conditions for the solidification of the Skaergaard intrusion: Eruption of East Greenland flood basalts in less than 300,000 years. Lithos, **92** (1-2), 181-197.

Latypov, R., Chistyakova, S. and Alapieti, T. (2007). Revisiting problem of chilled margins associated with marginal reversals in mafic-ultramafic intrusive bodies. *Lithos*, **99**, 178-206.

Leeman, W.P. and Dasch, E.J. (1978). Strontium, lead and oxygen isotopic investigation of the Skaergaard intrusion, East Greenland. *Earth Planet Sci. Lett.*, **41**, 47-59.

Lindsley, D.J. (1976). Experimental studies of oxide minerals. In: D. Rumble (Editor). *Oxide Minerals, MSA Reviews in Mineralogy*. **1**.

Lindsley, D.H., Speidel, D.H. and Nafziger, R.H. (1968). P-T-f_{O2} Relations for the system Fe-O-SiO_2. *American Journal of Science*, **266**, 342-360.

Larsen, R.B. and Brooks, C.K. (1994). Origin and evolution of gabbroic pegmatites in the Skaergaard intrusion, East Greenland. *J. Petrol.,* **35**, 1651-1679.

Longhi, J., Walker, D., and Hays, J.F. (1976) Fe and Mg in plagioclase. In: Proc Lunar Sci Conf 7th, pp. 1281-1300.

Lundgaard, K.L. and Tegner, C. (2004). Partitioning of ferric and ferrous iron between plagioclase and silicate melt. *Contrib. Mineral. Petrol.*, **147** (4), 470-483.

Macdonald, R., Sparks, R.S.J. Sigurdsson, H., McGarvie, D.A. and Smith, R.L. (1987). The 1875 eruption of Askja volcano, Iceland: combined fractional crystallization and selective contamination in the generation of rhyolitic magma. *Mineral. Mag.*, **51**, (360), 183-202.

Manning, C.E., & Bird, D.K., 1991. Porosity evolution and fluid flow in the basalts of the Skaergaard magma-hydrothermal system, East Greenland. *Am. J. Sci.,* **291**, 201-57.

Marsh, J.S. and Eales, H.V. (1984). Chemistry and petrogenesis of igneous rocks of the Karoo Central Area, Southern Africa. *Spec. Publ. Geol. Soc. S. Afr.,* **13**, 27-67.

McBirney, A.R. (1975). Differentiation of the Skaergaard intrusion. *Nature*, **253**, 691-694.

McBirney, A.R. (1989). The Skaergaard Layered Series I: structures and average compositions. *J.Petrol.,* **30**, 363-398.

McBirney A.R. and Nakamura, Y. (1974). Immiscibility in late stage magmas of the Skaergaard intrusion. *Carnegie Inst Washington Yearb,* **73**, 348-354.

McBirney, A.R. and Noyes, R.M. (1979). Crystallization and layering of the Skaergaard intrusion. *J. Petrol.*, **20**, 185-212.

McBirney, A.R. and Naslund, H.R. (1990). The differentiation of the Skaergaard Intrusion. A discussion of Hunter and Sparks. *Contributions to Mineralogy and Petrology*, **104**, 234-240.

McBirney, A.R. (1995). Mechanisms of differentiation in the Skaergaard intrusion. *J. Geol. Soc. London,* **152**, 421-435.

Morse, S.A. (1981). Kiglapait geochemistry IV: The major elements. *Geochimica et Cosmochimica Acta*, **45**, 461-479.

Morse, S.A., Lindsley, D.H. and Williams, R.J. (1980). Concerning intensive parameters in the Skaergaard Intrusion. *Am. J. Sci.*, **280-A**, 159-170.

Mysen, B.O., Virgo, D., Harrison, W.J. and Scarfe, C.M. (1980). Solubility mechanisms of H_2O in silicate melts at high pressures and temperatures: a Raman spectroscopic study. *Am. Mineral.*, **65**, 900-914.

Mysen, B.O. and Virgo, D. (1980). Trace element partitioning and melt structure: an experimental study at 1 atm pressure. *Geochim. Cosmochim. Acta,* **44**, 1917-1930.

Naldrett, A.J. (2004). Magmatic sulfide deposits: Geology, geochemistry and Exploration. Berlin, Springer, 727 p.

Naslund, H.R. (1980). *Part I. Petrology of the Upper Border Group of the Skaergaard Intrusion, East Greenland; and Part II. An Experimental Study of Liquid Immiscibility in Iron-Bearing Silicate Melts* (Ph.D. Dissertation), University of Oregon, Eugene, OR. -347pp.

Naslund, H.R. (1983). The effect of oxygen fugacity on liquid immiscibility in iron-bearing silicate melts. *Am. J. Sci.*, **283**, 1034-1059.

Naslund, H.R., 1984. Petrology of the Upper Border Series of the Skaergaard Intrusion. *J. Petrology,*
24, 185-212.

Naslund, H.R. (1989). Petrology of the Basistoppen sill, East Greenland: A calculated magma differentiation trend. *J. Petrol.*, **30**, 299-319.

Nielsen, T.F.D., 1978. The Tertiary dyke swarms of the Kangerdlugssuaq area, East Greenland. An example of magmatic development during continental break-up. Contr. Miner. Petrol., **67**, 63-78.

Norton, D., & Taylor, H.P. Jr, 1979. Quantitative simulation of the hydrothermal systems of crystallizing magmas on the basis of transport theory and oxygen

isotope data: an analysis of the Skaergaard Intrusion. J. Petrology, **20**, 421-86.

Osborn, E.F. (1959). The role of oxygen pressure in the crystallization and differentiation of basaltic magma. *Am Mineral*, **257**, 609-647.

Osborn, E.F. (1962). Reaction series for subalkaline igneous rocks based on different oxygen pressure conditions. *Am Mineral*, **47**, 211-226.

Philpotts, A.R. (1976). Silicate liquid immiscibility in tholeiitic basalts. *American Journal of Science,* **276**, 1147-1177.

Philpotts, A.R. (1982). Compositions of immiscible liquids in volcanic rocks. *Contributions to Mineralogy and Petrology*, **80**, 201-218.

Philpotts, A.R. (1990). *Principles of Igneous Petrology.* Prentice Hall: New Jersey.-237pp.

Philpotts, A.R. and Doyle, C.D. (1983). Effect of magma oxidation state on the extent of silicate liquid immiscibility in a tholeiitic basalt. *Am. J. Sci.,* **283**, 967-986.

Phinney, W.C. (1992). Partitioning coefficients of iron between plagioclase and basalts as a function of oxygen fugacity: implications for Archean and lunar anorthosites. *Geochim. Cosmochim. Acta,* **56**, 1885-1895.

Pitzer, K.S. and Sterner, S.M. (1994). Equations of state valid continuously from zero to extreme pressures for H_2O and CO_2. *J. Chem. Phys.,* **101** (4), 3111-3116.

Poldervaart, A. (1944). The petrology of the Elephant's Head dike and the New Amalfi sheet (Matatiele). *Trans. Roy. Soc. S. Afr.,* **30**, 85-119.

Poldervaart, A. (1946). The petrology of the Mount Arthur Complex (East Griqualand). *Trans. Roy. Soc. S. Afr.*, **31**, 83-110.

Ragland, P.C. (1989). *Basic analytical petrology.* Oxford University Press, New York.-369pp.

Redhammer, G.J., Beran A., Dachs E., and Amthauer G. (1993) A Mössbauer and X-Ray diffraction study of annites synthesized at different oxygen fugacities and crystal chemical implications. Phys Chem Minerals, **20**, 382-394.

Roeder, P.L. and Osborn, E.F. (1966). Experimental data for the system MgO-FeO-Fe_2O_3-$CaAl_2Si_2O_8$-SiO_2 and their petrogenic implications. *Am J Sci*, **264**, 428-480.

Roedder, E. & Weiblen, P.W. (1970). Lunar petrology of silicate melt

inclusions, Apollo 11 rocks. In:. Proceedings of the Apollo 11 Lunar Science Conference. Geochimica et Cosmochimica Acta, Supplement 1, 1, 507-528.

Roedder, E. & Weiblen, P.W. (1971). Petrology of silicate melt inclusions, Apollo 11 and Apollo 12 and terrestrial equivalents. In: Proceedings of the 2nd Lunar Science Conference. Geochimica et Cosmochimica Acta, Supplement 2, 1, 507-528.

Rollinson, H.R. (1993). *Using Geochemical Data: Evaluation, Presentation, Interpretation*. Longman Scientific and Technical.-352pp.

Sack, R.O., Carmicheal I.S.E., Rivers M., and Ghiorso M.S. (1980) Ferric-ferrous equilibria in natural silicate liquids at 1 bar. Contrib Mineral Petrol, **75**, 369-376.

Sato, H. (1989). Mg-Fe partitioning between plagioclase and liquid in basalts of Hole 504B OPD LEG 111: a study of melting at 1 atm. Proc ODP Sci Res, **111**, 17-26.

Sato, M. (1978). Oxygen fugacity of basaltic magmas and the role of gas-forming elements. *Geophysical Research Letters,* **5**, 447-449.

Schmidt, M.W., Connolly, J.A.D., Günther, D. and Bogaerts, M. (2006). Element partitioning-the role of melt structure and composition. *Science*, **312**, 1646-1650.

Sigurdsson, H. and Sparks, R.S.J. (1981). Petrology and rhyolitic and mixed-magma ejecta from the 1875 eruption of Askja, Iceland. *J. Petrol*., **22**, 41-84.

Sigurdsson, H. and Sparks, R.S.J. (1978). Rifting episodes in north Iceland in 1974-75 and the eruption of Askja and Sveinagja. *Bull. Volcanol.*, **41**, 1-19.

Smith, J.V. (1974). *Feldspar minerals, II. Chemical and textural properties*. Springer, Berlin, Heidelberg, New York.

Smith, J.V. and Brown, W.L. (1987). *Feldspar minerals*. Springer, Heidelberg.

Smith, P.M. and Asimow, P.D. (2005). Adiabat_1ph: A new public front-end to the MELTS, pMELTS, and pHMELTS models. *Geochem. Geophys. Geosyst.,* 6, art. no. Q02004, doi:10.1029/2004GC000816.

Snyder, D., Carmichael, I.S.E. and Wiebe, R.A. (1993). Experimental study of liquid evolution in an Fe-rich, layered mafic intrusion: constraints of Fe-Ti oxide

precipitation on the T-fO_2 and T-ρ paths of tholeiitic magmas. *Contributions to Mineralogy and Petrology,* **113**, 73-86.

Stewart, B.W. and DePaolo, D.J. (1990). Isotopic studies of processes in mafic magma chambers: II. The Skaergaard intrusion, East Greenland. *Contrib. Mineral. Petrol.,* **104**, 125-141.

Stolper, E. (1982). Water in silicate Glasses: An infrared spectroscopy study. *Conrib. Mineral. Petrol.,* **81**, 1-17.

Sugawara, T. (2000) Thermodynamic analysis of Fe and Mg partitioning between plagioclase and silicate liquid. Contrib. Mineral. Petrol., **138**, 101-113.

Sugawara, T. (2001). Ferric iron partitioning between plagioclase and silicate liquid: thermodynamics and petrological applications. *Contrib. Mineral. Petrol.*, **141**, 659-686.

Tegner, C. (1997). Iron in plagioclase as a monitor of the differentiation of the Skaergaard intrusion. *Contrib. Mineral. Petrol.,* **128**, 45-51.

Tegner, C., Delaney, J.S., Dyar, M.D. and Lundgaard, K.L. (2003). Iron in plagioclase as a monitor of oxygen fugacity in Skaergaard, Bushveld, and Bjerkreim-Sokndal layered intrusions, and anorthosite if the Rogaland Igneous Province, EGS-AGU-EUG Joint Assembly, Geophysical Research Abstracts, Nice, pp. 08789.

Thorarinsson, S. and Sigvaldason, G.E. (1972). The Hekla eruption of 1970. *Bull. Volcanol.*, **36**, 269-288.

Thy, P. and Lofgren, G.E. (1994). Experimental constraints of the low-pressure evolution of the transitional and mildly alkali basalts: the effect of the Fe-Ti oxide minerals and the origin of basaltic andesites. *Contrib. Mineral. Petrol.,* **116**, 340-351.

Thy, P., Lesher, C.E., Nielsen, T.F.D. and Brooks, C.K. (2006). Experimental constraints on the Skaergaard liquid line of descent. *Lithos*, **92**, 154-180.

Thy, P, Lesher, C.E. and Tegner, C. (2009). The Skaergaard liquid line of descent revisited. *Contrib. Mineral. Petrol.,* **157**, 735-747.

Toplis, M.J. and Carrol, M.R. (1995). An experimental Study of the Influence of Oxygen Fugacity on Fe-Ti Oxide Stability, Phase Relations, and Mineral-Melt Equilibria in Ferro-Basaltic Systems. *Journal of Petrology*, **36**, 1137-1170.

Toplis, M.J. and Carrol, M.R. (1996). Differentiation of ferro-basaltic magmas under conditions open and closed to oxygen: implications for the Skaergaard intrusion and other natural systems. *Journal of Petrology,* **37**, 837-858.

Toplis, M.J. and Corgne, A. (2002). An experimental study of element partitioning between magnetite, clinopyroxene and iron-bearing silicate liquids with particular emphasis on vanadium. *Contrib. Mineral. Petrol.*, **144**, 22-37.

Toplis, M.J., Dingwell, D.B. and Libourel, G. (1994). The effect of phosphorus on the iron redox ratio, viscosity, and density of an evolved ferro-basalt. *Contrib. Mineral. Petrol.,* **117**, 293-304.

Tormey, D.R., Grove, T.L. and Bryan, W.B. (1987). Experimental petrology of normal MORB near the Kane Fracture Zone: 22°-25°N, mid-Atlantic ridge. *Contributions to Mineralogy and Petrology,* **96**, 121-139.

Veksler, I.V. (2009). Extreme iron enrichment and liquid immiscibility in mafic intrusions: Experimental evidence revisited. *Lithos*, **111** (1-2), 72-82.

Veksler, I.V., Dorfman, A.M., Borisov, A.A., Wirth, R. and Dingwell, D.B. (2007). Liquid immiscibility and the Evolution of Basaltic Magma. *Journal of Petrology*, **48** (11), 2187-2210.

Veksler, I.V., Dorfman, A.M., Danyeshevksy, L.M., Jakobsen, J.K. and Dingwell, D.B. (2006). Immiscible silicate liquid partition coefficients: implications for crystal-melt element partitioning and basalt petrogenesis. *Contributions to Mineralogy and Petrology*, **152**, 685-702.

Vincent, E.A. and Phillips, R. (1954). Iron-titanium oxide minerals in layered gabbros of the Skaergaard intrusion, East Greenland, Part I. Chemistry and ore-microscopy. *Geochim. Cosmochim. Acta*, **6**, 1-26.

Wager, L.R., & Deer, W.A., 1938. A dyke swarm and coastal flexure in East Greenland. *Geol. Mag.,* **75**, 39-46.

Wager, L.R., & Deer, W.A., 1939. Geological investigations in East Greenland, Part III. The petrology of the Skaergaard Intrusion, Kangerdlugssuaq, East Greenland. *Meddr. Gronland.,* **105**, 352 pp.

Wager, L.R. and Mitchell, R.L. (1951). The distribution of trace elements during strong fractionation of basic magma – a further study of the Skaergaard intrusion, East Greenland. *Geochim. Et Cosmoch. Acta*, **1**, 129-208.

Wager, L.R., 1960. The major element variation of the Layered Series of the Skaergaard Intrusion and a re-estimation of the average composition of the Hidden Layered Series and of the successive residual magmas. J. *Petrology* **1**, 364-398.

Wager, L.R. and Brown, G.M. (1967). Layered igneous rocks. Freeman, San Francisco.-588pp.

Wager, L.R. and Brown, G.M. (1968). Layered igneous rocks. Oliver & Boyd, Edinburgh London,-588pp.

White, C.M., Geist, D.J., Frost, C.D. and Verwoerd, W.J. (1989). Petrology of the Vandfaldsdalen Macrodike, Skaergaard region, East Greenland. *J. Petrology,* **30**, 271-98.

Wilke, M., Farges, F., Petit, P.E., Brown Jr., G.E. and Martin, F. (2001). Oxidation state and coordination of Fe min minerals: An Fe K-XANES spectroscopic study. *Am. Mineral.*, **86**, 714-730.

Williams, R.J. (1971). Reaction constants in the system Fe-MgO-SiO_2-O_2: intensive parameters in the Skaergaard intrusion, East Greenland. *Am. J. Sci.,* **271**, 132-146.

Wood, D.A. (1978). Major and trace element variations in the Tertiary lavas of East Greenland and their significance with respect to the Iceland Geochemical anomaly. *J. Petrol.,* **19**, 393-436.